INFRARED EMISSION SPECTRA FROM OPERATING

ELASTOHYDRODYNAMIC' SLIDING CONTACTS

by

James L. Lauer

SUN OIL COMPANY

prepared for

NATIONAL AERONAUTICS AND SPACE ADMINISTRATION

NASA Lewis Research Center

NAS3-18531

1. Report No. NASA CR-134973	2. Government Accession No.	3. Recipient's Catalog No.
4. Title and Subtitle INFRARED EMISSION SPECTRA FROM OPERATING ELASTOHYDRODYNAMIC SLIDING CONTACTS		5. Report Date March 8, 1976
		6. Performing Organization Code
7. Author(s) James L. Lauer		8. Performing Organization Report No.
		10. Work Unit No.
9. Performing Organization Name and Address Sun Oil Company P. O. Box 1135 Marcus Hook, PA 19061		
		11. Contract or Grant No. NAS 3-18531
		13. Type of Report and Period Covered Contractor Report
12. Sponsoring Agency Name and Address National Aeronautics and Space Administration Washington, DC 20546		
		14. Sponsoring Agency Code

16. Abstract

Infrared emission spectra from an operating EHD sliding contact were obtained through a diamond window for an aromatic polymer solute present in equal concentration in four different fluids. Three different temperature ranges, three different loads, and three different speeds for every load were examined. Very sensitive Fourier spectrophotometric (interferometric) techniques were employed. Band intensities and band intensity ratios -- though for the same spectral bands -- were, nevertheless, found to depend both on the operating parameters and on the fluid. Fluid film and metal surface temperatures were calculated from the spectra and their dependence on the mechanical parameters plotted. The difference between these temperatures could be plotted against shear rate on one curve for all fluids. However, at the same shear rate the difference between bulk fluid temperature and diamond window temperature was much higher for one of the fluids, a traction fluid, than for the others.

ORIGINAL PAGE IS
OF POOR QUALITY

17. Key Words (Suggested by Author(s)) elastohydrodynamic lubrication infrared emission spectroscopy lubricating film temperatures bearing surface temperatures high pressures Fourier infrared spectroscopy		18. Distribution Statement Unclassified - Unlimited	
19. Security Classif. (of this report) Unclassified	20. Security Classif. (of this page) Unclassified	21. No. of Pages 86	22. Price* $3.00

FOREWORD.

The work reported here is the second phase in a program of applying infrared spectroscopy to EHD contacts. In the first phase it was shown that infrared emission spectra could be obtained from the very small fluid volumes in a high pressure diamond cell. The present work demonstrates the feasibility of infrared emission spectroscopy of the extremely thin fluid films in operating contacts through a diamond window. As a first step information on temperatures in the Hertzian region was obtained for a variety of operating conditions. Subsequent phases of this work will deal with temperature distributions, molecular alignment and, above all, with chemical and physical changes of fluids under the most severe stresses.

TABLE OF CONTENTS

LIST OF TABLES

LIST OF FIGURES

LIST OF FIGURES (Cont'd)

SUMMARY

Infrared emission spectra were obtained from both the lubricant and the metallic surface of an operating elasto-hydrodynamic sliding contact. For this purpose a device resembling an inverted Four-Ball Tester was constructed, which permitted the application of different loads to a test ball rotating about a horizontal axis above a diamond window in the bottom of a cup filled with test fluid at a controlled temperature (20-50°C). The radiation from the entire Hertzian region which passed through the window was collected by an all-reflecting microscope objective lens and analyzed by an infrared Fourier spectrometer (interferometer) over the 630-730 wavenumber region.

Four representative fluids, (1) a naphthenic mineral oil, (2) a pentaerythritol ester, (3) a synthetic paraffin, and (4) a cycloaliphatic traction fluid, were examined at three different loads and three different sliding velocities. Every fluid was diluted 33% by polymethylstyrene so that the same 700 and 760 cm^{-1} bands could be examined. These fluid infrared bands stood out over the continuous background of graybody radiation from the metal surface. By appropriate calibrations the intensities of the 700 cm^{-1} band and the background intensities in the spectra could be related to the fluid and ball surface temperatures. The temperature registered by a thermocouple attached to the diamond window was considered the Hertzian inlet temperature.

The analysis of the data is incomplete and subject to revision in the light of further related work. However, these observations already stand out: (i) For equal shear rates the difference between diamond temperature and bulk fluid temperature was considerably larger for the traction fluid than for the others while (ii) the difference between diamond and metal surface temperature was generally least for the ester fluid; (iii) the fluid film temperature was barely higher than the diamond temperature for the synthetic paraffin for which the film thicknesses were relatively quite high -- and hence the shear rates relatively low -- but for the other fluids the film temperature generally decreased with increasing shear rate; and (iv) a plot of the difference between fluid film and metal surface temperature versus shear rate was very nearly one parabola for all the fluids, the temperature difference increasing with shear rate at low shear rates and decreasing with shear rate at higher shear rates.

In some instances, the ratios of the 700/760 cm^{-1} band intensities changes markedly with change of load, possibly indicating a change of physical state or molecular alignment.

1. INTRODUCTION

When, late in 1973, we embarked on a program of applying infrared -- primarily emission -- spectroscopy to elastohydrodynamic (EHD) contacts, we set ourselves as objectives the determination of fluid temperatures, metal surface temperatures, and of changes of fluid composition and state under various operating conditions. While infrared emission spectra of dielectrics generally consist of discrete bands, which are characteristic of the composition and state of the material, those of metallic surfaces are continuous, "graybody", and generally depend only on temperature. Composites of these spectra are, therefore, easily separated. From the accumulated data useful deductions regarding the effects of EHD processes on the fluids, especially those leading to bearing failure, were considered to be likely results.

We realized, of course, from the start, that major hurdles would have to be overcome before we could hope to arrive at meaningful information. We had background in infrared Fourier spectroscopy, the most sensitive procedure of obtaining infrared spectra, and had gathered and analyzed absorption spectra of fluids contained in the small volumes of high pressure diamond cells. But Fourier infrared emission spectroscopy, the only procedure that appeared to hold much promise in the study of operating EHD bearing contacts, had never been applied to such small samples, and dynamic conditions introduce into the spectroscopy the additional complications of even thinner fluid films and the graybody radiation from moving metal surfaces whose temperature is different from the film temperature. Though calculations based on the available theory showed that our experimental objectives were entirely possible, we decided to work up to them in stages and thereby provide a sound basis for our eventual conclusions. Our report to NASA a year ago[1] described work proving our ability to obtain emission spectra under static conditions from contact regions simulated in the diamond cell. Now we reached the stage where we can produce emission spectra from operating contacts and derive fluid film and boundary surface temperatures from them. We are very confident that later stages will bring us closer to an understanding of the interactions of EHD processes in the metal and fluid parts of the contact region.

2. TEST FLUIDS

The basic test fluids were selected and supplied by NASA. Fluids of pertinent properties (especially viscosity) as different as possible were chosen. Because of our limitations of sensitivity, spectral range, and time, every fluid was diluted 2/3 to 1/3 by volume with polymethylstyrene (Monsanto Fluid 276 V-2). The differences between the fluids were thereby reduced, but the advantage of having the same two exceedingly intense and non-interfered infrared bands as indicators in every spectrum certainly made up for this loss. The same calibration spectra could be used throughout this work.

Polymethylstyrene may not be necessary in the future because of our advances in technique. Infrared bands of the fluids themselve will become available to us for analysis.

Viscosities and densities of fluids used in this investigation were determined by standard procedures at two temperatures and are listed in Table I. These data provided the basic information for the film thicknesses calculated during the course of our data reduction process.

A routine infrared absorption spectrum obtained for one of the fluids, which is essentially merely the spectrum of the polymethylstyrene indicator fluid, is shown in Figure 1. In the spectral region used for the emission spectra from EHD contacts ($630-930$ cm^{-1}) only two bands are outstanding, one at about 700 cm^{-1} and the other at about 760 cm^{-1}. These are the characteristic vibration bands of a monosubstituted aromatic ring. The former vibration is describe as every other sextant of the ring going up out of the plane while the intervening sextants go down; a large change in dipole moment is thereby produced, resulting in a very strong band. The latter vibration is also very strong in monosubstituted aromatics; it is the derivative of the in-phase out-of-plane vibration of the six adjacent hydrogens in benzene (which gives rise to the extremely strong 671 cm^{-1} benzene "umbrella" vibration) and corresponds to out-of-plane wagging of five adjacent hydrogens with respect to the ring substituent considered more or less stationary (Figure 2). This wagging mode is very sensitive to the molecular environment (temperature, liquid or glassy state) and therefore a potentially useful probe for it. On the other hand, the 700 cm^{-1} band strength is nearly unaffected by the molecular environment and, therefore, a good temperature indicator.

Polymethylstyrene has a molecular weight in the lubricating oil range and is soluble in all the test fluids. It does not interfere with the trends for which the test fluids were selected.

3. TEST APPARATUS

3.1 MECHANICAL SECTION

Since one of the ultimate objectives of our study is an understanding of the processes leading to bearing failure and failure

is more likely to occur in sliding contacts, our test apparatus
was constructed for sliding contacts. (At some later time
rolling contacts should also be examined.) A ball-on-plate
is the simplest contrivance to obtain such a contact; we
adapted Professor Winer's version[2], which is essentially a
Four-Ball-Machine with the test ball being rotated about a
horizontal (instead of the usual vertical) axis (Figure 3).
However, while Winer locates his contact at a sapphire window
in a plane above the ball, we had to place it below the ball
at a diamond window in the bottom of the cup containing.
the test fluid, in order to introduce the transmitted radia-
tion into our interferometer over the shortest possible dis-
tance. Otherwise, a long optical lever arm would have been
required, which would have amplified any mechanical instabilities.
Indeed, only by extensive precautions (e.g. sponged rubber
supports) to mechanically isolate the EHD apparatus from the
interferometer could the necessary radiometric sensitivity be
achieved. Placing the contact in the fluid reservoir cup
causes interactions between the fluid flow in the reservoir
and in the contact zone. Thus the only practical way to remove
the heat generated in the contacts was to insert an aluminum
coil containing cooling water into the cup itself. Winer's
method of circulating the test fluid through a heat exchanger
caused our contact temperatures and/or film thicknesses to
become unstable.

The temperature of the water circulating through the coil
was controlled by two constant temperature baths to provide
three basic temperature levels for every test fluid. For
calibration purposes (the test ball stationary), the entire
assembly can be heated by circulating warm water through the
coil. Then the test fluid functions merely as a heat transfer
medium.

Basically then, our EHD unit is an upside-down Four Ball
Machine, in which the test ball is rotated about a horizontal
axis to form a sliding contact at a diamond window mounted in
the bottom plate of a cup containing the test fluid.

The essential parts of our EHD apparatus (items 1 to 18)
and the interferometer entrance optics are shown in Figure 3.
It will be noted that the two units are mechanically isolated
(the spectrometer is supported only at its center by several
layers of sponge rubber.

The load is applied to the test ball by a lever arm (not
shown) resting on the top of it on three point contacts,
symmetrically located on three coplanar steel balls in such a
way that the resultant load is directed perpendicularly downward
through the center of the test ball. On suggestion of Professor
Winer, these three contacts were padded by small sapphire
discs to increase the contact areas and thereby reduce the
danger of scoring the test ball. Applying the load to the test
ball from above also fixes its position on the diamond window
of the primary EHD contact in the cup. The shaft turning the
ball is deliberately kept flexible. Fine adjustment screws

4

allow the diamond window to be placed tangentially to the ball. Another set of adjustment screws moves the entire cup assembly in the focal plane of the objective lens of the interferometer entrance optics, and permits location of the contact on the optic axis.

At least three temperatures in the fluid cup were continuously monitored during every experiment: (a) the temperature at the diamond window by a thermocouple touching it within the mounting cement, (b) the temperature at the ball by a thermocouple loosely touching it, and (c) the temperature at a relatively quiescent location within the fluid. The constancy of these temperatures to better than 0.2°C during a spectral scan (about 20-25 minutes) was essential. Because of the extremely high thermal conductivity of the diamond window (a specially ground 4 mm diameter, 2 mm thick disc of natural Type II A diamond chosen for near perfect infrared transparency and oriented so as to minimize stress in the direction of sliding), the temperature recorded at (a) was assumed to be equal to -- or at least closely parallel to -- the fluid inlet temperature at the Hertzian contact. Changes of rotational speed or load were reflected instantly by changes of this temperature. Temperature (b) rather than temperature (c) was chosen as the best measure of the bulk fluid temperature because the many temperature gradients and currents in the main body of the cup made precise relocation of the thermocouple at (c) impossible.

The largest readily available stainless steel ball (440C, diameter 0.0572m) was chosen so as to provide a large Hertzian contact region for analysis. Only minor changes of the loading lever -- mainly the location of the three stationary loading (0.025 mm diameter) balls -- will be necessary to accommodate the even larger steel balls (440C, diameter 0.680m), which SKF (Sweden) recently donated to us for this program. The latter balls have a certified roughness of less than 0.01 μm (or 100Å), which is just about 10% of the smallest fluid film thickness calculated. However, the balls used in this study could according to SKF, be up to five times rougher.

The pertinent mechanical properties of ball and window are listed in Table II.

3.2 ENTRANCE OPTICS FOR EMISSION SPECTROSCOPY

Since essentially the same interferometer entrance optics were described in our earlier report[1], it is not necessary to go into many details here. The essentials are also shown in Figure 3. An important element is a Beck lens (it is called a "lens" even though it has no refracting elements, because it functions like one), which gathers the radiation emitted by the contact zone and transmitted by the diamond window. All of the work reported here was done with a 15X lens. The Beck lens forms a real image of the contact

region (the field of view of this lens equals the area of the contact region under our smallest load) at the focus of the collimating mirror and this image is the effective source for the interferometer (or Fourier spectrometer). The area of the collimating mirror filled by this "source" is, however, only a fraction of the total mirror area. By contrast, the aperture effective for radiation from the chopper blade, located just downstream of the "source" is the full mirror area. The electronic circuitry of our Beckman-RIIC FS-720 Fourier Spectrometer is so constructed that only the difference of the radiant flux falling on the detector window at half-cycle intervals is amplified. By restricting the aperture of the chopper radiation, though the insertion of "restrictors" into the collimated beam, the graybody radiation emitted in the EHD region by the surface of the test ball can, therefore, be balanced by radiant flux of nearly equal magnitude coming from the chopper blade. The chopper is thus an effective temperature reference and was thermostatted by a jet of nitrogen.

Another image of the contact region is projected in the interferometer absorption cell compartment in front of the detector. A diaphragm was placed there to limit both the portion of the contact area and of the chopper blade seen by the detector.

The exitance (radiant power emitted) of the chopper blade which is detected, is, therefore, the effective reference of radiant energy in our experiments. By balancing this exitance against that of the ball surface in the contact region at the chopper frequency of 15 cycles per second, emission spectra of fluid films only 0.1 μm thick and less than 100°C have been recorded.

3.3   INTERFEROMETER MODIFICATIONS

Although the same basic Beckman-RIIC FS-720 Fourier Interferometer was used in this work as in our earlier studies[1], so much of it was changed that not much more than the original shell remained. Already some time ago we extended the frequency range from 50-400 cm^{-1} to 50-1100 cm^{-1} by changes in the triggering circuitry (reading at 4 μm retardation intervals instead of 8 μm intervals) and by adapting a thinner Mylar beam-splitter (2.5 μm thick)[3]. However, to make this work possible, (a) the Golay detector was replaced by a ten times more sensitiveone with solid state circuitry (bringing us close to the theoretical limit for thermal detectors), (b) the original phase-sensitive amplifier was replaced by a modern Ithaco Model 391A Lock-In Amplifier, and (c) the digitizer and punch circuitry, which transforms our signals into punched paper tape data points, was replaced by a new Novatronics unit with a range of +3999 to -39999, giving us a dynamic range of 16 bits (our previous range of 0-399 was inadequate to detect the extremely small emission signals from the bearing fluid in presence of the overwhelming graybody radiation from the ball surface.

To make full use of the new parts, the computer programs were improved considerably. Figures 4 and 5 illustrate the power of these programs. The interferogram of Figure 5 represents the recorded signal of an actual sample run in the form of a scan of interferometer mirror displacement versus amplitude. No particular regularities can be discerned in this record and it looks like random noise only. In fact, not even the center burst, the maximum or stationary phase, which is characteristic of every interferogram, is very apparent since this interferogram was obtained at near balance of chopper blade and EHD ball surface irradiance of the Golay detector. Nevertheless our data processing package was able to extract the respectable spectrum of Figure 5. It shows the emission bands of polymethylstyrene at 700 and 760 cm^{-1} as well as the absorption band of the Mylar beamsplitter at 730 cm^{-1}. This absorption band is present in all our spectra and can be confusing when the fluid spectrum has a band nearby. We will replace the beamsplitter soon by germanium which does not absorb in this region.

The interferometer optics of the FS-720 was realigned for proper interfacing to the new entrance optics. An inexpensive low-power laser was most helpful in this endeavor.

3.4 ALIGNMENT

While the methods used for obtaining interferograms and spectra were essentially the same as those used in our earlier work on emission spectra under static conditions[1], the nature of the new work required some special considerations. Above all, it was necessary to exercise extreme care to make certain that the optical alignment was proper -- no mean task since the Hertzian region is not visible. The procedure finally adopted for aligning the EHD contact region on the optic axis of the interferometer entrance optics and at the focus of the Beck objective lens (Figure 3) was the following:

(i) The "Four-Ball Section" was turned upside down so that the diamond window faces up. A tiny amount of a liquid was placed into the conjunction of window and test ball. An optical microscope of low power was placed above the window. With a reasonably strong lamp reflecting light at the window, it was not difficult to see the conjunction region from the outline of the droplet. The fine adjustment screws on the window mounting plate were used to center the conjunction region on the diamond window.

(ii) Since the position of the test ball on the window was now defined by the three coplanar holding balls at the bottom of the loading platform, the assembly could be turned over. The ball was removed, and some diluted black paint was applied to the diamond window. When the test ball was put back, paint from the contact region was transferred to the ball and a small round opening was found on the window precisely at the position of the conjunction.

(iii) The assembly (without the ball) was placed above the Beck lens and the diamond window was illuminated by a strong light bulb. With the second set of adjustment screws the enlarged image of the hole in the paint was oriented at the "proper" position in the image plane of the interferometer cell compartment ahead of the detector. The up-and-down adjustment on the Beck lens holder was then used to focus the image exactly (the ragged edges became sharply outlined).

(iv) The paint was removed from the window and the cup filled with the fluid to be studied.

The diaphragm in the image plane of the cell compartment was mentioned before. For all the experiments described here later, it was opened to correspond to the Hertzian area under smallest load. For this purpose a mask with the correct diameter hole was placed over the diamond window. Some experiments were done in which both the diaphragm opening and its position were varied under EHD operating conditions. However, for this work the diaphragm remained unchanged. The proper position of the diamond window on the optic axis of the Beck lens could also be determined with the mechanical section in operation by varying the cup adjustment screws. When the minimum was reached for both the X and the Y adjustment (Figure 6), the contact region was on the axis. The asymmetry of the plot of Figure 6 for the inlet and outlet regions should be noted.

Future work will be designed to study different portions of the Hertzian contact region. At this time we know from a number of observations that further reduction of the radiating area results in somewhat higher calculated film temperatures. This is just as one would expect.

3.5 CONTROL OF CHOPPER BLADE TEMPERATURE AND EMISSIVITY

The Beckman RIIC FS-720 Interferometer uses a chopper-modulated amplifying system in conjunction with a Golay detector. As was mentioned earlier, the amplified signal is "locked-in" so as to represent the difference of radiant power incident on the detector from the source and the blade, which are 180° apart in phase. Under normal operating conditions, i.e. for absorption spectrophotometry, the source is the hot quartz envelope of a mercury arc in front of the chopper so that the radiation from the chopper blade is negligible by comparison. The chopper wheel is turned by a constant speed motor next to it to provide a chopping frequency of 15 Hz. Heat is transferred from the motor to the chopper blade by conduction through the shaft and by radiation (the blade is deliberately painted black), so that its normal operating temperature is slightly above ambient. However, even though the temperature rise is very small, a large area of the blade is seen by the collimator so that -- under our conditions of very high sensitivity -- the total radiant power from the blade is

not at all negligible compared to that from our weak source
(i.e. the EHD region). Indeed, it is often greater than the
latter, thereby giving rise to an "inverted" interferogram.
Reducing the effective blade area by insertion of "restrictors"
(masks with precisely dimensioned holes) into the collimated
beam, may then "rectify" the inverted interferogram. The
reason for this is the rather small spread of the source
beam by the Beck lens (it uses only the central section of
the collimating mirror) so that the restrictor -- provided
its hole is not so small that part of the source beam is also
cut off -- changes the ratio of radiant power between source
and blade. Since the part of the source beam that originates
from the ball surface in the contact region is graybody in
nature just as the radiant emission from the blade and since
ball and blade temperatures are not too different, it is
possible to balance these two sources and effectively monitor
the radiant emission from the fluid alone. In practice, an
exact balance is not desirable, for the radiation emitted by
the fluid alone is so weak compared to random noise that the
center burst of the interferogram is difficult to locate (its
location on an interferogram provides the primary reference for
the computation of spectra). Hence it seemed best to operate
near a minimum center burst, which can be either positive or
negative in the interferogram. If it is positive, the compu-
tation of the spectra by the Fourier transformation was straight-
forward, but if negative, the interferogram had to be inverted
first to conform with computer processing. In that case spectral
emission bands of the fluid look like absorption bands, but the
absorption band of the beamsplitter (Mylar) remains as an
absorption band.

To illustrate these considerations, Figure 7 is shown,
representing spectra obtained under the identical operating
conditions except for differences of restrictor size. The
correspondence of the 700 and 760 cm^{-1} apparent absorption
bands to emission bands is evident, while the 730 cm^{-1} Mylar
absorption band has remained as an absorption band. Since base
line band areas are used (vide infra) as measures of band
intensity, it does not matter whether the peaks are maxima or
minima; only the absolute values count. On the other hand,
when spectral amplitudes at particular frequencies are compared,
e.g. in the determination of ball surface temperatures (vide
infra) amplitudes of inverted spectra must be assigned a
minus sign for consistency.

Since the chopper blade radiation is thus an effective
reference source for all the spectral runs, it must remain
constant or known. Throughout this work a jet of ice-cooled
nitrogen at constant flow velocity was directed at the blade.
The nitrogen was then used to flush the entire interferometer.
It was also necessary to replace the black blade surface by
shiny aluminum to reduce the emissivity. No run was started
before the chopper assembly had reached equilibrium temperature.

One of three restrictors (masks of different apertures) was used to balance the graybody radiations as closely as possible to maximize fluid band areas in the spectra.

The use of an extended reference source, such as the chopper blade, in an interferometer may be questioned, for it produces a distribution of retardations. We do not believe this matter is serious because the graybody spectrum at our frequencies and temperatures is almost flat. For this reason it is not difficult to balance graybody emissions at somewhat different temperatures. A more serious defect, we think, is the location of the chopper downstream of the Beck lens, making us vulnerable to possible changes of stray radiation or temperature in the entire interferometer entrance optics. We tried to minimize this potential source of error by shielding (e.g. the aluminum reflector, item 15 in Figure 3). To solve this problem in the future and to gain much more flexibility in the temperature balance and control, a small reflecting chopper (vibrating tuning fork) was designed to be placed directly below the diamond window. Radiation from a source of variable intensity will be reflected by the chopper blade and used to balance the graybody radiation from the ball; in this way both source and reference radiations will follow the same optical path. This modification, now on order, will eliminate many other questions and problems as well.

4. EHD CONTACT TEMPERATURES BY I.R. EMISSION SPECTROSCOPY

Once we became convinced that we could obtain reproducible "dynamic" emission spectra from the fluid in an EHD contact region -- the most crucial step of the program -- we had to develop effective procedures for extracting the most information from these spectra. As mentioned earlier, the 700 cm^{-1} band of our polymethylstyrene indicator fluid should be nearly unaffected by the physical conditions in the EHD region; its strength should, therefore, be a good measure of fluid film temperature. The ball's surface temperature in the EHD region should be inferable from its graybody radiation at frequencies not overlapped by film radiation. Our present spectra are averages over most of the Hertzian contact region because of our lens and diaphragm settings (different sections of the Hertzian region will be explored later) and the temperatures inferred from the spectra are, therefore, also average temperatures. Although this report deals primarily with these temperatures, their determination is only one aim of this investigation. Molecular orientation, changes of composition and state, are other objectives. However, the deduction of consistent fluid and metal surface temperatures in the contact region is a necessary first and important step. This work is, we believe, the first to be published in which contact region temperatures are compared for different fluids under different operating conditions.

Before we could arrive at film and ball temperatures from our spectra, a theoretical analysis of thermal emission from semi-transparent films sandwiched between metal surfaces and windows had to be made. Its results are more general than needed for our purposes so that they could be useful elsewhere.

10

4.1 THERMAL EMISSION FROM SEMITRANSPARENT FILMS ON METALLIC SURFACES THROUGH TRANSPARENT WINDOWS

In all the work reported on infrared emission spectroscopy from thin layers of materials on metal surfaces equality of the temperatures of the layer and the metal was assumed. Low[4], for example, studied the emission spectra of oleic acid spread on aluminum in this way. Inverted peaks in his spectra are indicative of a temperature gradient through his thicker films, but these were considered artifacts to be avoided. In EHD contact regions, the fluid film temperature must be assumed, under steady operating conditions, to be always different from the surface temperature of the sliding ball and from the temperature of the diamond window as well. McMahon's widely quoted equations of his paper on "Thermal Radiation from Partially Transparent Reflecting Bodeis"[5] apply to thick (wavelengths small compared to thickness) slabs with equal boundary conditions on both surfaces. Our situation is that of thin radiating films bounded by different materials at different temperatures. A separate analysis of our case is therefore required.

If an accepted mathematical model of the EHD situation were available for a few standard fluids, the spectra of these fluids could be employed for apparatus calibrations and a calculation of fluid temperatures from their spectra would be simple. Such a model is still lacking, although excellent effort in this direction is underway. Our approach has, therefore, been to use fluid emission spectra obtained with the diamond anvil cell under static conditions for calibration. The physical differences between a real EHD contact and one simulated with the diamond cell do, however, require a model to map static into dynamic data. The main difficulties are (a) the absence of shear under static conditions (b) the near impossibility of producing fluid films statically as thin as those sheared (0.1-0.5 μm), (c) providing for equivalent film boundaries (diamond vs. metal), and (d) different heat transfer characteristics. The following sections will describe a model approaching these requirements. It is based on the radiation transfer theories developed by the astrophysicists for estimating temperatures in stellar atmospheres. However, drastic simplifications could be made.

Since our Hertzian contact consists essentially of a flat plate of dielectric, the fluid, sandwiched between a flat metal surface (the flattened portion of a ball surface) and a diamond window, the schematic diagram of Figure 8 will represent the situation. Following a more detailed analysis made by Viskanta, Hommert and Groninger[6] of a similar situation encountered with a heated glass sheet, the starting equation is the steady-state radiative transfer equation for a plane layer of a nonscattering, semi-transparent dielectric (the fluid film in our case) in local thermodynamic equilibrium. With azimuthal symmetry and -- for the moment -- restriction to one-dimensional radiation transfer and one spectral frequency, this equation is

$$\frac{dI(y)}{dy} = -k \left[n^2 I_B(t) - I(y) \right] \qquad (1)$$

where $I(y)$, k, n, and I_B are respectively the monochromatic intensity (radiance), spectral absorption coefficient*, index of refraction, and Planck blackbody function at absolute temperature t, all at wavenumber ν. It is convenient to separate $I(y)$ into two contributions: the intensity in the forward direction (increasing negative y), $I^+(y)$, and that in the negative direction, $I^-(y)$. By solving Eq. (1) in the standard way, using the appropriate boundary conditions, the outwardly emerging intensity at wavenumber ν turns out to be proportional to

$$I^+(0) = A+B, \text{ with}$$
$$A = (1-R_1)(1-R_1 R_2 T^2)^{-1}(1-R_2)TB_M \quad \text{and} \qquad (2)$$
$$B = (1-R_1)(1-R_1 R_2 T^2)^{-1}(1-T)(1+R_2 T) B_F$$

where R_1 and R_2 are the reflectivities** at the two boundaries, $T = \exp(-kh)$ is the transmissivity through the fluid, h is the fluid film thickness, B_M and B_F are $I_B(t_M)$ and $I_B(t_F)$, i.e. the Planck radiation functions evaluated for the metal surface and average film temperatures respectively. Equation (2) corresponds to Eq. (18) of the article by Viskanta, Hommert and Groninger[6].

It is evident that equations (2) could have been derived from first principles without formally solving Eq. (1), for A is evidently the radiant intensity emerging from the fluid as a result of radiation from the metal surface, which is transmitted through the two interfaces and attenuated on its way and B is the radiant intensity of sources within the fluid radiating in the positive and negative y direction, which are transmitted through interface 1 with or without reflection at interface 2 after appropriate attenuation. For both A and B the multiple reflection factor $(1-R_1-R_2 T^2)^{-1}$ takes an infinite number of bounces at both interfaces into account. This factor comes out naturally from the integration of Eq. (1), but could easily be missed in a direct accounting procedure of propagating rays. However, the main advantage of Eq. (1) over first principles methods of solution is its solvability for both a distribution of angles (here totally neglected) and temperatures along y (or rays at angles with y). The solution given by Eq. (2) assumes an average temperature throughout the thickness of the fluid film. By measuring an intensity proportional to $I^+(0)$ for several frequencies, and preferably for several angles with respect to the y direction, an estimate of the temperature distribution could be obtained.

*assumed to be independent of t

**assumed independent of temperature

Emission band intensities of the fluid measured by a baseline method, i.e. by subtracting the background graybody radiation of the metal surface (Figure 7), do not include that part of the metal surface radiation which is absorbed by the fluid film. However, they do include that part which undergoes multiple reflections within the film.

Subtracting the reflected protion (T=1) from A in Eq. (2) gives

$$A' = (1-R_1)(1-R_1 R_2 T^2)^{-1}(1-R_2)(T-1)B_M \qquad (3)$$

so that the effective intensity I+(eff) is

$$I^+ eff = A' + B \qquad (4)$$

and the effective emissivity of the fluid film is proportional to

$$E_F(eff) = \frac{A'+B}{B_F} = (1-R_1)(1-R_1 R_2 T^2)^{-1}(1-T)\left[1+R_2 T - (1-R_2)\frac{B_M}{B_F}\right] \qquad (5)$$

where, according to Planck's law

$$\frac{B_M}{B_F} = \frac{e^{\frac{C_2}{\lambda T_F}} - 1}{e^{\frac{C_2}{\lambda T_M}} - 1} \qquad (6)$$

for $B_M/B_F \ll 1$, $(1-R_2)$
B_M/B_F is neglected in Eq. 5

Here T_F and T_M are the absolute film and metal surface temperatures, λ is the absorption band wavelength in meters and $C_2 = 0.014388$ mK, the universal radiation constant. The baseline band intensity is proportional to

$$I^+ eff = E_F{}^{eff} B_F \qquad (7)$$

13

In the high pressure diamond anvil cell, schematically shown in Figure 9 , the fluid film is sandwiched between two diamond windows and the entire setup is isothermal. The outwardly emerging intensity is proportional to

$$I^+(0) = \frac{(1-R_1)(1-T)}{1-R_1 T} B_F = E_D B_F \qquad (8)$$

an equation readily derived from Eq. 2 by setting $B_M = 0$ and $R_1 = R_2$.

A calibration of band intensity in the diamond cell versus temperature (it is not necessary to compute B_F explicitly) for a fluid layer of known thickness will thus yield E_D, from which E_F^{eff} can be calculated when R_2, B_M/B_F, and h are known (say from separate experiments). Once E_F^{eff} is known, the temperature of the EHD film can be determined from the corresponding emission band intensity of an EHD film.

The effect of the front diamond window on the emission of the fluid film has been assumed to amount to an attenuation factor equal for both the diamond cell and the contact film so that calibration takes care of it automatically. If the reflected portion of the emerging radiation at the front diamond surface returns into the fluid and re-emerges to a significant extent, this argument may not be strictly true. However, the difference due to this assumption will be much less than our various experimental errors. It also seems unlikely that thermal radiation from the fluid film could be coherent enough to cause significant interference phenomena; none were observed in our work.

Perhaps the neglect (in the work reported here) of the last term in Eq. (5), viz. $(1-R_2) B_M/B_F$, in temperature calculations is a more serious error than the foregoing. It can be accounted for computationally by a loop-type correcting procedure, since knowledge of B_M/B_F must precede the determination of B_F from Eq. (7). Omitting the term is equivalent to assuming $(1-R_2) B_M/B_F$ small compared to $1+R_2 T$. Typically for $R_2 = 0.72$, $T = 0.5$, $t_M = 50°C$ and $t_F = 80°C$, this amounts to an E_F^{eff} that is 16% too small. Our present radiometrically deduced temperatures could thus be too low, especially for thick films absorbing considerable radiation (small T). This problem will be attended to later, when better film thickness values (h) and calibration data will be available to us.

14

4.2 LUBRICANT FILM THICKNESSES

The best way to obtain fluid film thicknesses in Hertzian contacts under various conditions of linear speed, load, and fluid inlet temperatures appears to be optical interferometry. This procedure has been used by Cameron and coworkers[7] and by Winer and coworkers[8] and is readily adaptable to our own apparatus and experimental conditions. It will be carried out later for all our fluids under our standard experimental conditions. To correlate our present data, film thicknesses were calculated from viscosity and density measurements by well-established empirical equations.

Wedeven's equation[9], which is applicable to our experimental conditions, is

$$h = 1.73R \left(\frac{\alpha \eta u}{R} \right) \left(\frac{w}{E'R^2} \right)^{-\frac{1}{21}} \tag{9}$$

where h is the film thickness, R the reduced radius of contact, which is the ball radius in our case, η the ambient viscosity of the lubricant, u the combined surface velocity, which is one-half the ball's surface velocity in our case, w the load on the bearing contact, E' is the reduced elastic modulus defined by

$$\frac{1}{E'} = \frac{1}{2} \left(\frac{1-\sigma_1^2}{E_1} + \frac{1-\sigma_2^2}{E_2} \right) \tag{10}$$

and α is the pressure/viscosity coefficient.

For the fluid compositions used in this work kinematic viscosities v_1 and v_2, were obtained by standard methods at the same two temperatures (t_1 and t_2). Densities were obtained at standard temperatures and spot checks showed that the empirical equation

$$d(t) = d(t_3) - (t_3-t) \times 0.00065 \tag{11}$$

was a good approximation to the density at any temperature t. In Eq. (9) the parameters characterizing the fluid are α and η and they must be known at the Hertzian inlet temperature to permit the computation of h.

The kinematic viscosity at any temperature between t_1 and t_2 can be found with considerable confidence for all of our fluids by making use of the ASTM viscosity charts or, equivalently, by the Walther formula[10]

$$\log \log (v_1 + a) = b + c \log t_1$$

$$\text{or} \quad \log \log (v_2 + a) = b + c \log t_2 \tag{12}$$

whence
$$c = \log \left[\log(v_1 + a) / \log(v_2 + a) \right] / \log(t_1/t_2) \tag{13}$$

and
$$b = \log \log (v_1 + a) - c \log t \tag{14}$$

so that, in general,
$$v(t) = 10^q - a \tag{15}$$

$$\text{where} \quad q = 10^b \cdot t^c$$

and, following Cameron[10], $a = 0.6$

The viscosity η is obtained by multiplying the kinematic viscosity by the density, viz.

$$\eta = v \cdot d \tag{16}$$

For the calculation of the pressure-viscosity coefficient the data and formulations of Jones, Johnson, Winer, and Sanborn[11] were used. To make maximum use of the available experimental data, i.e. the viscosities, a viscosity-pressure index Z was chosen from this report by linear interpolation for the chemical types composing our fluids. The Z values are quite characteristic of chemical type and are nearly independent of temperature or vary very little about a temperature in the middle between t_1 and t_2. The slope of the tangent to $\log \eta$ as a function of pressure at atmospheric pressure, designated as α_{ot}, can be calculated from Z and η_o, the viscosity at ambient pressure,

$$\log \alpha_{ot} = \log Z + H_o - 2.9388 \tag{17}$$

where

$$H_o = \log (\log \eta_o + 1.2) \tag{18}$$

The so-called "reciprocal asymptotic isoviscous pressure α^* takes into account all variations of viscosity with pressure over the entire pressure range and it is therefore the least

16

dependent of all the (pressure-viscosity) parameters on measurement techniques"[11]. However, in the absence of experimental data on viscosity at elevated pressures it is also very difficult to evaluate. Therefore α_{ot} is believed to be a better choice of pressure-viscosity coefficient under our circumstances.

The relations of this section have been incorporated into a (Fortran IV) computer program. Because the measured viscosities and some of the empirical equations employ the customary cgs system of units, a number of statements were introduced into the program to translate them into S.I. units.

Tables I, II, and III contain the fundamental data used in the computer calculations. Tables IV provide the film thicknesses h for all the four fluids as a function of Hertzian inlet temperature. As mentioned previously, the temperature registered by our thermocouple next to the diamond window was considered to be this temperature. Indeed, part of the diamond window, about 10% of its area, is in the contact region, but its contribution to the overall temperature measured should be small, especially in view of the excellent thermal conductivity of diamond. If the temperature registered by the thermocouple near the ball were taken as the inlet temperature, the thicknesses h would come out to be appreciably higher. Our fluid film temperatures would then come out lower, for we would attribute the radiant power measured to a larger radiating volume. All this uncertainty will be removed when measured film thicknesses will become available to us.

4.3 REDUCTION OF EMISSION SPECTRAL DATA TO TEMPERATURES

The procedures for obtaining film and ball surface temperatures will now be detailed. For the reasons discussed in Section 2, the film temperatures were based on the intensities of the 700 cm^{-1} band of polymethylstyrene. The ball surface temperatures were based on the spectral responses at 660 and 810 cm^{-1}. At these frequencies the fluids have no infrared bands so that the responses are entirely graybody.

For the following discussions, two definitions are needed:

(i) Spectral response, r, is defined at a wavenumber, ν, as the fraction of the maximum signal -- assigned a value of unity -- (which almost invariably occurred at the same frequency recorded between 630 and 930 cm^{-1}) multiplied by (a) the greatest unnormalized amplitude computed in our standard way and (b) the amplifier gain factor.

(ii) Band strength, P, is defined as the base line band area measured in a spectrum in units of spectral response times wavenumber.

17

The procedure of drawing baselines is admittedly arbitrary, but with consistent criteria it is quite reproducible. In our case, we drew average lines on both sides of the band to be measured in such a way that they would meet near the wavenumber of the band peak. Often a shoulder in the band contour indicated the location of the baseline quite naturally Our procedure is illustrated by the baselines drawn in Figure 7.

4.3.1 Ball Surface Temperatures

Simple calibration experiments are sufficient to determine the ball surface temperatures from the spectra in all cases. All that was needed experimentally was to record spectra under our standard conditions for the stationary ball while the fluid in the cup was kept at a constant elevated temperature by circulating warm water through the coil. Figures 10 and 11 show the spectral responses for our three standard restrictors. All these curves, which are very similar, are straight lines within our limits of error ($\pm 2°$). They cross zero near 38°C; at this temperature the ball surface happens to send the same radiant flux to the detector as the chopper blade.

From these curves and corresponding spectral responses for the EHD runs, ball surface temperatures could be estimated to within $\pm 2°C$.

4.3.2 Fluid Film Temperature

An attempt was made to obtain the necessary calibrations from contact region spectra at zero rotational speed in a way analogous to the calibrations for the ball temperature. For this purpose the ball was held in the fluid-filled cup in such a way above the diamond window as to just make contact. Under these conditions the film thickness was taken as the distance between the circumference of the ball and its tangent, the flat plate formed by the diamond window, averaged over the diameter of the instrument's field of view. However, this idea failed when it proved to be impossible to locate the ball at the precise tangent position. Accordingly a high-pressure diamond anvil cell was aligned in place of the ball/plate apparatus and emission spectra were recorded under known conditions. The interferometer was not changed for these measurements except for substitution of restrictors; in particular, the diaphragm in the cell compartment was left unaltered. Since it is impossible to measure fluid films in the diamond cell of thicknesses comparable to those encountered in EHD experiments, emission spectra were obtained with a 25 μm spacer for a 10% solution of polymethylstyrene in one of the test fluids. The 700 cm^{-1} base line band areas were measured as shown in Figure 7 and converted to band strengths, P^D_{700}. These P^D_{700}'s were found to be a function of the temperature according to the empirical equation.

$$P^D_{700} = ae^{bt} \tag{19}$$

where a and b are empirical constants (a=0.2627, b=0.0668) and t is the temperature. It turned out, as expected, that the plots were almost independent of restrictor size. Absorption spectra were also obtained under analogous conditions and a mean absorption coefficient of k = 2000 cm^{-1} was determined for the 700 cm^{-1} band area. The emissivity for the diamond cell was calculated according to Eq. (8), using a reflectivity of R_1=0.04432 for the diamond/fluid interface. This value was computed from the Fresnel equation[12] for normal incidence using n = 2.23 for the refractive index of diamond at 700 cm^{-1} and n=1.5 for the mean refractive index of the fluids in the temperature range considered.

Emissivities for the fluid films in the contact region were calculated by Eq. (5) for the same polymethylstyrene band at 700 cm^{-1} for a range of thicknesses h. For the reflectivity of the metal/fluid interface Winer's value of R_2=0.72 was chosen while the same value of R_1=0.04432 was used for the diamond/fluid interface as before for the diamond cell. A table of E_F/E_D versus h was computed. With the help of this table E_F/E_D values corresponding to any experimental film thickness could be found which, when divided into the experimental bandstrengths P_{700}, would yield P^D_{700} bandstrengths, i.e. bandstrengths for the diamond cell equivalent to those observed from the contact region. The empirical equation, Eq. (19) in the tabular form was then used to calculate average film temperatures.

It should be noted that the h used in Eq. (19) was only one-third of the actual (computed) film thickness. The reason is, of course, that the polymethylstyrene diluent responsible for the 700 cm^{-1} band was present in a dilution of one-third. Furthermore, it was noted that changes in R_1 even as great of a factor of two would not affect the ratio E_F/E_D very much. Thus temperature variations and even anomalous dispersion of refractive index would not seem to be important. This advantage is, of course, based on our use of the same diluent for all the fluids.

5. EXPERIMENTAL CONDITIONS

5.1 INTERFEROMETER SETTINGS

Since the EHD contact region is an extremely weak radiation source, the operating conditions of the interferometer were selected with great care and kept constant throughout this work. The amplifier time constant was 1.25 seconds corresponding to a bandwidth of 0.1 Hz, and the retardation rate (twice the speed of the movable interferometer mirror) was about 1 μm/s. About 1000 samples were read per run, at retardation intervals of 4 μm, so that the time per run was about 20 minutes. The maximum optical path difference from the position of stationary

19

phase was only about 1000 points x 4 μm/point or 4000 μm = 4 mm, corresponding to a theoretical resolution (the reciprocal of this value) of 2.5 cm^{-1}. However, by the technique of "zero filling" (assuming zero readings for sampling points beyond the actual range of mirror travel), which we used to the fullest possible extent, one can gain about a factor of two in effective resolution at the expense of higher computer cost -- as we showed some time ago[13] and as Griffith recently confirmed[14] -- so that we estimate our resolution of bands in the spectra to be about 1 cm^{-1}. Our spectra were calculated at 0.6 cm^{-1} intervals; however, a shift in band peak position of less than 1 cm^{-1} is probably not significant. No apodization function was used and every spectrum was truncated ("boxcar" method) at precisely the same number of points to maintain the same resolution throughout this work. The uniformity of resolution thus achieved makes it possible to compare band intensities of different runs. Only the 630 to 930 cm^{-1} spectral region was calculated and plotted. Extensive mathematical filtering was employed.

Our balance of spectral resolution and running time proved to be a good compromise for this study. Instrumentation now under construction should permit improvement of both factors.

The amplifier gain was set at 30 or 40 db. The Ithaco 391A amplifier permitted zero suppression by 1000%, which was essential, especially for recording inverted interferograms. Under these conditions the 700 cm^{-1} band could still be measured reasonably well in films 0.1 μm thick (or 0.03 μm in terms of polymethylstyrene alone) at temperatures as low as 300°K. A thickness of 0.03 μm (or 300 Å) corresponds to only about ten molecular diameters. The (10-20% of the actual film thickness in this case). Gribov[15] estimated the band intensity of the 1100 cm^{-1} C-F band to be about ten times that of the 700 cm^{-1} aromatic band and that of the 1700 cm^{-1} C=O band to be about 20 times that. The blackbody spectral radiance at 300 to 350°K does not change appreciably between 700 and 1700 cm^{-1}. A 100 Å layer of a C=O containing molecule, e.g. an ester or a carboxylic acid salt should, therefore, be detectable with our interferometer and detector (provided the wavelength range is extended)!

5.2 BALL/PLATE PARAMETERS. GENERAL COMMENTS

Table III lists the experimental conditions used for the four fluids. Three rotational speeds, loads, and bath temperatures were used to make the results representative of actual bearing conditions within the constraints of our apparatus. The bath temperatures are those of the circulating water reservoir, not those of the fluid reservoir. As explained earlier, the fluid temperatures were monitored by three thermocouples, one at the diamond window (t_D, assumed representative of the inlet temperature), one at the ball surface (t_B) and one at a quiescent spot in the cup. Temperature t_B was considered to be most representative of the bulk fluid temperature. Space limitations in the fluid cup (the cooling coil could not be

20

changed) made it impossible to keep the fluid temperatures precisely constant under the various load and speed conditions. At least 27 experiments were, therefore, run per fluid. For one of the fluids, however, Fluid No. 2 (ester) (Table I), every experiment was repeated with each of the three restrictors in the reference beam to observe their relevance, for a total of at least 81 experiments. As a result of this work only one of the three restrictors was used for a particular t_B range, viz. the 0.75 in. size for t_B <30°C, 1.00 in. for 30°C <t_B<40°C, and 1.5" for t_B>40°C, and only the spectra corresponding to this decision were evaluated further. Duplicates were also run when necessary. In addition, there were the calibration runs. The results analyzed in the following section therefore derive from more than 250 valid spectra, which took at least 500 hours just to collect, to compute and to plot. No valid spectrum could be obtained unless all the fluid temperatures monitored by the thermocouples were kept constant for half an hour to within about 0.2°C. These estimates do not take into account the necessary cleaning times and the inevitable equipment maintenance and down times.

We do not believe that a different interferometer would have reduced the time needed for our experiments by a significant amount since weak radiation sources can be measured properly only in long observation times and a large fraction of the working time was consumed in reaching steady operating conditions[16].

Figures 12 to 14 show representative spectra for the "most typical" fluid, Fluid No. 1 (naphthenic mineral oil) of Table I. This fluid came out to be near average in the subsequent temperature analyses. All the spectra were obtained for the middle bath temperature. Restrictors were different for them, depending on the criteria just stated. The effects of pressure and velocity changes on the 700 and 760 cm^{-1} bands are illustrated. Since all the spectra were normalized, only relative band strengths can be compared. Evidently both emission bands are well-defined, but only the strength of the 700 cm^{-1} was used for film temperature determination. Variations of intensity ratio between the two bands are undoubtedly significant and will be subjected to further study. They are briefly discussed in a following section.

Since film thickness enters into the expressions for film temperature (t_F) the sensitivity of the latter to errors of film thickness (h) is important. Fortunately the influence of h on t_F in our range of t and h is not very great. A 10% error in h corresponds to an error of less than 2°C near 80°C film temperature. Estimating h too high produces an estimate of t which is too low.

6. RESULTS

6.1 CONTACT REGION TEMPERATURES

This report concentrates on fluid film and ball surface emission temperatures from the contact region as they were

obtained from the infrared emission spectra. These temperatures
as well as other measured parameters such as the temperature
at the diamond window, are listed for every fluid in Table IV
with the operating parameters such as film thicknesses, emission
band strengths, the temperatures of the water bath supplying
cooling water for the coil immersed in the test fluid surrounding
the ball/plate contact, the ball speeds and loads. From the
measured parameters temperature differences and shear velocities
were calculated and these are also shown in Table IV. These
temperatures and temperature differences are defined as follows:

t_F = fluid film temperature in °C, derived from
infrared spectra

t_D = diamond window temperature in °C, also con-
sidered as the Hertzian inlet temperature,
measured by a thermocouple at the window

t_B = bulk fluid temperature in °C, measured by a
thermocouple.

t_M = ball surface temperature in °C, derived from
infrared spectra

From these definitions, the following temperature differences
are derived:

$$\Delta t_1 = t_F - t_D$$

$$\Delta t_2 = t_M - t_D$$

$$\Delta t_3 = t_D - t_B$$

$$\Delta t_4 = t_F - t_M$$

Figure 15 shows these quantities graphically.

The data of Tables IV constitute the main experimental
data of this report. The emissivity ratios, E_F/E_D, for the
fluid films in the contact region compared to fluid layers in
the diamond anvil cell used for the temperature calibration
are listed for completeness to make it possible to check the
calculations in particular instances.

When comparing results for the different fluids listed in
Tables IV, the reader should be aware that the three temperature
ranges (water bath temperatures controlling the cooling in the
fluid cup and thereby the fluid viscosity ranges) were not the
same for all the fluids, although at least two temperatures
overlapped. Thus, for example, the water bath temperatures for
Fluid #1 (Naphthenic Mineral Oil) were 0, 15 and 28°C, but they
were 0, 15, and 40°C for Fluid #2 (Ester). The reason for this

22

inconsistency is our original plan for four temperature ranges which had to be abandoned for lack of time. It is, therefore, not possible to average all the data to compare the fluids, but it is possible to average them for a particular bath temperature, since the other parameters, load and speed, were the same. Such averages were calculated in Table V.

To facilitate comparisons between the fluids, all the temperature data as well as the averages for the temperature ranges were plotted versus shear rate separately for the individual fluids and for all fluids on one plot in Figures 16 to 40. The tables and plots will now be discussed.

6.1.1 Diamond Temperature (t_D) versus Shear Rate

These temperatures were continuously recorded during every experiment. As soon as speed and loads were changed with any fluid, a new diamond temperature was established almost immediately (within seconds). These temperatures were found to be very characteristic of a given fluid. Figures 16-19 show that the diamond temperatures (t_D) increased with shear rate (U/h) for all fluids in a near-linear fashion. A slight decrease of slope is noticeable for the highest shear rates. Fluid #3 (Synthetic Paraffin) exhibits the steepest slope and it is also the most viscous of all the fluids and has the highest film thicknesses (h). The slopes are essentially the same for all the other fluids, but the temperatures (t_D) are generally higher for Fluid #4 (Traction Fluid).

Since the diamond temperatures (t_D) were considered to be the inlet temperatures and thus our reference levels, the relations just noted should be kept in mind for the following discussions.

6.1.2 Diamond Temperature Rise (Δt_3) versus Shear Rate, Speed and Load

The difference between the bulk fluid temperature and the diamond temperature (Δt_3) was plotted against shear rate in Figures 20-24. This temperature difference was thought to be a measure of the balance between the energy input represented by the shear rate and the energy removal, primarily by the cooling coil, while the diamond temperature itself (t_D), which was discussed in the preceding section was considered to be a more direct indication of the energy input by itself. Not surprisingly, since the points do represent a balance condition, the scatter of the points is large. The general trend is still for Δt_3 to increase with U/h of the three fluids for which comparable shear rates were possible (all but Fluid #3, the synthetic paraffin). Fluid #4, the traction fluid, had the highest Δt_3. This behavior is also evident by comparing Δt_3 for this fluid at any of the water temperatures in Table V.

The differences between the fluids with respect to Δt_3 are shown in a different way in Figures 25 and 26, containing plots of Δt_3 vs. speed at two constant loads and vs. load at two constant speeds for all fluids at 0°C water bath temperature.

In all cases the sequence of the Δt_3's remains the same, with the highest values for Fluid #4 (Traction Fluid) and the lowest for Fluid #3 (Synthetic Paraffin). All the plots for Fluid #4 are essentially straight lines of positive slope, while those for the other fluids have diminishing slopes for the higher loads or speeds. The Δt_3's for Fluid #1 (Naphthenic Hydrocarbon Oil) and even more so for Fluid #2 (Ester) exhibit negative slopes for increasing speeds at the (low) 11 kg load. Evidently cooling due to increased ball speed becomes more important there for these fluids than heating by viscous shear in the fluid film, but for Fluid #4 the heat input always easily overcomes the losses.

6.1.3 Ball Surface Temperature Rise (Δt_2) versus Shear Rate

It may appear surprising that the ball surface temperature t_M was nearly always lower than the diamond temperature t_D ($\Delta t_2 = t_M - t_D < 0$). For it will be recalled that t_D is not the temperature of the diamond surface at the contact -- which could conceivably be just below the high fluid film temperature but more nearly an average temperature of the diamond window, since diamond is a most excellent heat conductor and the contact area, as mentioned, is only a small portion of the total diamond face. Indeed, t_D is likely to be even less than the average window temperature because the thermocouple junction measuring it is located in the mounting cement rather than in the window itself. On the other hand, t_M is measured by radiation from the Hertzian area only. The explanation seems clear from the general tendency of Δt_2 to decrease with increasing shear rate (Figures 27-31). At high shear rates, cooling of the ball surface by the reservoir fluid is more efficient than heating by the sheared fluid. Note that the averaged Δt_2 increases with shear rate (Figure 31) for Fluid #3 (Synthetic Paraffin).

The slopes of the Δt_2 vs. U/h curves for the different fluids are also suggestive. Fluid #3 (Synthetic Paraffin) has the highest viscosity, the lowest density (Table I) and the lowest thermal conductivity of the fluids and it shows the largest decrease of Δt_2 with increasing shear rate. Fluid #2 (Ester) has the highest density and thermal conductivity and it shows the least change of Δt_2 with shear rate. Again the heat transfer mechanism is indicated.

6.1.4 Film Temperature Rise (Δt_1 and Δt_4) versus Shear Rate

In Figures 32-36, the difference between the film temperature t_F and the diamond temperature t_D (considered the Hertzian inlet temperature) and in Figures 37-41 the difference between the film temperature t_F and the metal surface temperature t_M were plotted against shear rate (Δt_1 and Δt_4 respectively). All these temperature differences are positive, showing that heat is generated in the fluid film as it passes the contact region. In some instances the trends are toward larger Δt_1 or Δt_4 with increasing shear rate, in others the trends are opposite.

24

Such opposing trends were noted even for the same fluid, depending on the operating conditions.

Figures 42 & 43 show that all the separate plots can be put on common curves, one for Δt_1 vs. U/h, the other for Δt_4 vs. U/h. The scatter of the points is large, especially toward the high shear rates -- where the film thicknesses are very small -- but the general shapes of the curves are clear. They are parabolas with apices corresponding to a shear rate near 6×10^6 sec^{-1} for maximum Δt_1 and Δt_4. Evidently our experimental conditions were such that the balance of heat generated by shear in the fluid and heat lost through the solid surfaces was maintained there at the highest temperature.

The result that common curves of Δt_1 or Δt_4 vs. U/h (Mr. William R. Jones, Jr., of NASA-Lewis, suggested this type of plot) can be drawn for all the fluids does not mean that the nature of the fluid is unimportant. It was shown in the preceding sections that the absolute values of t_D were quite different for the fluids and, in particular, highest for Fluid #4 (Traction Fluid). However, the physical phenomena are certainly the same for all the fluids.

6.2 BAND STRENGTH RATIOS

Comparison of the spectra shown in Figures 12 to 14 is a good starting point for an analysis of the state of the fluid in the contact zone. The bands peaking near 700 and 760 cm^{-1} are the only ones concerning us now. The base lines have been drawn in so that relative band strengths can be compared at a glance. As a preliminary aside it will be noted that the spectrum for the lowest load (11 kg) and speed (240 RPM) is inverted: Radiation flux from this film was effectively less than radiation from the chopper blade. However, closer examination will reveal that in this spectrum the intensity of the 760 cm^{-1} band exceeded that of the 700 cm^{-1} band. When the load is further increased to 19.5 kg at the same speed, the corresponding spectrum shows the band strengths to be about equal and when the load is further increased to 28.5 kg, the strength of the 700 cm^{-1} band is relatively greater. Equal band strength is shown for the other spectra at 11 kg load.

Corresponding comparisons for the other fluids also show trends. A detailed analysis of the band strength ratios is not yet completed.

One reason for the relative band strength changes can be film thickness changes. The absorption coefficients for the two bands are different. If this were the only reason, film thicknesses could be directly determined from the band ratios. The largest thickness changes occur, however, for changes of speed and not load, hence the trend mentioned for the 11 kg series is likely to have another reason.

An intriguing possibility is improved molecular alignment in the contact with increasing load. If the direction of the change in dipole moment, which produces the band, is thereby turned into the plane of the ball surface, the band intensity should go up. Changes of bandwidth and structure could correlate with such a picture. Infrared polarization spectra would be useful to have to substantiate this mechanism, if possible.

Evidently more work is needed in this area.

7. DISCUSSION

The pattern shown by the data is consistent with a mechanism in which heat is generated by shearing of the fluid in the contact region and removed by the solid surfaces and cooling in the reservoir. Especially Figures 37-41 are instructive; the differences between the fluid film and ball or diamond surface temperatures fall on common curves when plotted against shear rate. Figure 44 and Tables VI and VII permit a quick overview of all the trends.

A very interesting finding is the high average Δt_1 and especially Δt_3 (diamond temperature increase above ambient fluid temperature) for Fluid #4 (Traction Fluid), which is very clearly shown in Figure 24, in which average Δt_3 is plotted against shear rate. That high traction would generate more heat is, on reflection, not unexpected, but the occurrence of the phenomenon even in our diluted fluid was surprising. Since shear rate already takes film thickness -- and hence a measure of viscosity -- into account, a factor besides viscosity must be responsible.

One way to explain traction and some of these phenomena might be that discussed by Johnson[17], viz. solid grains are formed in the inlet zone as the fluid becomes highly compressed. The grains are then pushed into the contact where they are already beginning to relax. This picture is consistent with heat generation in the inlet zone. However, no real evidence of solidification has emerged from our spectra (although our analysis is still incomplete). Another way would be analogous to that applied under certain conditions to polyphenyl ether by Hirst, et al[18], viz. the fluid becomes "elastic" under stress. By this mechanism the heat generated in the inlet zone is caused by the squeezing out of a film in a preferred direction and bunching is likely to occur in the outlet zone. The film in the contact zone is thinner than predicted from the viscosity relations; indeed, viscosity has lost much of its meaning. Such a model would be consistent with the observed band intensity ratio changes under increased load. Our work planned for the near future includes testing for polarization effects in the contact emission spectra; if observed, for Fluid 4 in particular, they might lead to a preferred model. On the other hand, the ester fluid (Fluid #2) would have less orientation in the bulk of the contact area, because its affinity for the metal surfaces makes for easier flow.

26

Band intensity ratios, especially if caused by polarization in the contact region might also be correlatable with a model of a flow of "sticks" within a flow of spheres. As long as the sticks are aligned in the direction of flow, their "viscosity", if you will, is low, but crosswise they are difficult to move. As the bundles move down the Hertzian region, their alignment changes. Our projected spatially resolved spectra of the region might clarify these ideas.

In any case, the film thickness measurements planned for the immediate future might have a very important bearing on the direction of our future work.

A preliminary comparison between our temperatures and those calculated and experimentally inferred by A. W. Crook[19] was made. Considering the differences of technique, the discrepancies are not bad. Crook's assumptions for energy balance in the contact zone were basically (i) all heat generated by viscous friction within the fluid and (ii) all heat lost to the solid surfaces by conduction only. Cameron[20] improved on Crook's equations by substituting more modern and better relations for the viscosity/temperature and viscosity/pressure relationships. His final equation (in our notation)

$$\frac{T_F}{n_F} = U^2 \cdot \frac{M+1}{8K} + \frac{T_M}{n_o} \tag{20}$$

where U is the sliding velocity, m is an adjustable empirical parameter (between 2 and 3) and K the thermal conductivity of the fluid, can be reconciled with our data, at least in a general way. This examination is not complete.

8. CONCLUSIONS

The most important result of this work is the successful demonstration that good infrared emission spectra from fluid films in EHD contact regions can be obtained and that these spectra show differences depending on the operating parameters and on the type of fluid used.

Temperatures of the fluid films and the metal surface in the contact region can be determined from these spectra. For the former temperatures, knowledge of the film thicknesses is also required. Since proper thicknesses were not available, admittedly inadequate values calculated from low shear viscosities were used and the resulting temperatures still came out reasonable. They are always higher than the metal surface temperatures, depend on the nature of the fluid and vary with the operational parameters in a consistent manner.

27

One mechanism of heat generation and loss appears to obtain for all the fluids -- one plot of film temperature rise against shear rate can generally accommodate all the fluids. However, the base level, i.e. the diamond temperature (or the inlet temperature by our assumptions) was significantly higher for one of the fluids (Traction Fluid).

Work is underway on a unifying model to reconcile the temperature variations.

Infrared spectroscopy is likely to become a very valuable tool for EHD studies. In the present work EHD conditions likely to cause failure were diligently avoided, since the emphasis was on laying the groundwork. However, the principal advantage of the technique is its sensitivity to chemical and structural changes of the fluid molecules. Since the EHD films are so thin, we established that the time scale of the experiments is adequate to observe new chemical entities even if they are formed on the solid boundaries and have to diffuse from there. Much of our future effort will be in this area. Immediate targets will also include spatially resolved spectra of traverses of the Hertzian region and the determination of molecular orientation in contacts from band intensity ratios and polarized infrared spectra.

28

APPENDIX A

List of Symbols

A radiation intensity, as defined by Eq. (2)

A' radiation intensity defined by Eq. (3)

B radiation intensity, as defined by Eq. (2)

$B_F = I_B(t_F)$ blackbody radiance at fluid film temperature t_F

$B_M = I_B(t_M)$ blackbody radiance at metal surface temperature t_M

$C_2 = 0.014388$ mK   radiation constant

E_1 Young's modulus of steel

E_2 Young's modulus of diamond

E_D emissivity of fluid in diamond anvil cell

$E_F(eff)$ effective fluid film emissivity

$E' = \frac{1}{2} \left[\frac{1-\sigma_1^2}{E_1} + \frac{1-\sigma_2^2}{E_2} \right]$ reduced elastic modulus

H_o quantity defined by Eq. (18)

I monochromatic radiation intensity

$I_B(t)$ blackbody radiation intensity at temperature t and wave-number υ

I^+eff radiation intensity defined by Eq. (4)

$I^+(y)$ monochromatic radiation intensity in the forward direction

$I^-(y)$ monochromatic radiation intensity in the backward direction

P_{700} film band intensity at 700 cm^{-1}

P^D_{700} fluid band intensity at 700 cm^{-1} measured in diamond cell

List of Symbols (Cont'd)

R	ball radius, generally the reduced radius of contact
R_1	monochromatic reflectivity at fluid/diamond interface
R_2	monochromatic reflectivity at fluid/ball interface
$T = \exp(-kh)$	fluid transmittance at wavenumber ν
Z	viscosity /pressure index
a	empirical constant in Eq. (12)
a	empirical constant in Eq. (19)
b	empirical constant in Eq. (12)
b	empirical constant in Eq. (19)
c	empirical constant in Eq. (12)
d(t)	fluid density at temperature t
h	fluid film thickness
k	spectral absorption coefficient at wavenumber ν and temperature t
q	quantity defined by Eq. (15)
t	temperature in °C
t_F	fluid film temperature in °C
t_M	metal surface temperature in °C
u	combined surface velocity at contact
w	load on the bearing contact
y	coordinate in the direction of radiation propagation
α	pressure coefficient of viscosity
α^*	reciprocal asymptotic isoviscous pressure
α_{ot}	slope of tangent to log η as a function of pressure

List of Symbols (Cont'd)

η	absolute viscosity
λ	wavelength
$\nu(t)$	kinematic viscosity
σ_1	Poisson ratio of steel constituting the ball
σ_2	Poisson ratio of diamond

Fluid	Density			Kinematic Viscosity		Absolute Viscosity		Viscosity-Pressure Index
	20°	38°C	99°C	38°C	99°C	38°C	99°C	Z
				centistokes		N.sec/m^2		dimensionless
	kg/m^3	kg/m^3	kg/m^3					
Diluted Naphthenic Mineral Oil (N-1)	952.8	941.1	901.4	43.9	4.77	.0413	.00430	0.63
Diluted Pentaerythritol Ester	997.3	985.6	945.9	42.2	6.01	.0416	.00568	0.50
Diluted Synthetic Paraffin	904.0	892.3	852.6	291.1	24.4	.2597	.02080	0.48
Diluted Cycloaliphatic Traction Fluid	925.2	913.4	873.7	48.2	5.31	.0440	.00463	0.72

TABLE 11

Mechanical Constants of Ball and Window

	Young's Modulus N/m^2	Poisson's Ratio	Radius m
Ball (440 C Steel)	0.200×10^{12}	0.29	0.0286
Diamond	1.05×10^{12}	0.177	∞
Reduced Elastic Modulus	0.364×10^{12}		

$$\frac{2}{E'} = \frac{1-\sigma_1^2}{E_1} + \frac{1-\sigma_2^2}{E_2}$$

TABLE III

Operating Parameters

Loads		Hertzian Radius m	Average Hertzian Pressure N/m^2	Max. Hertzian Pressure N/m^2
kg	N			
11.0	107.9	2.334×10^{-4}	6.301×10^8	0.9451×10^9
19.5	191.2	2.825×10^{-4}	7.626×10^8	1.1439×10^9
28.5	279.4	3.206×10^{-4}	8.654×10^8	1.2980×10^9

TABLE IVa

Experimental and Calculated Data

Fluid #1 (Diluted Naphthenic Mineral Oil (N-1))

Water Temp C	Load kg	Speed RPM	t_B °C	t_D °C	t_M °C	P_{700}	E_{F/E_D}	t_P °C	μ^h_m	U/h (sec^{-1}).10^6	Δt_1 t_P-t_D °C	Δt_2 t_M-t_D °C	Δt_3 t_P-t_B °C	Δt_4 t_P-t_M °C
0	11	240	26.5	35.5	35.8	2.99	.065	77.3	0.225	·3.2	41.8	0.3	9.0	41.5
		360	26.5	34.0	32.6	4.14	.096	76.3	0.332	3.3	42.3	-1.4	7.5	43.7
		480	26.5	34.5	30.2	3.43	.111	71.3	0.388	3.7	46.8	-4.3	8.0	41.1
	19.5	240	28.5	40.0	38.2	6.03	.052	91.1	0.181	4.0	51.1	-1.8	11.5	52.9
		360	30.5	46.0	35.3	5.41	.054	88.9	0.187	5.8	42.9	-10.7	15.5	53.6
		480	33.5	48.5	39.0	8.88	.059	95.0	0.203	7.1	46.5	-9.5	15.0	56.0
	28.5	240	31	45	39.3	6.61	.042	95.7	0.143	5.0	50.7	-5.7	14.0	56.4
		360	34.3	51.5	40.0	7.11	.042	96.8	0.145	7.4	45.3	-11.5	17.2	56.8
		480	37.5	55.5	44.7	8.48	.044	98.7	0.153	9.4	43.2	-10.8	18.0	54.0
15	11	240	29.5	37	35.6	1.97	.062	74.3	0.214	3.4	37.3	-1.4	7.5	38.7
		360	30.5	41	38.9	5.00	.068	84.3	0.238	4.5	43.3	-2.1	10.5	45.4
		480	32	44	37.3	8.16	.074	90.4	0.256	5.6	46.4	-6.7	12.0	53.1
	19.5	240	32.5	43	36.0	6.58	.046	94.3	0.159	4.5	51.3	-7.0	10.5	58.3
		360	34.5	48	41.3	9.50	.050	98.5	0.172	6.3	50.5	-6.7	13.5	57.2
		480	37.0	52	43.0	10.48	.052	99.2	0.181	8.0	47.2	-9.0	15.0	56.2
	28.5	240	36	48	42.0	8.40	.037	101.0	0.127	5.7	53.0	-6.0	12.0	59.0
		360	38.5	54	46.6	6.27	.039	96.0	0.134	8.1	42.0	-7.4	15.5	49.4
		480	40.5	59	50.4	9.56	.040	101.8	0.138	10.4	42.8	-8.6	18.5	61.4
28	11	240	37	44	42.2	5.96	.045	93.1	0.156	4.6	49.1	-1.8	7.5	50.9
		360	38	48	46.6	10.65	.051	99.8	0.177	6.1	51.8	-1.4	10.0	53.2
		480	38.5	50.5	48.4	6.45	.056	91.0	0.193	7.5	40.5	-2.1	12.0	42.6
	19.5	240	41	50	49.0	5.67	.035	96.1	0.119	6.1	46.1	-1.0	9.0	47.1
		360	43	55	50.7	6.65	.038	97.3	0.132	8.2	42.3	-4.3	12.0	46.6
		480	43.5	58	54.6	9.78	.042	101.9	0.145	9.9	43.9	-3.4	14.5	47.3
	28.5	240	44.5	56	55.3	6.29	.027	101.3	0.093	7.7	45.3	·-0.7	11.5	46.0
		360	47	62	59.6	8.22	.030	104.1	0.101	10.7	42.1	-2.4	15.0	44.5
		480	48	65	61.5	6.07	.033	98.0	0.113	12.7	33.0	-3.5	17.0	36.5

TABLE IVb

Experimental and Calculated Data

Fluid #2 (Diluted Pentaerythritol Ester)

Water Temp °C	Load kg	Speed RPM	t_B °C	t_D °C	t_M °C	P_{700}	E_F/E_D	t_F °C	μ_m^h	U/h (sec^{-1}).10^6	Δt_1 t_F-t_D °C	Δt_2 t_M-t_D °C	Δt_3 t_D-t_B °C	Δt_4 t_F-t_M °C
0	11	240	21	26.5	26.8	.90	.080	56.3	.278	2.6	29.8	0.3	5.5	29.5
		360	21	26	25.3	1.08	.111	54.0	.389	2.8	28.0	-0.7	5	28.7
		480	22	26.5	23.2	1.53	.130	56.9	.457	3.2	30.4	-3.3	4.5	33.7
	19.5	240	23.5	34	33.9	3.27	.057	80.6	.199	3.6	43.6	-0.1	10.5	46.7
		360	24.5	35	30.0	2.72	.074	73.9	.256	4.2	38.9	-5	10.5	43.9
		480	26	36	33.3	3.01	.086	73.2	.301	4.8	37.2	-2.7	10	39.9
	28.5	240	26	40	37.5	4.84	.044	90.3	.154	4.7	50.3	-2.5	14	52.8
		360	28	45	39.2	2.49	.050	78.5	.171	6.3	33.5	-5.8	17	39.3
		480	29.5	46	41.4	3.76	.059	82.2	.203	7.1	36.2	-4.6	16.5	40.8
15	11	240	31.5	38	36.8	7.40	.050	94.8	.174	4.1	56.8	-1.2	6.5	58.0
		360	32.5	45	42.8	6.50	.052	92.2	.179	6.0	47.2	-2.2	12.5	49.4
		480	35.5	43	42.0	12.25	.068	97.7	.237	6.1	54.7	-1	7.5	55.7
	19.5	240	35	46	45.0	4.27	.037	91.0	.126	5.7	45.0	-1	11	46.0
		360	34.5	46.5	40.3	9.37	.047	99.2	.162	6.7	52.7	-6.2	12	58.9
		480	35.5	48.5	43.0	10.64	.054	99.0	.186	7.7	50.5	-5.5	13	56.0
	28.5	240	38.5	52.5	50.1	6.96	.029	101.9	.098	7.3	49.4	-2.4	14	51.8
		360	39	55	47.6	7.41	.036	99.7	.122	8.9	44.7	-7.4	16	52.1
		480	38	55	51.2	9.60	.044	100.6	.150	9.6	45.6	-3.8	17	49.4
40	11	240	45	50	57.6	3.30	.033	88.9	.113	6.4	38.9	7.6	5	31.3
		360	45	52	55.6	4.17	.041	89.2	.141	7.7	37.2	3.6	7	33.6
		480	46	54	60.7	4.13	.047	87.0	.162	8.9	33.0	6.7	8	26.3
	19.5	240	45	55	45.8	0.88	.027	72.1	.093	7.7	17.1	-9.2	10	26.3
		360	46.5	58.5	63.9	4.13	.032	92.7	.110	9.8	34.2	5.4	12	28.8
		480	46	59.5	62.3	4.65	.038	91.9	.131	11.0	48.4	2.8	13.5	29.6
	28.5	240	47	60	58.9	3.26	.023	94.1	.079	9.1	34.1	-1.1	13	35.2
		360	46	62.5	62.0	5.20	.028	98.2	.096	11.3	35.7	-0.5	16.5	36.2
		480	46.5	65	65.7	1.71	.032	79.5	.112	12.9	14.5	0.7	18.5	13.8

TABLE IVc

Experimental and Calculated Data

Fluid #3 (Diluted Synthetic Paraffin)

Water Temp °C	Load kg	Speed RPM	t_B °C	t_D °C	t_M °C	P_{700}	E_{P/E_D}	t_P °C	$\lambda \frac{h}{m}$	U/h $(sec^{-1}).10^6$	Δt_1 $t_P - t_D$ °C	Δt_2 $t_M - t_D$ °C	Δt_3 $t_D - t_B$ °C	Δt_4 $t_P - t_M$ °C
0	11	240	23.5	27	30.3	1.05	.351	36.4	1.301	0.6	9.4	3.3	3.5	6.1
		360	24	28	32.3	2.06	.434	43.2	1.648	0.7	15.2	4.3	4	10.9
		480	24	28.5	30.9	2.85	.498	46.0	1.920	0.8	17.5	2.4	4.5	15.1
	19.5	240	26	32	31.0	4.34	.268	61.7	.975	0.7	29.7	-1	6	30.7
		360	27	34.5	33.2	4.55	.306	60.4	1.123	1.0	25.9	-1.3	7.5	27.2
		480	29	37.5	34.5	5.59	.424	62.7	1.195	1.2	25.2	-3	8.5	28.2
	28.5	240	33.5	43	33.5	5.35	.161	72.4	.570	1.3	29.4	-9.5	9.5	38.9
		360	35	50	38.5	7.58	.160	77.7	.566	1.9	27.7	-11.5	15	39.2
		480	36.5	49.5	38.7	4.02	.195	65.3	.695	2.1	15.8	-10.8	13	26.6
17	11	240	30.0	34	35.9	2.02	.250	51.3	.907	0.8	17.3	1.9	4	15.4
		360	30	35	34.0	5.01	.314	61.5	1.154	0.9	26.5	-1	5	27.5
		480	31.5	36	34.7	5.23	.363	59.9	1.350	1.1	23.9	-1.3	4.5	25.2
	19.5	240	33.5	41	37.2	3.16	.178	63.1	.634	1.1	22.1	-3.8	7.5	25.9
		360	34	44.5	39.3	4.02	.199	65.0	.710	1.5	20.5	-5.2	10.5	25.7
		480	35.5	44	39.0	4.67	.252	63.7	.911	1.6	19.7	-5	8.5	36.7
	28.5	240	38.5	48.5	41.8	4.28	.126	72.8	.441	1.6	24.3	-6.7	10	31.0
		360	38.5	54	43.8	3.76	.137	69.5	.483	2.2	15.5	-10.2	15.5	25.7
		480	45	59.5	45.0	3.03	.135	66.5	.474	3.0	7.0	-14.5	14.5	21.5
29	11	240	36.5	40	41.0	2.90	.191	60.7	.682	1.1	20.7	1	3.5	19.7
		360	37.5	43	42.5	5.72	.221	68.7	.796	1.4	25.7	-0.5	5.5	26.2
		480	38.5	44.5	42.6	9.79	.248	80.4	.896	1.6	35.9	-1.9	6	37.8
	19.5	240	42	49	47.4	5.18	.128	75.4	.449	1.6	26.4	-1.6	7	28.0
		360	41.5	52.8	47.8	7.00	.145	78.0	.511	2.1	25.5	-4.7	11	30.2
		480	45	54	45.9	5.97	.170	73.2	.604	2.4	19.2	-8.1	9	27.3
	28.5	240	46	58	46.7	9.07	.090	89.0	.311	2.3	31.0	-11.3	12	42.3
		360	48	62	51.0	11.57	.103	90.6	.359	3.0	28.6	-11	14	39.6
		480	49	64	53.5	9.36	.117	85.6	.411	3.5	21.6	-10.5	15	32.1

TABLE IVd

Experimental and Calculated Data

Fluid #4 (Diluted Sun Traction Fluid)

Water Temp °C	Load kg	Speed RPM	t_B °C	t_D °C	t_M °C	p_{700}	E_{F/E_D}	t_P °C	μ_m^h	U/h $(sec^{-1}).10^6$	Δt_1 t_P-t_D °C	Δt_2 t_H-t_D °C	Δt_3 t_D-t_B °C	Δt_4 t_P-t_M °C
0	11	240	28.5	38	36.0	3.83	.068	80.3	.237	3.0	42.3	-2	9.5	44.3
		360	28.5	41	34.5	7.87	.079	88.8	.277	3.9	47.8	-6.5	12.5	54.3
		480	29.5	44	37.9	3.47	.086	75.3	.299	4.8	31.3	-6.1	14.5	37.4
	19.5	240	31.5	44.5	40.2	9.31	.050	98.2	.170	4.2	53.7	-4.3	13	58.0
		360	35	50.5	43.3	9.40	.052	97.8	.179	6.0	47.3	-7.2	15.5	54.5
		480	36	54	47.6	8.17	.056	94.6	.196	7.3	40.6	-6.4	18	47.0
	28.5	240	34.5	51	41.3	9.36	.038	102.2	.131	5.5	51.2	-9.7	16.5	60.9
		360	38	58.5	46.8	12.85	.038	107.0	.131	8.2	48.5	-11.7	20.5	60.2
		480	41	64	53.3	8.41	.040	100.0	.137	10.5	36.0	-10.7	23	46.7
29	11	240	34.5	46	41.7	3.28	.049	82.9	.167	4.3	36.9	-4.3	11.5	41.2
		360	35	50	48.7	4.71	.056	86.3	.191	5.7	36.3	-1.3	15	37.6
		480	36.5	53.5	52.3	5.13	.058	87.1	.202	7.2	33.6	-1.2	17	37.4
	19.5	240	34	51.5	47.5	2.91	.038	84.9	.129	5.6	33.4	-4.0	17.5	58.5
		360	34.5	56.5	50.1	15.61	.042	108.6	.143	7.6	52.1	-6.4	22	54.7
		480	40	58.5	47.9	12.02	.048	102.6	.164	8.8	44.1	-10.6	18.5	48.3
	28.5	240	38	57	53.9	7.53	.031	102.2	.105	6.9	45.2	-3.1	19	46.5
		360	40	65.6	61.6	11.14	.031	108.1	.105	10.3	42.6	-3.9	25.5	38.3
		480	41	68.5	67.9	11.05	.034	106.2	.117	12.3	37.7	-0.6	27.5	
39	11	240	35.5	44.5	49.8	6.42	.050	92.6	.175	4.1	48.1	5.3	9	42.8
		360	39	51	49.9	10.0	.053	98.4	.184	5.9	47.4	-1.1	12	48.5
		480	37.5	54.5	50.9	4.20	.056	84.6	.194	7.4	30.1	-3.6	17	33.7
	19.5	240	38.5	51	52.3	7.37	.039	98.4	.134	5.4	47.4	1.3	12.5	46.1
		360	39	56	52.8	11.0	.044	102.8	.149	7.2	46.8	-3.2	17	50.0
		480	43	62	64.7	11.88	.044	103.9	.149	9.7	41.9	2.7	19	39.2
	28.5	240	42.5	59	51.7	9.98	.029	97.3	.098	7.3	38.3	-7.3	16.5	45.6
		360	45	66	55.1	12.86	.031	100.2	.105	10.3	34.2	-10.9	21	45.1
		480	45	68	60.3	7.18	.035	99.4	.121	11.9	31.4	-7.7	23	39.1

TABLE V

Film Thicknesses, Shear Rates, Temperatures, and Temperature Differences for the
Four Fluids Averaged over Speeds and Loads

Fluid	Water Temp °C	t_B °C	t_D °C	t_M °C	t_P °C	h μm	U/h $(sec^{-1}).10^6$	Δt_1 $t_F{-}t_D$ °C	Δt_2 $t_M{-}t_D$ °C	Δt_3 $t_D{-}t_B$ °C	Δt_4 $t_F{-}t_M$ °C	h.Δt_3	$\dfrac{\Delta t_1}{(U/h)}$	$\dfrac{\Delta t_4}{(U/h)}$	$\dfrac{\Delta t_2}{(U/h)}$
#1, Diluted Naphthenic Mineral Oil (N-1)	0	30.5	43.4	37.2	87.9	0.217	5.4	44.5	-6.2	12.9	50.7	2.80	8.24	9.39	-1.15
#2, Diluted Pentaerythritol Ester		24.6	35.0	32.3	71.8	0.268	4.4	47.2	-2.7	10.4	39.5	2.79	10.72	8.98	-0.61
#3, Diluted Synthetic Paraffin		28.7	36.7	33.7	58.4	1.110	1.1	21.7	-3 0	8.0	24.7	8.88	19.7	22.5	-2.73
#4, Diluted Sun Traction Fluid		33.6	49.5	42.3	93.8	0.195	5.9	60.2	-7.2	15.9	51.5	3.10	10.15	8.68	-1.21
#1, Diluted Naphthenic Mineral Oil (N-1)	15	34.6	47.3	41.2	93.3	0.180	6.3	46.0	-6.1	12.7	52.1	2.29	7.30	8.27	-0.97
#2, Diluted Pentaerythritol Ester		35.6	47.7	44.3	97.3	0.159	6.9	49.6	-3.4	12.1	53.0	1.92	7.19	7.68	-0.49
#3, Diluted Synthetic Paraffin		35.2	44.1	39.0	63.7	0.785	1.5	19.6	-4.1	8.9	24.7	6.99	13.1	16.5	-2.73
#4, Diluted Sun Traction Fluid		--------------------------------NOT					AVAILABLE--								
#1, Diluted Naphthenic Mineral Oil (N-1)	28	42.3	54.3	52.0	98.1	0.137	8.2	43.8	-2.3	12.0	46.1	1.64	5.34	5.62	-0.28
#2, Diluted Pentaerythritol Ester		-----------------------------------NOT					AVAILABLE--								
#3, Diluted Synthetic Paraffin		42.7	51.9	46.5	78.0	0.558	2.1	26.1	-5.4	9.2	31.5	5.13	12.4	15.0	-2.57
#4, Diluted Sun Traction Fluid		37.1	56.3	54.2	96.5	0.147	7.6	40.2	-2.1	19.2	42.3	2.82	5.29	5.57	-0.28
#1, Diluted Naphthenic Mineral Oil (N-1)	40	--------------------------------------NOT					AVAILABLE---								
#2, Diluted Pentaerythritol Ester		45.9	57.4	59.2	88.2	0.115	9.4	30.8	+1.8	11.5	29.0	1.32	3.28	3.09	0.19
#3, Diluted Synthetic Paraffin		-----------------------------------NOT					AVAILABLE--								
#4, Diluted Sun Traction Fluid		40.6	56.9	54.2	97.5	0.145	7.7	40.6	-2.7	16.3	43.3	2.36	5.27	5.62	-0.35

TABLE VI

Effect of Increases of Speed and Load on Various Δt's[a]

Fluid	Δt_1		Δt_2	t_D or Δt_3	Δt_4		Film Thickness
	Change-1[b]	Change-2[c]	Change-1 or -2	Change-1 or -2	Change-1	Change-2	h
#1 (Naphthenic Mineral Oil)	+-	-	-	+	-	-	Large
	-	-	-	-	+-	-	Medium
	-	-	-	+	+	+-	Small
#2 (Ester)	+	-	-	+	+	-	Large
	-	-	-	+	+-	+-	Medium
	-	-	-	+	+-	+-	Small
#3 (Synthetic Paraffin)	+	-	-	+	+	+-	Large
	-	-	-	+	+-	+-	Medium
	+	-	-	+	+	+-	Small
#4 (Traction)	+	-	-	+	+	-	Large
	+	-	+	+	+-	-	Medium
	-	-	-	+	+	+-	Small

Notes: (a) $\Delta t_1 = t_F - t_D$, $\Delta t_2 = t_M - t_D$, $\Delta t_3 = t_D - t_B$, $\Delta t_4 = t_F - t_M$, where t_F, t_D, t_M, and t_B are the

the fluid film, diamond (inlet), ball surface, and bulk fluid temperatures

respectively

(b) Change-1: Effect of increased load at constant speed

(c) Change-2: Effect of increased speed at constant load

TABLE VI.I

Average and (Maximum) Δt's and t_D (in °C) [a]

Fluid	Δt_1 [b]	Δt_2 [b]	Δt_3 [b]	Δt_4 [b]	t_D [b]
#1 (Naphthenic Mineral Oil)	44.8(51.8)	-4.9(0.3)	12.5(18.5)	49.6(61.4)	48.3(65)
#2 (Ester)	45.7(56.8)	-2.3(3.2)	11.4(17.7)	44.5(58.9)	45.1(70.0)
#3 (Synthetic Paraffin)	22.5(35.9)	-4.2(4.3)	8.7(15.5)	35.9(42.3)	39.7(64.4)
#4 (Traction)	50.2(51.2)	-4.7(-0.6)	17.6(27.5)	46.9(60.9)	52.9(68.5)

Notes: (a) $\Delta t_1 = t_F - t_D$, $\Delta t_2 = t_M - t_D$, $\Delta t_3 = t_D - t_B$, $\Delta t_4 = t_F - t_M$, where t_F, t_D, t_M, and t_B are the the fluid film, diamond (inlet), ball surface, and bulk fluid temperatures respectively

(b) The averages are for the same set of cooling water temperatures. Whenever a set was unavailable, interpolated values were used.
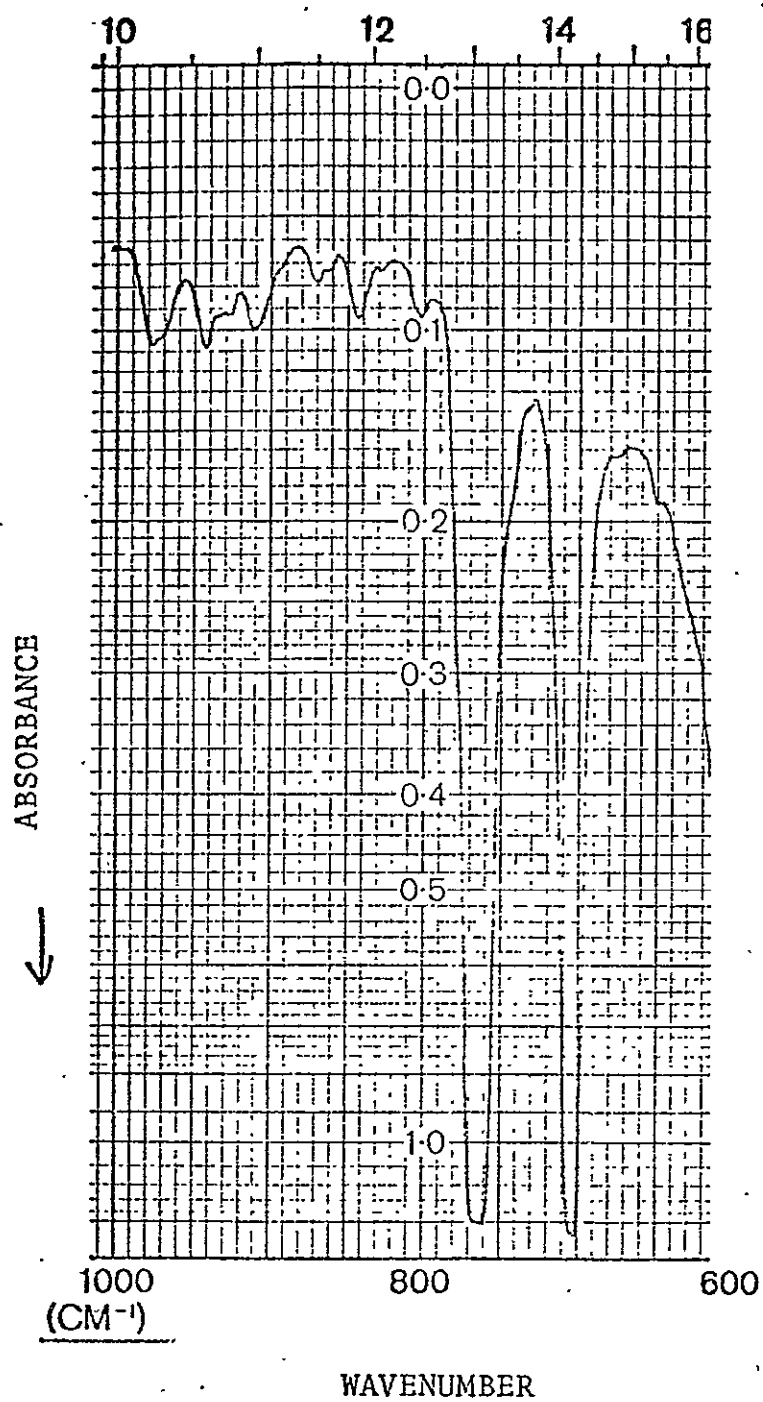
FIGURE 1

ROUTINE INFRARED SPECTRUM OF POLYMETHYL STYRENE FLUID
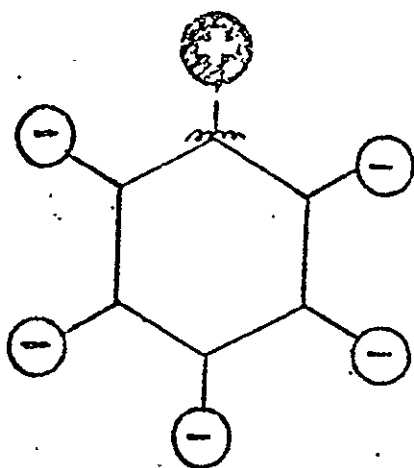
WAGGING MODE
760 cm^{-1}

+ = Motion into Paper Plane

- = Motion out of Paper Plane
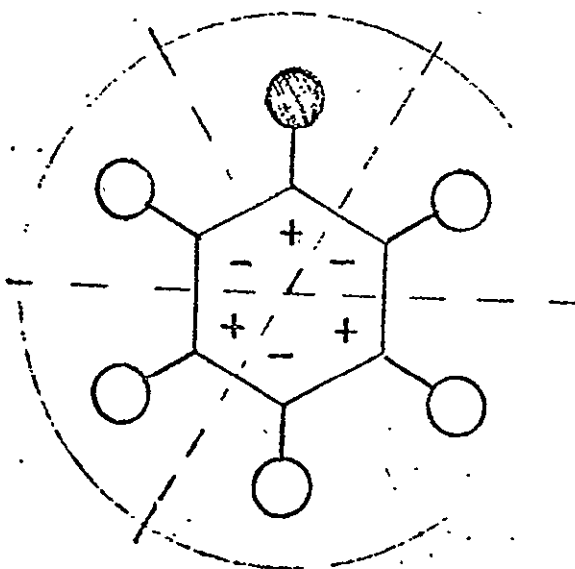
CH OUT OF PLANE
DEFORMATION MODE

700 cm^{-1}

FIGURE 2

TWO INFRARED-ACTIVE VIBRATIONAL MODES OF POLYMETHYLSTYRENE

43

FIGURE 3   EHD APPARATUS AND INTERFEROMETER ATTACHMENT FOR EMISSION
            MEASUREMENTS

1. FLUID CUP
2. FLUID
3. DIAMOND HOLDER
4. DIAMOND WINDOW
5. CONTACT REGION
6. ROTATING BALL
7. HOLDER
8. DIAMOND HOLDER x/y ADJUSTMENT SCREW
9. FLUID CUP x/y ADJUSTMENT SCREW
10. FLEXIBLE SHAFT
11. MOTOR DRIVE
12. COOLING WATER OUT
13. COOLING WATER IN
14. INTERFEROMETER SOURCE COMPARTMENT COVER

15. ALUMINUM REFLECTOR
16. BECK LENS SUPPORT
17. BEARING TABLE SURFACE
18. BEARING TABLE SUPPORT
19. BECK LENS
20. CHOPPER BLADE
21. ADAPTER TUBE FOR EMISSION SPECTRA
22. CHOPPER MOTOR
23. INTERFEROMETER COLLIMATING MIRROR
24. GAS COOLER
25. REAL IMAGE OF CONTACT REGION
26. GAS NOZZLE
27. INFRARED TRANSPARENT WINDOW

44

CENTER BURST

FIGURE 4 - INTERFEROGRAM OF FLUID #4 FOR ESSENTIALLY
BALANCED SAMPLE AND REFERENCE RADIATION
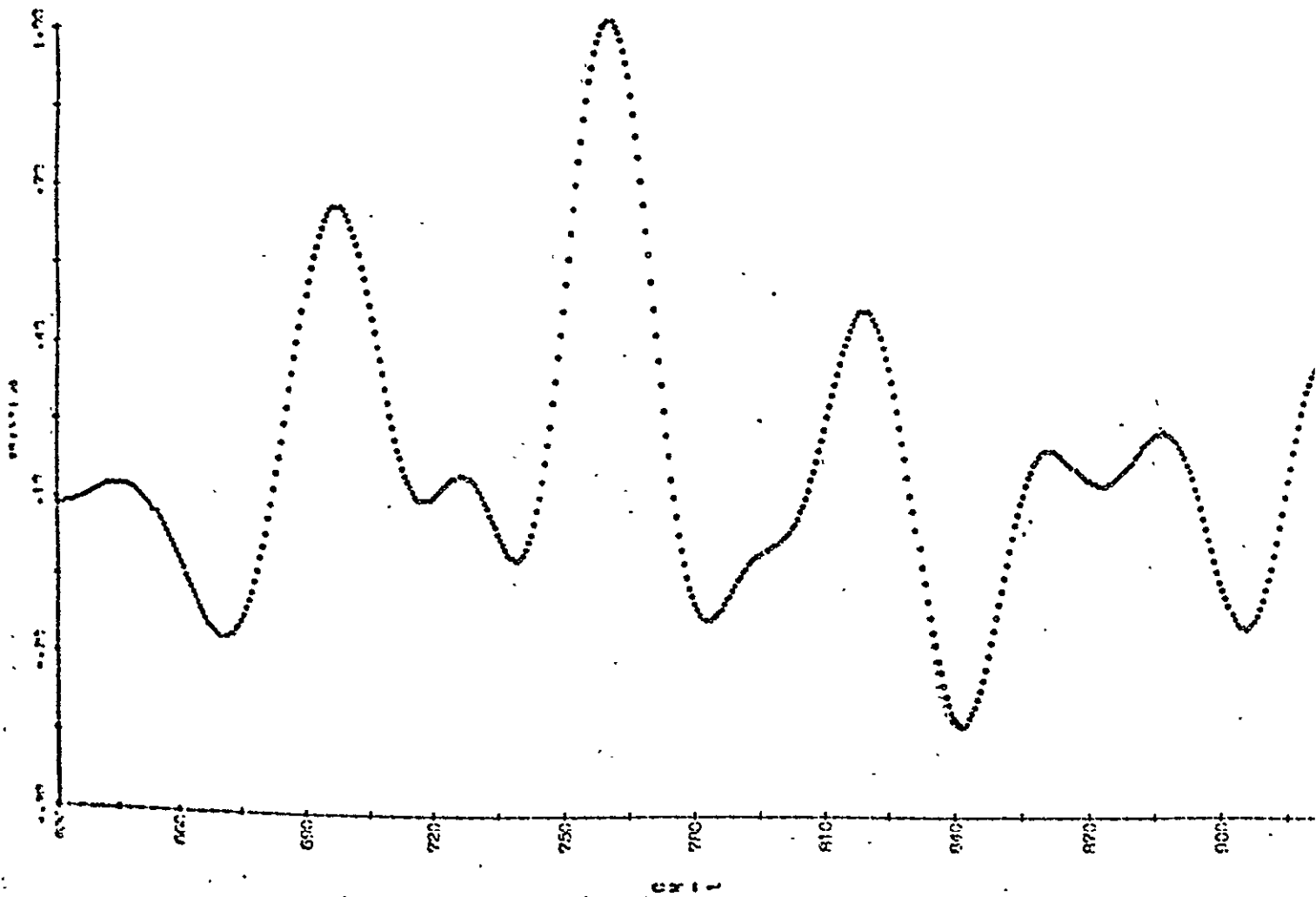
FIGURE 5 - SPECTRUM OF FLUID 4 DERIVED FROM INTERFEROGRAM
SHOWN ABOVE
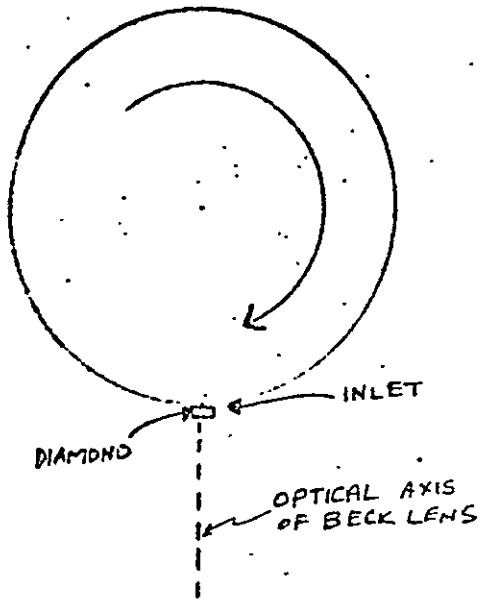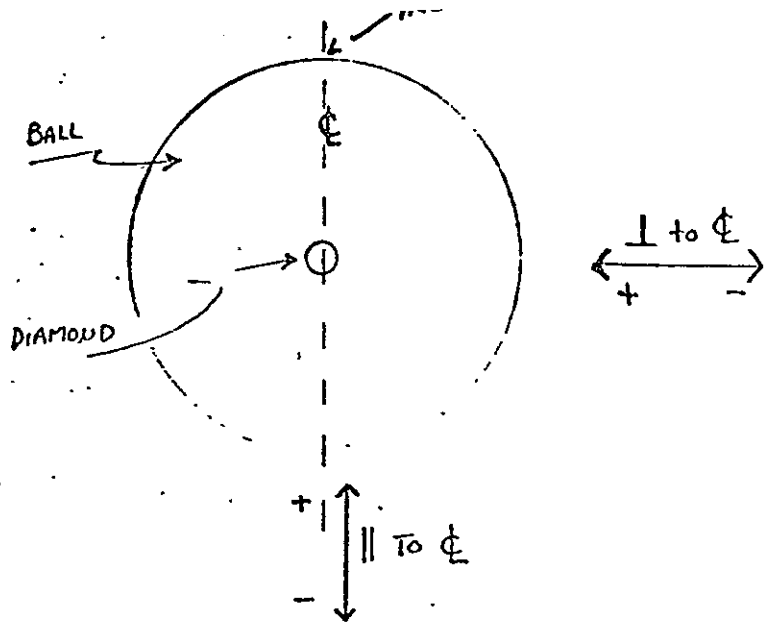
SIDE VIEW   TOP VIEW
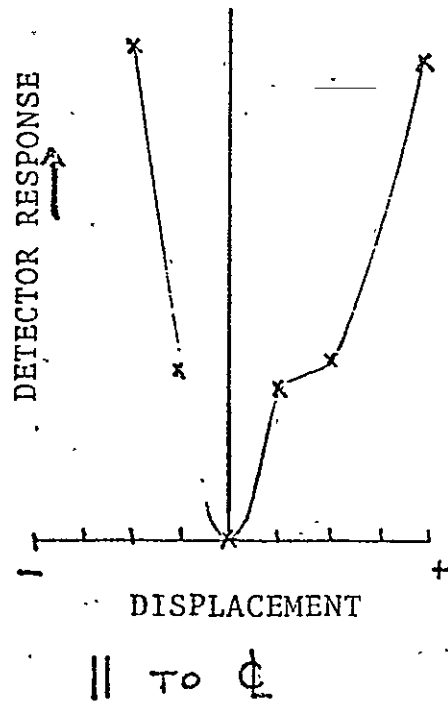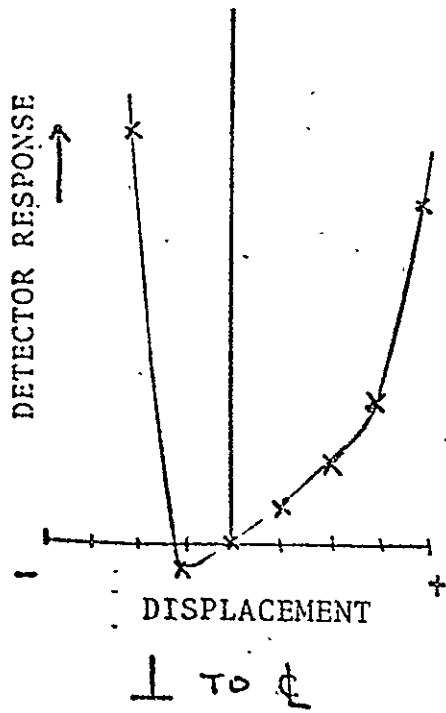
FIGURE 6

EFFECT OF MOVING CONTACT ZONE ACROSS FOCAL PLANE OF BECK LENS

46.
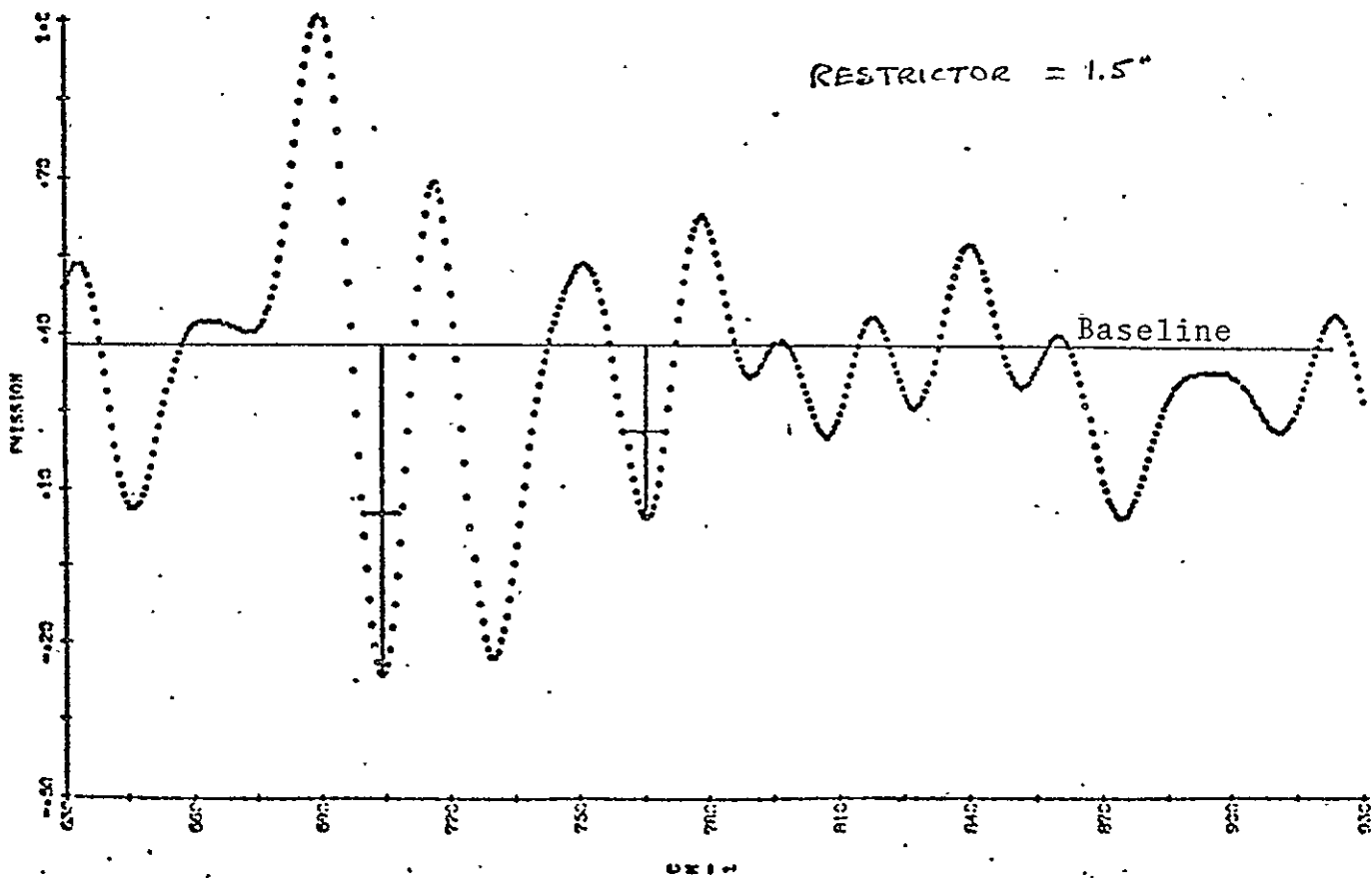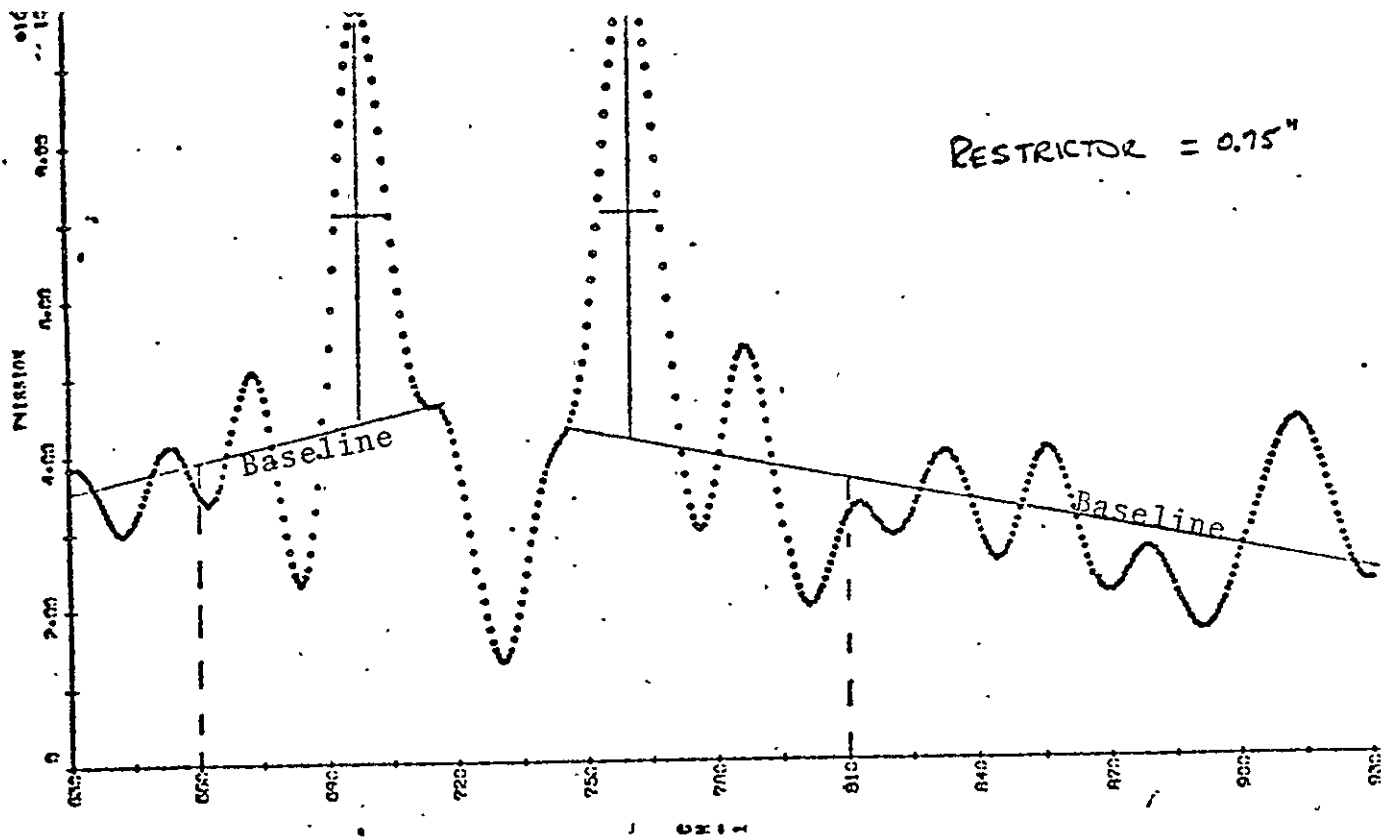
FIGURE 7 - EFFECT OF RESTRICTOR SIZE ON DIRECTION OF EMISSION
PEAK.   Fluid 2   480 RPM   28.5 KG   Bath at 24.5°C

47

$I^+(0)$ effective

Diamond Window
refractive index n

$I^+(0)$

Interface 1
reflectivity R_1

$y=0$

y

$I^-(0)$

Semi-transparent Fluid Film
refractive index n' spectral absorption coefficient k

$I^+(h)$

$y=h$

Interface 2
reflectivity R_2

Ball (opaque)
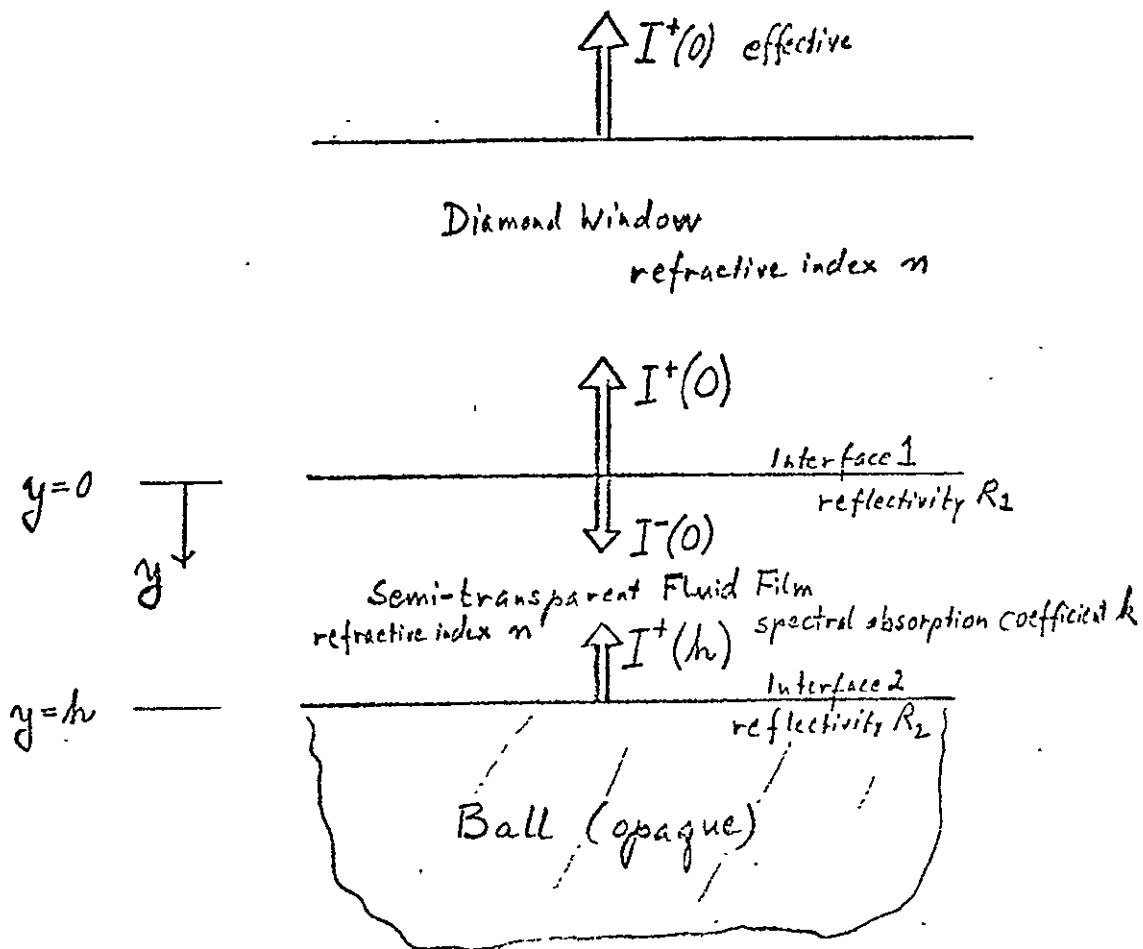
FIGURE 8

RADIATION FROM AN E.H.D. CONTACT

$I^+(0)$ effective

diamond window

refractive index n_D

$I^+(0)$

$y = 0$

y

$I^-(0)$

fluid film   refractive index n_F

$I^+(L)$

$y = L$

$I^-(L)$

diamond window
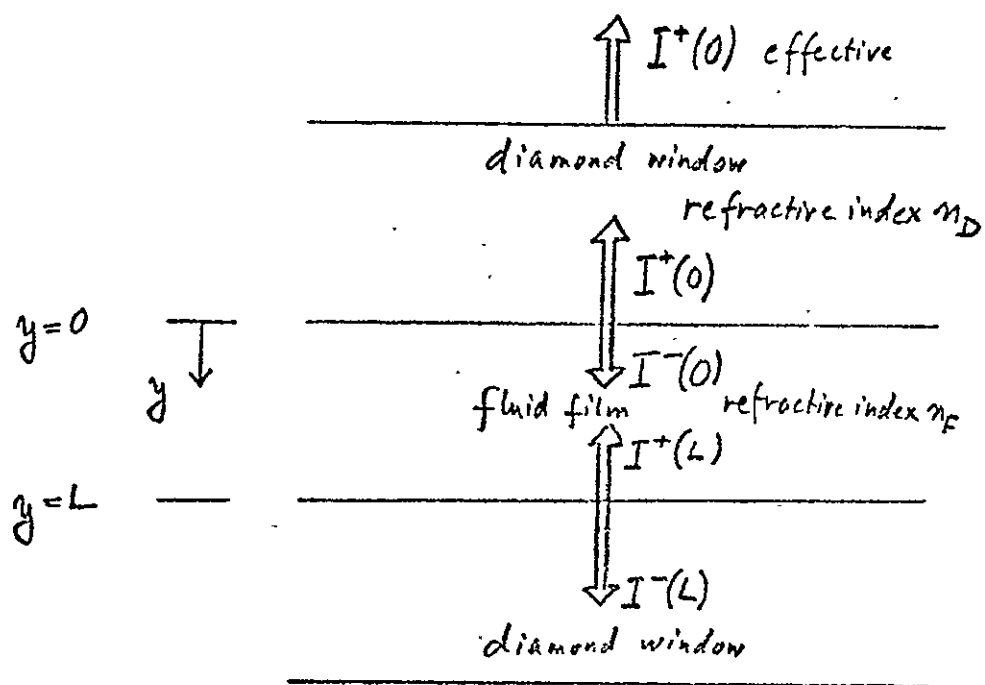
FIGURE 9

RADIATION FROM A DIAMOND ANVIL CELL
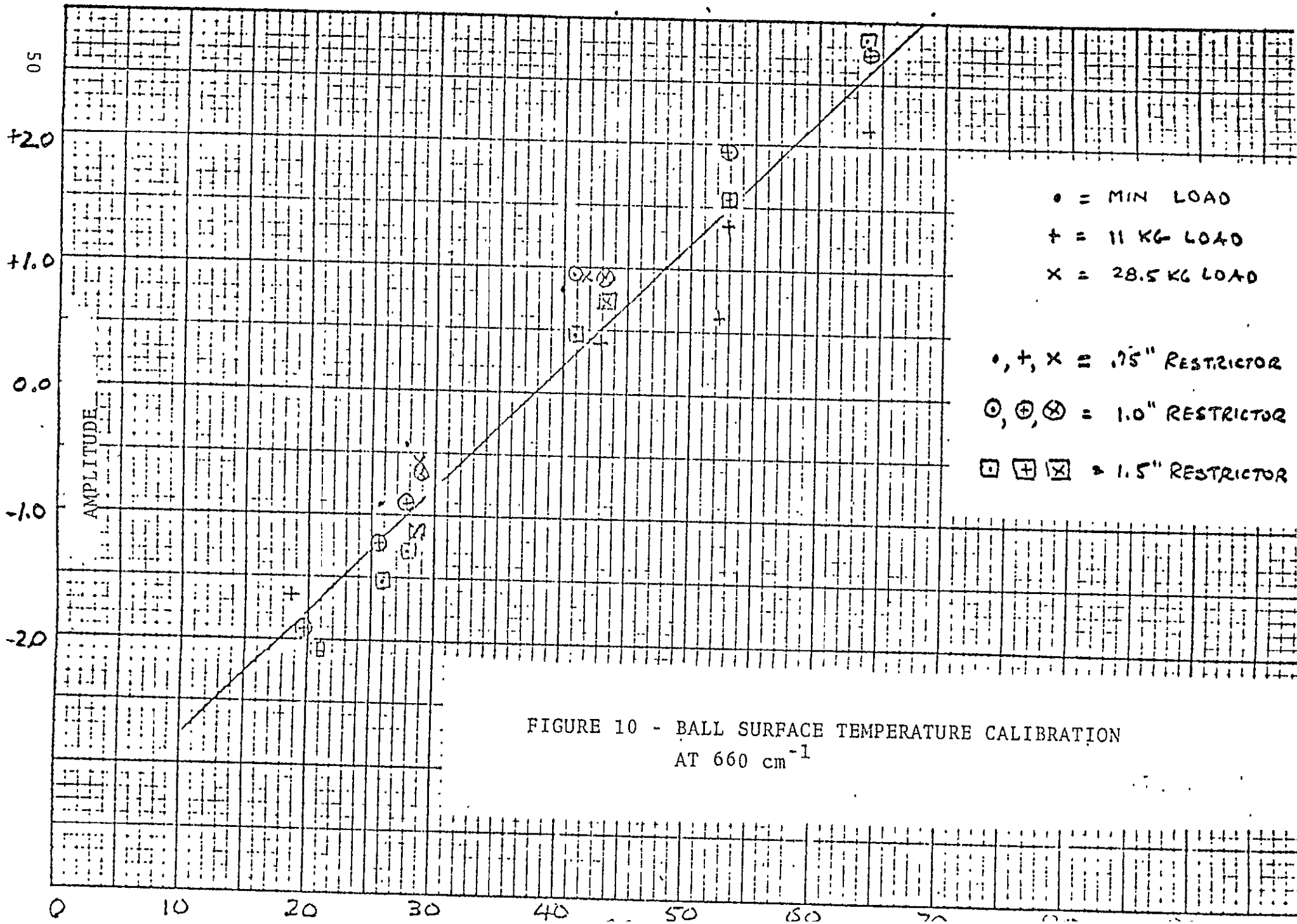
FIGURE 10 - BALL SURFACE TEMPERATURE CALIBRATION AT 660 cm^{-1}
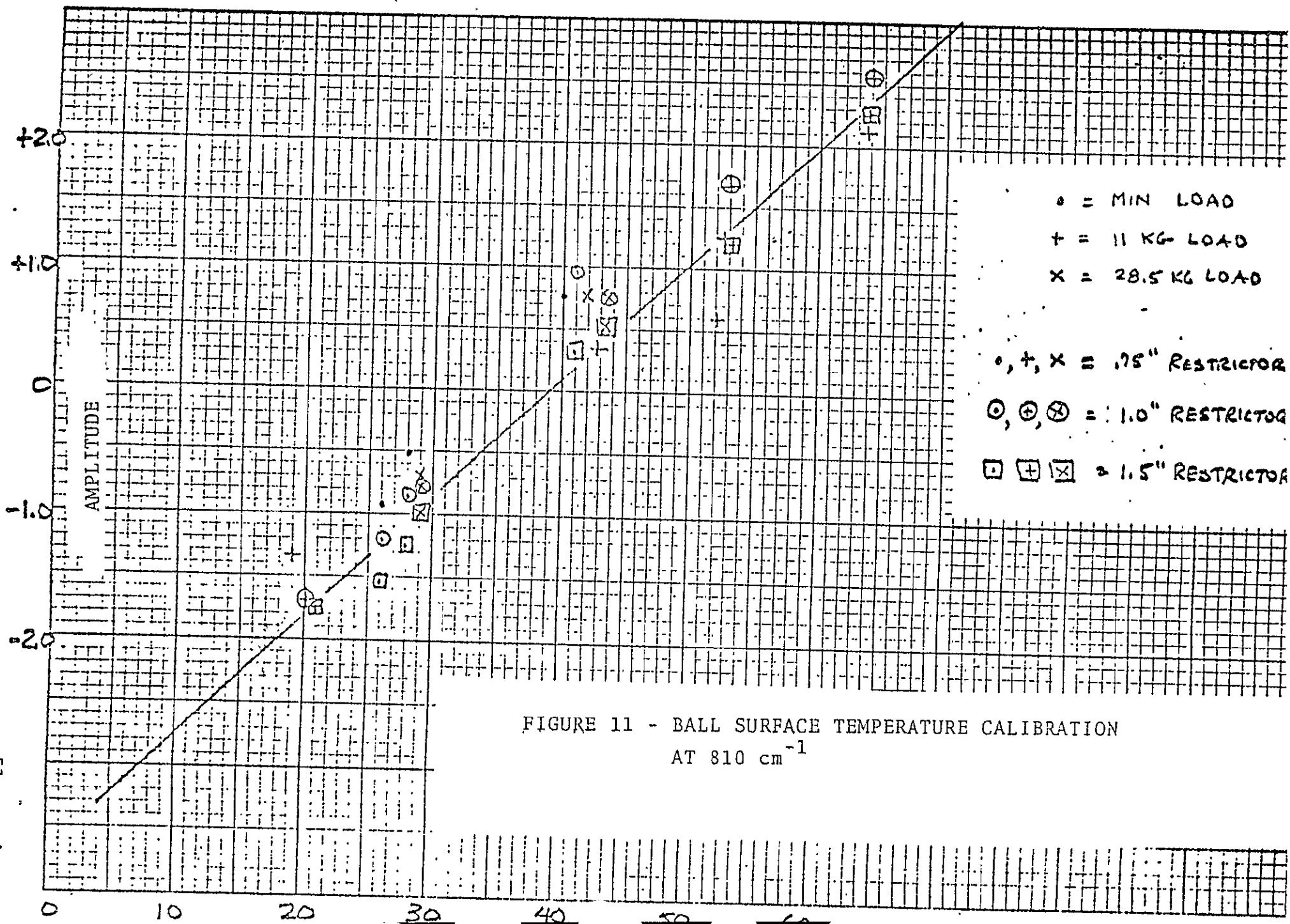
FIGURE 11 - BALL SURFACE TEMPERATURE CALIBRATION
AT 810 cm^{-1}

Legend:
- • = MIN LOAD
- + = 11 KG LOAD
- × = 28.5 KG LOAD

- •, +, × = .75" RESTRICTOR
- ⊙, ⊕, ⊗ = 1.0" RESTRICTOR
- ⊡, ⊞, ⊠ = 1.5" RESTRICTOR

240 RPM
11 kg
R = .75"

360 RPM
11 kg
R = .75"

480 RPM
11 kg
R = 1"

630   690   750   810   870   930
cm^{-1}
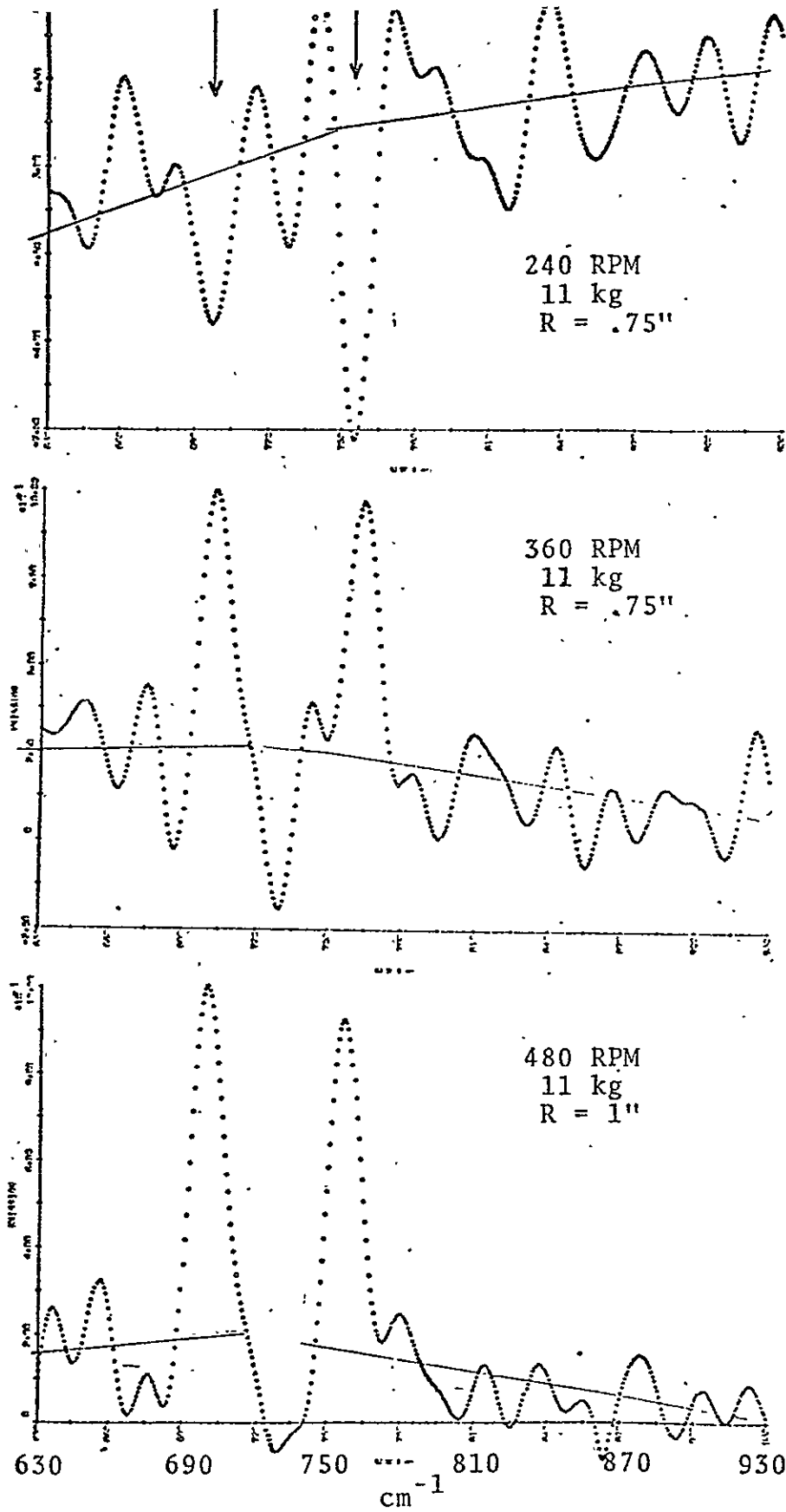
FIGURE 12 - FLUID 1 CONSTANT LOW LOAD   INCREASING
                    SPEED

240 RPM
15.5 kg
R = 1"

360 RPM
19.5 kg
R = 1"

480 RPM
19.5 kg
R = 1"

630   690   750 cm⁻¹ 810   870   930
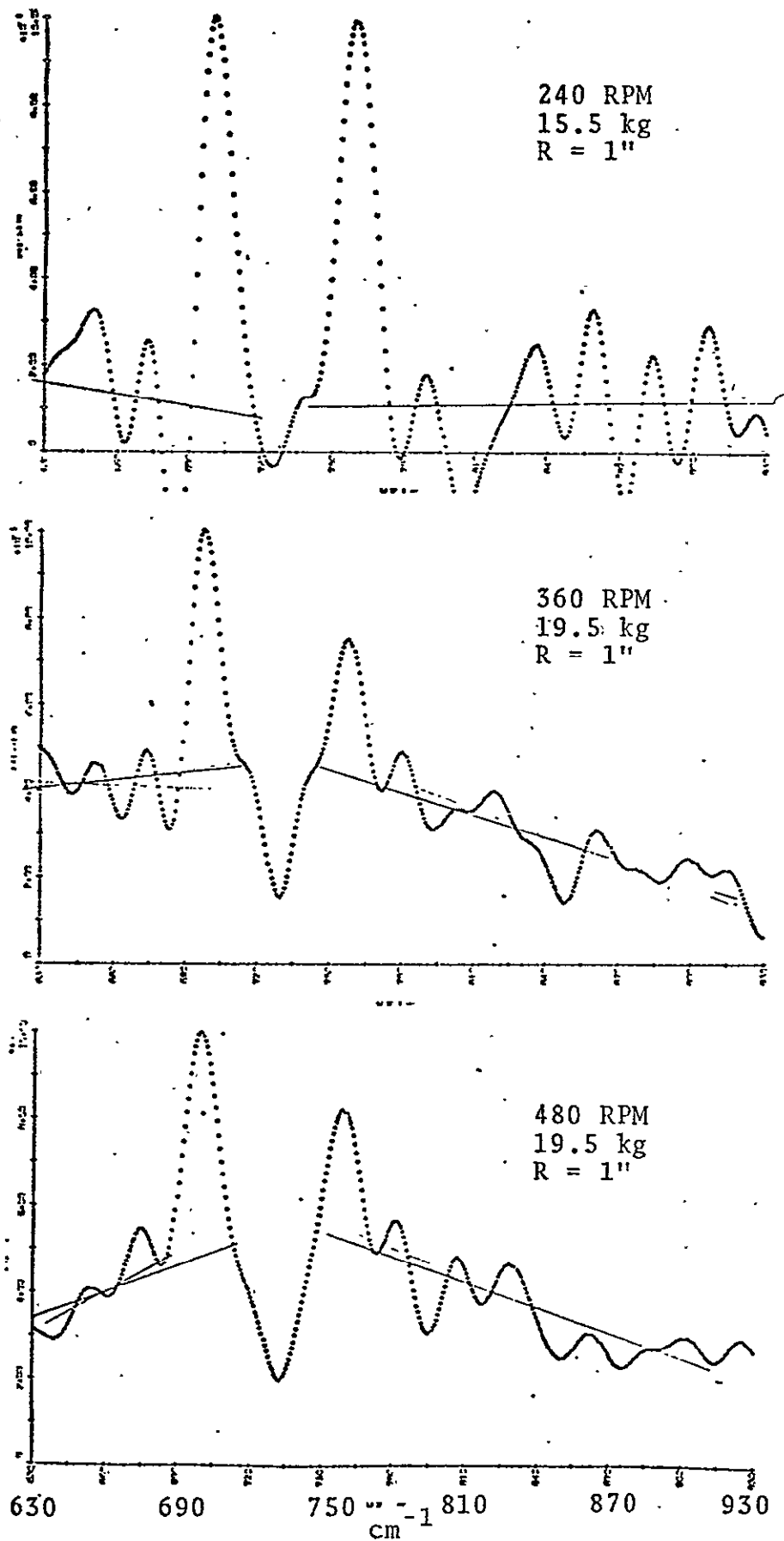
FIGURE 13 - FLUID 1 CONSTANT MED LOAD   INCREASING
                    SPEED

240 RPM
28.5 kg
R = 1"

360 RPM
28.5 kg
R = 1"

480 RPM
28.5 kg
R = 1.5"

630   690   750   810   870   930
cm^{-1}
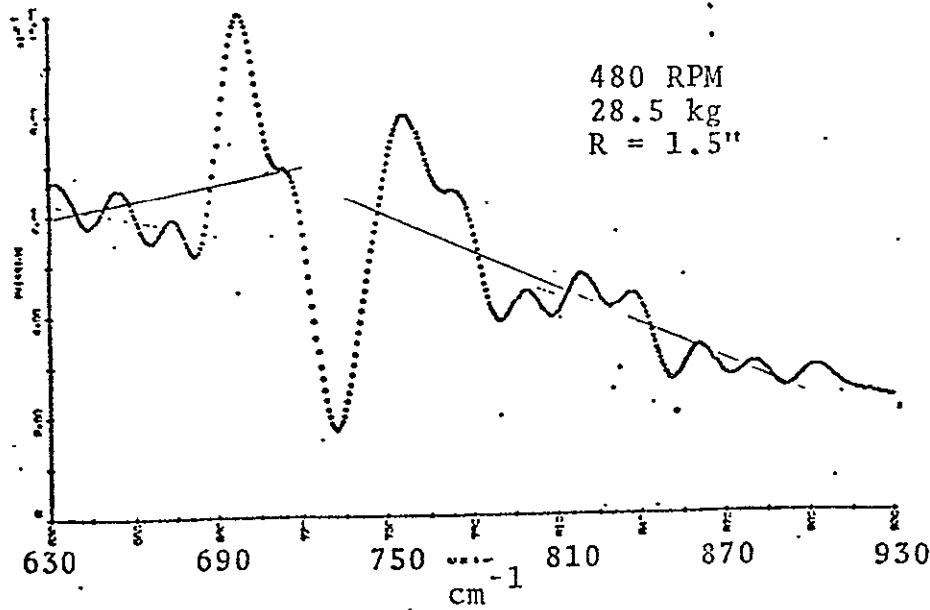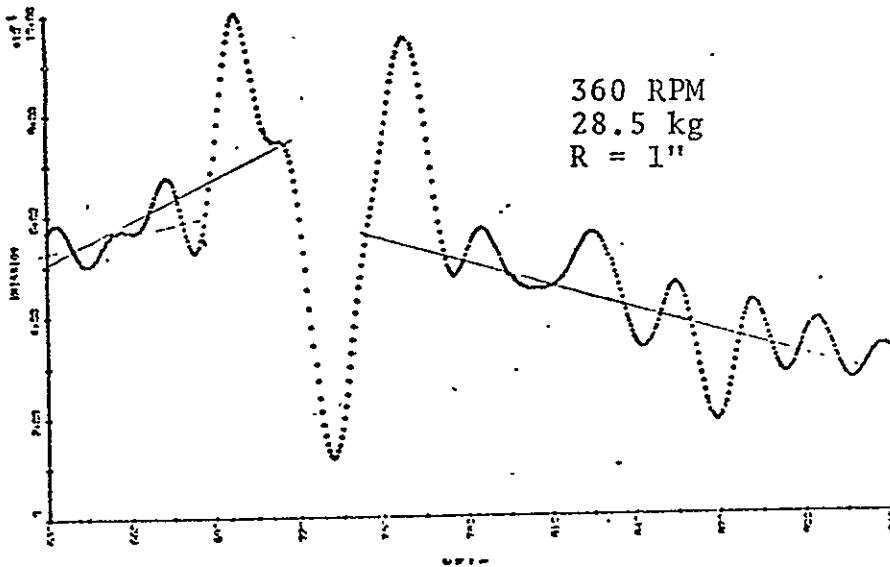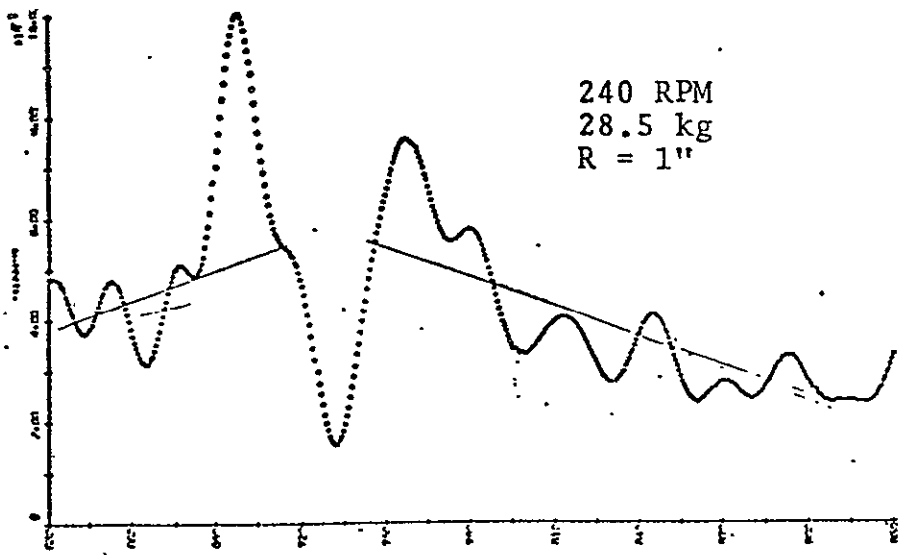
FIGURE 14 - FLUID 1 CONSTANT HIGH LOAD   INCREASING
           SPEED

ball

t_B

t_M

Δt_3

fluid flow

Δt_4

Δt_2

t_D

Δt_1

t_F

Diamond Window

o   by Thermocouple

⊏⊐   by Radiation
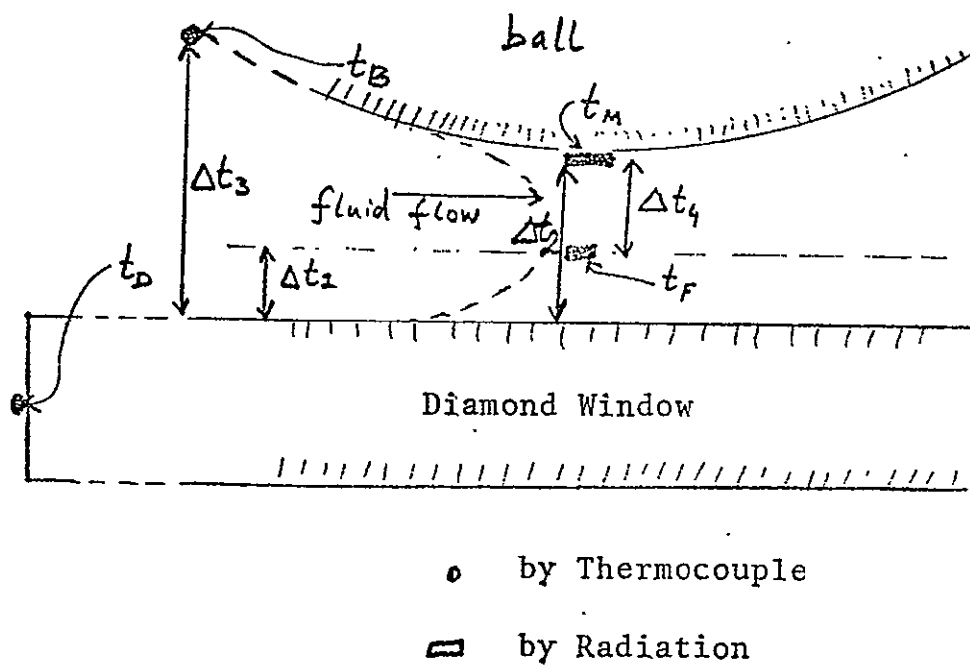
FIGURE 15 - EHD CONTACT TEMPERATURES

tD°C VS SHEAR RATE, U/h

FIGURE 16

Fluid No. 1
(Naphthenic Hydrocarbon Oil)

56

Shear Rate (sec^{-1} x 10^6)
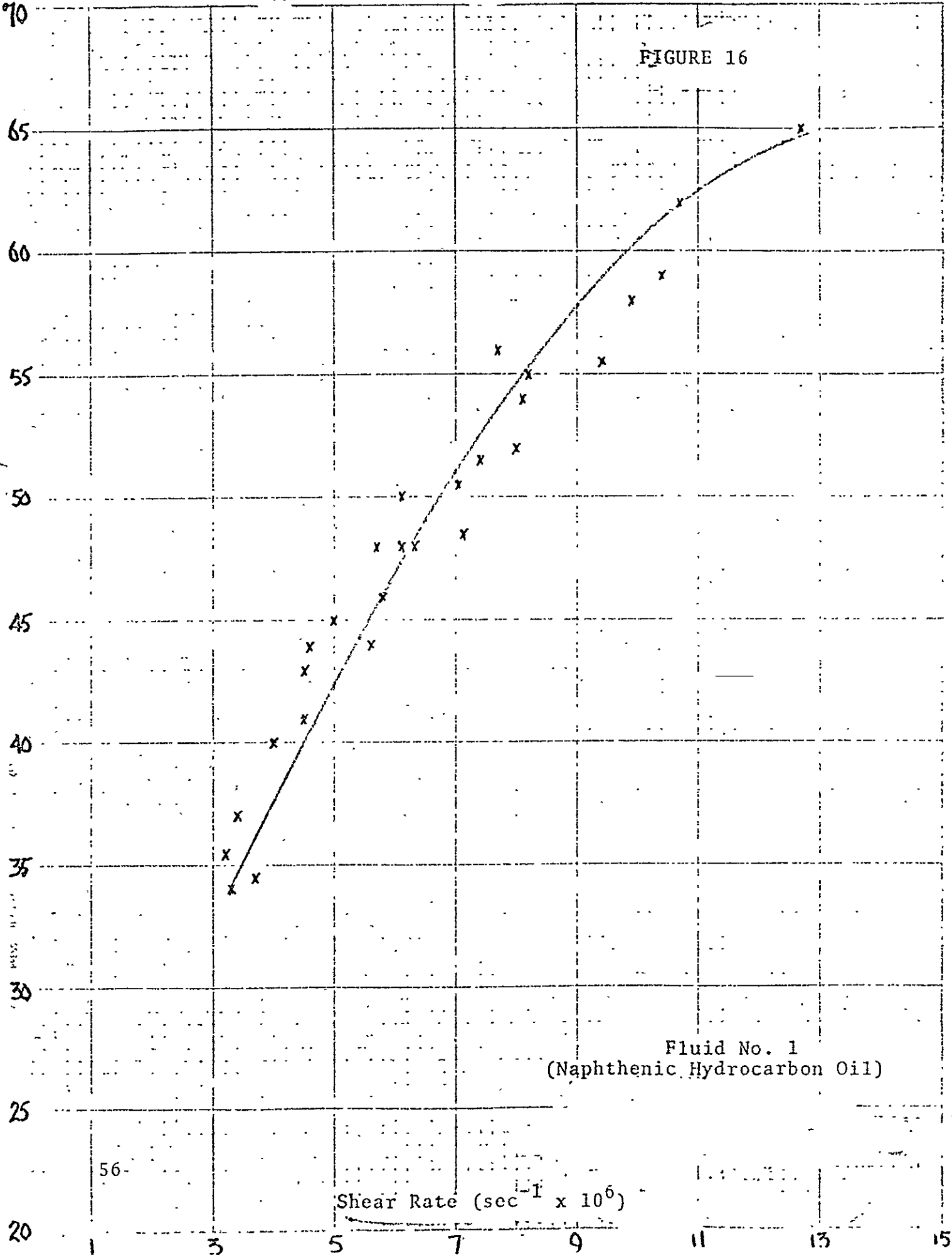
tD°C VS. SHEAR RATE

FIGURE 17

Fluid No. 2 (Ester)

Shear rate (sec^{-1} · 10^6)

57

tD°C VS SHEAR RATE

FIGURE 18
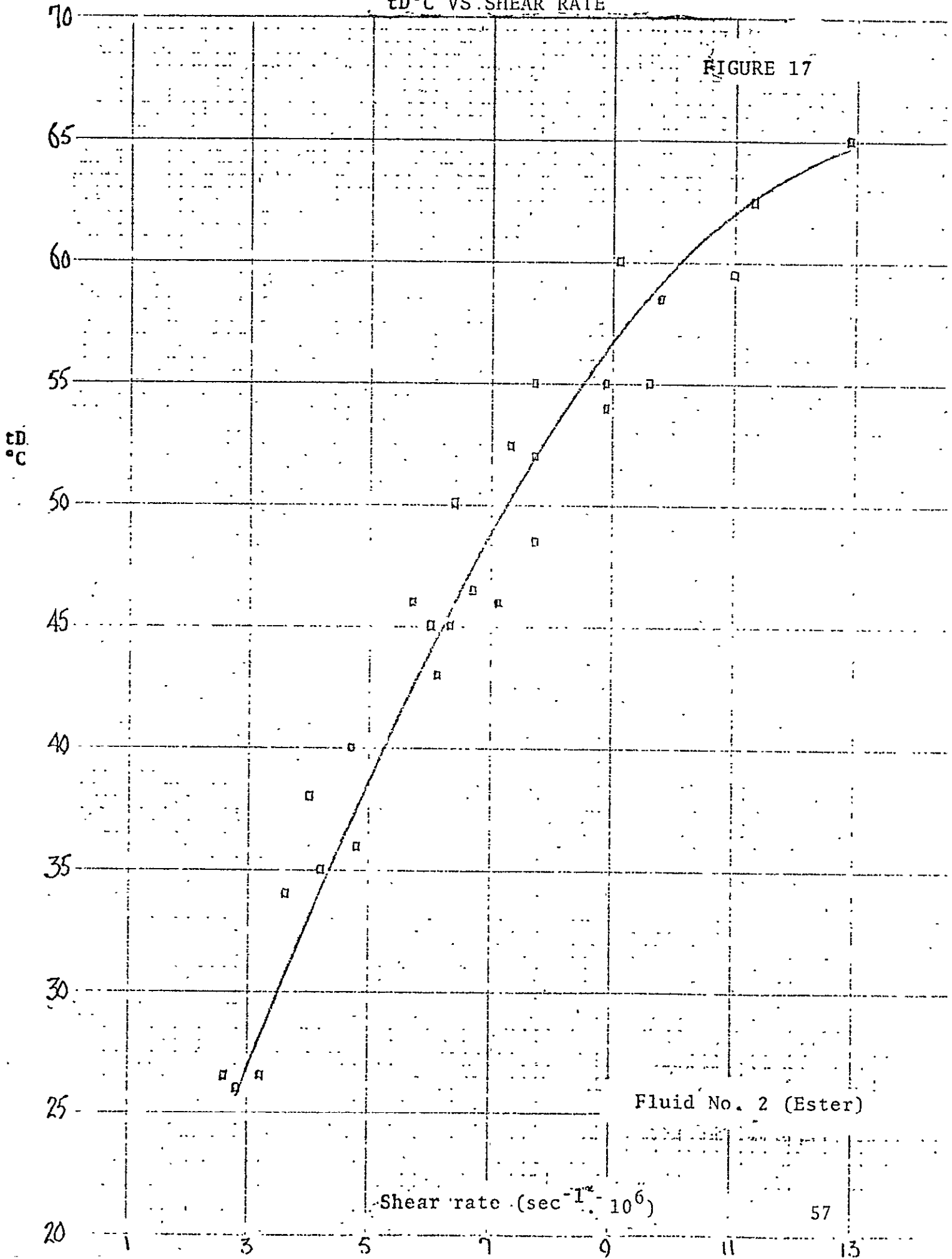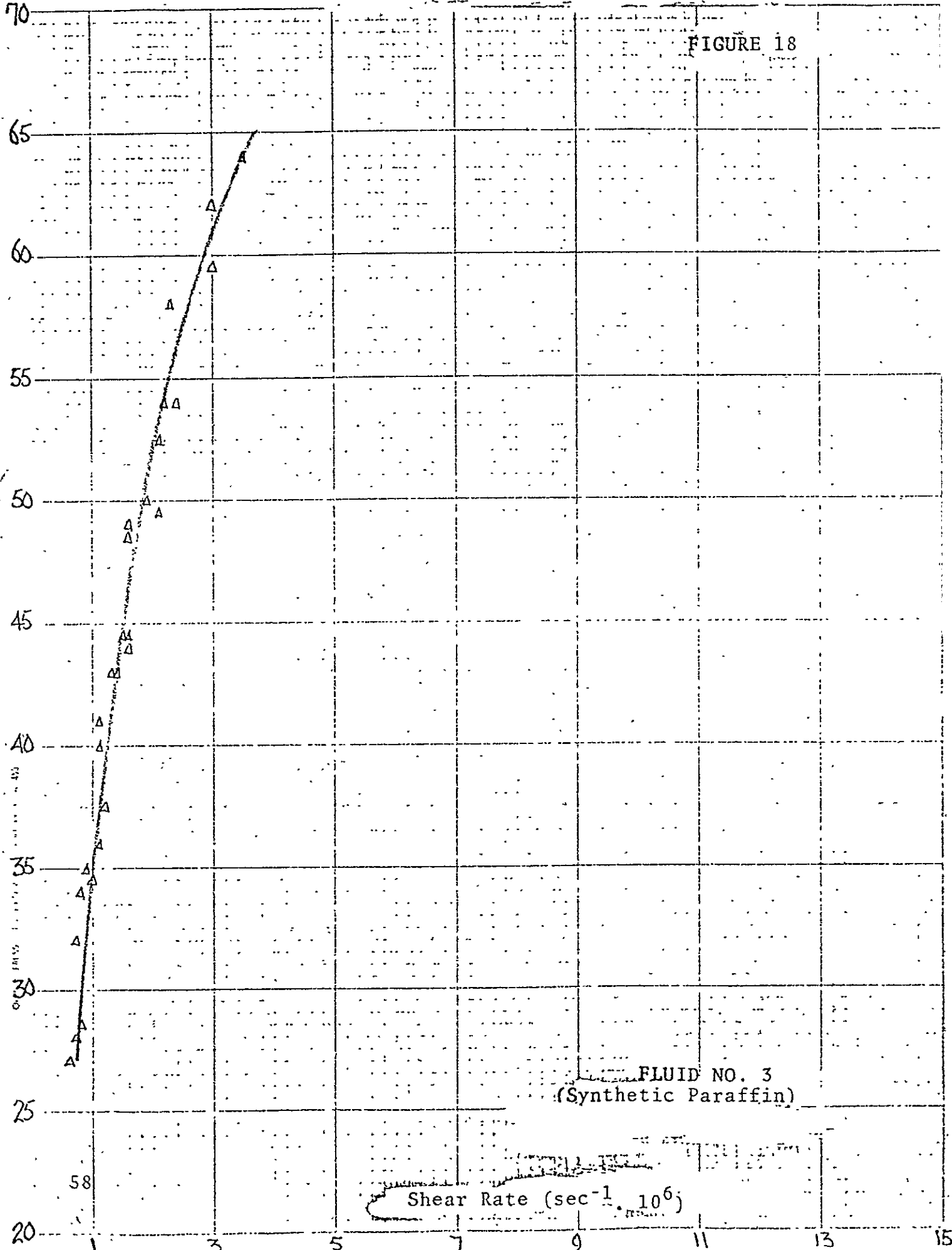
FLUID NO. 3
(Synthetic Paraffin)

Shear Rate (sec^{-1} . 10^6)

tD°C VS SHEAR RATE

FIGURE 19

FLUID NO. 4
(Traction Fluid)

tD
°C

Shear rate (sec^{-1} . 10^6)

A+3 VS SHEAR RATE

FIGURE 20

$(t_D - t_B)$

FLUID NO. 1
(Naphthenic Mineral Oil)
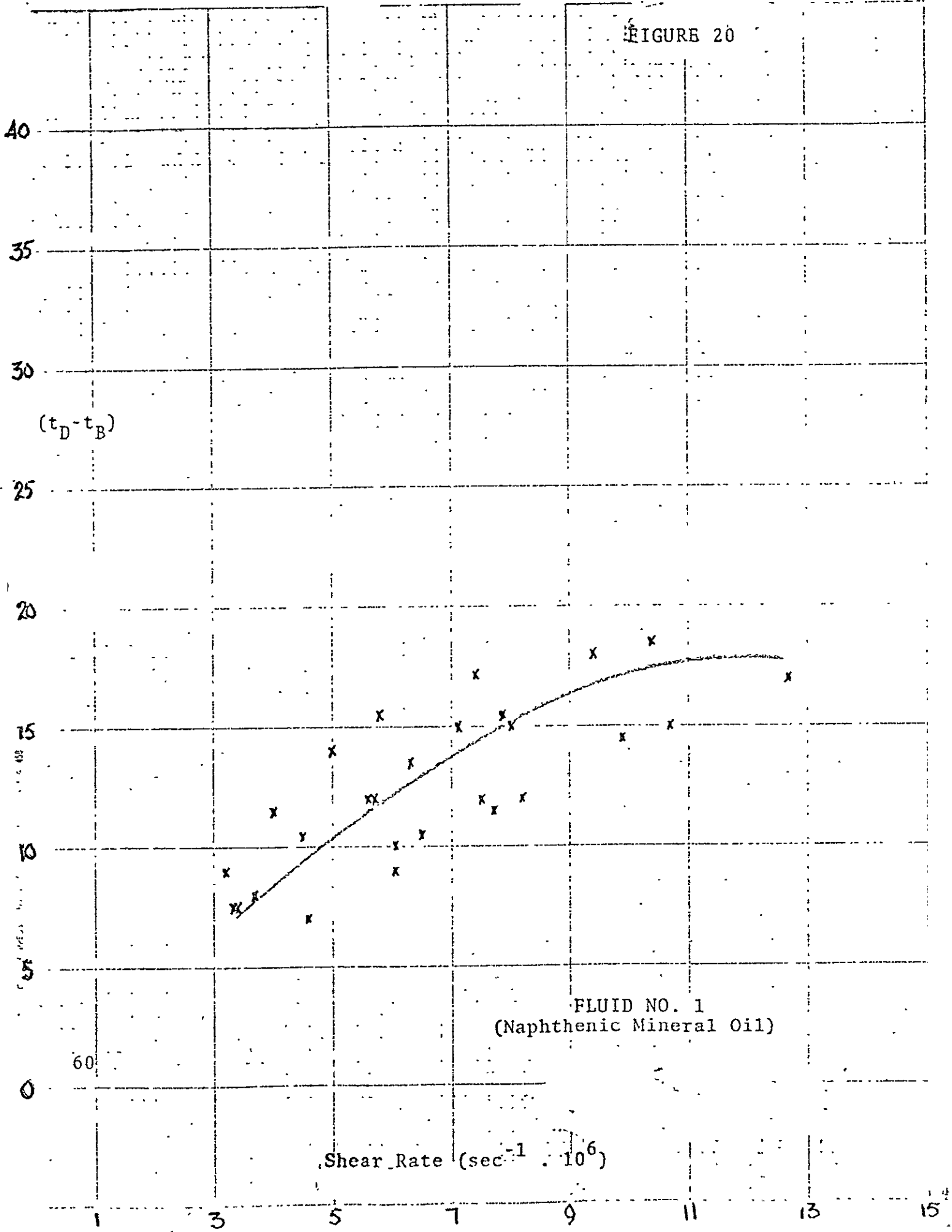
Shear Rate (sec^{-1} . 10^6)

Δt3 VS SHEAR RATE

FIGURE 21

$\Delta t3 (t_D - t_B)$
°C

FLUID NO. 2 (ESTER)

Shear rate (sec^{-1} . 10^6)

61
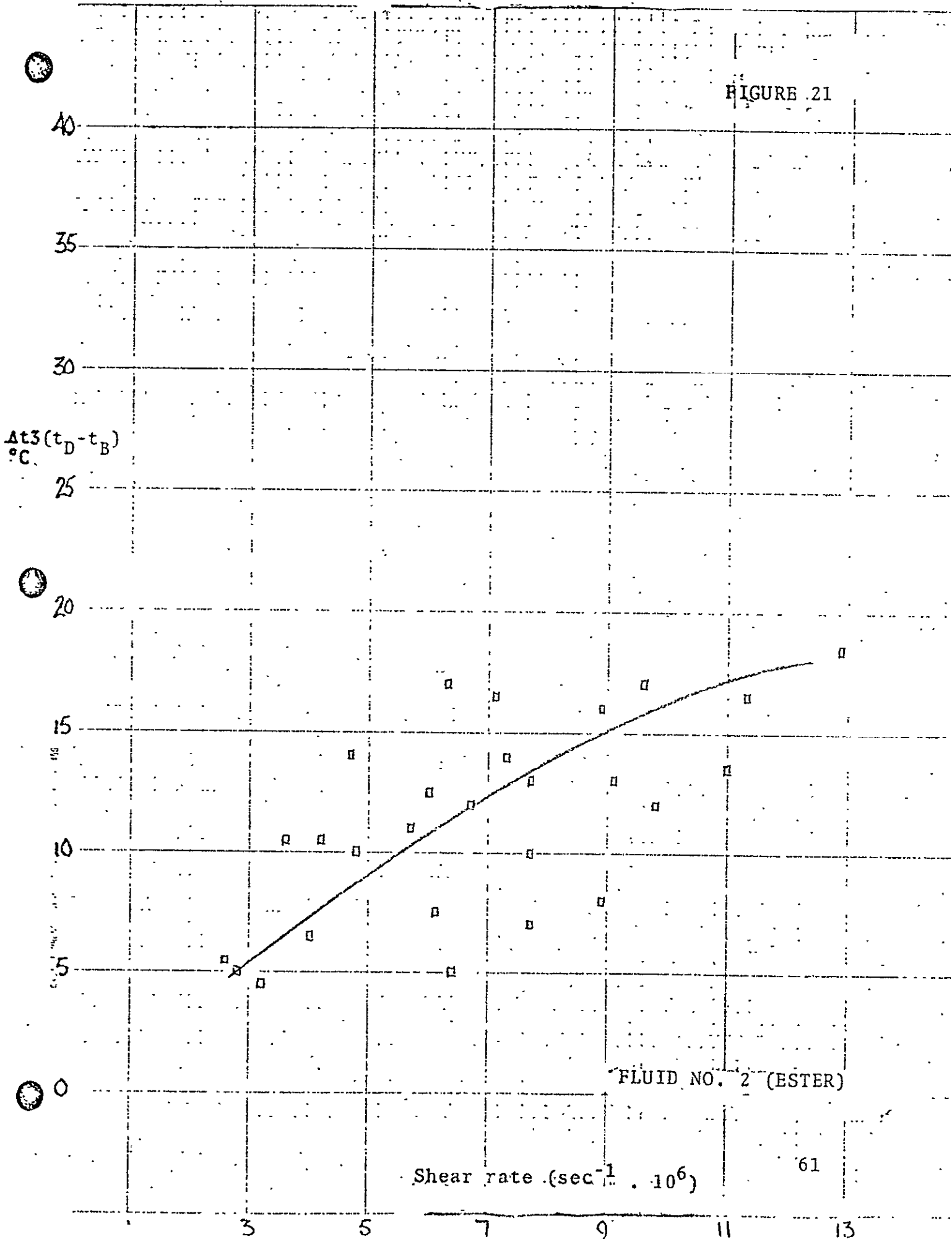
Δt3 VS SHEAR RATE

FIGURE 22

$\frac{\Delta t3}{\circ C}$ $(t_D - t_B)$

FLUID NO. 3
(Synthetic Paraffin)

Shear rate (sec^{-1} x 10^6)

DOUBLE POINT $\Delta t3$ VS SHEAR RATE

FIGURE 23
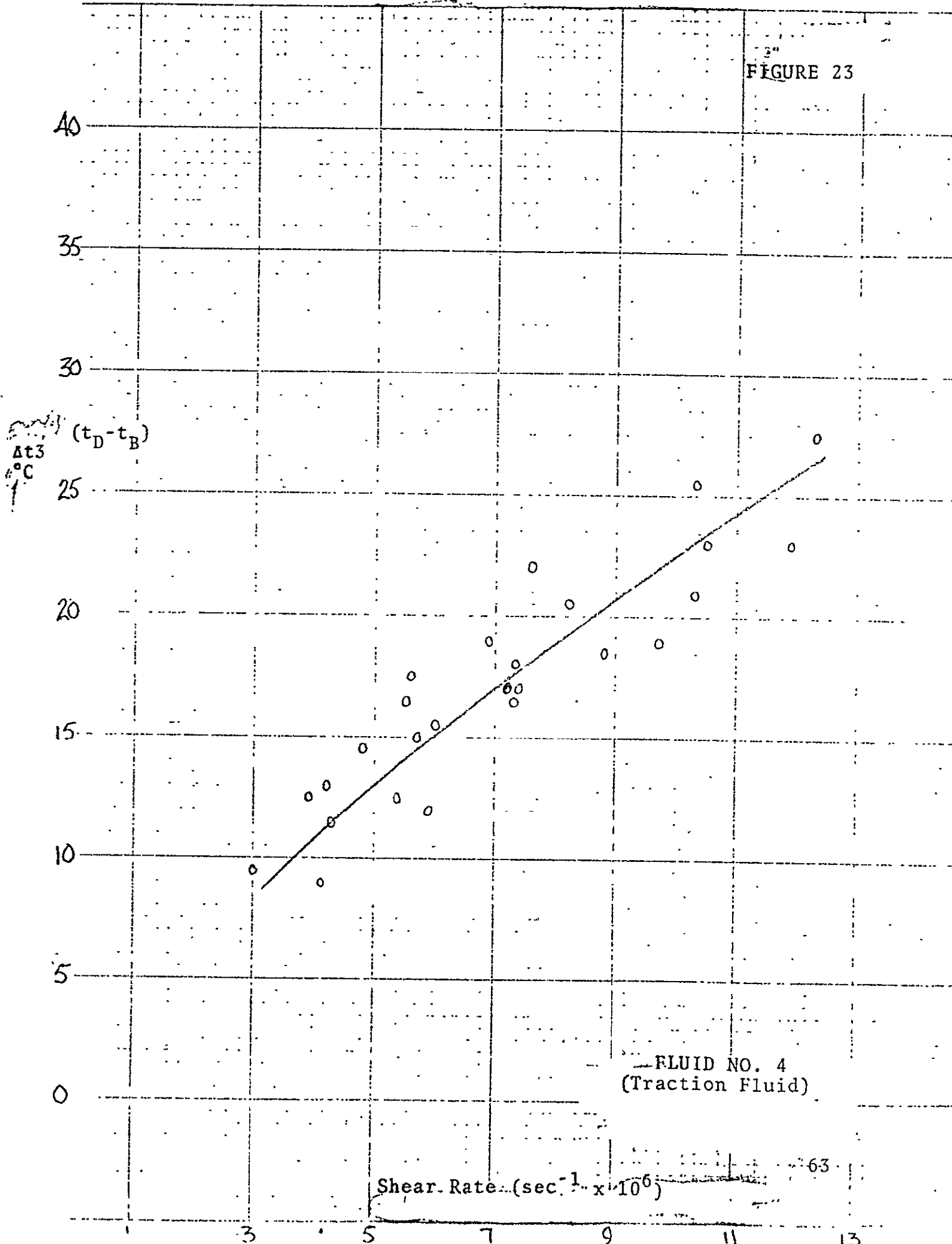
$\Delta t3$ $(t_D - t_B)$ °C

FLUID NO. 4
(Traction Fluid)

Shear Rate (sec^{-1} x 10^6)

63

FIGURE 24

Δt3 AVERAGED OVER SPEED AND LOAD
VS AVERAGED SHEAR RATE

FIGURE 25

Fluid #4 (traction)

20

Fluid #1 (mineral oil)

Fluid #2 (ester)

15

Fluid #3 (synthetic paraffi

10

5

Δt3
°C

28 kg

11 kg

Fluid No.	1	2	3	4
	X	□	△	o

20

15

Fluid #4 (traction) — o

10

Fluid #1 (mineral oil)

5 Fluid #2 (ester)

Fluid #3 (synthetic paraffin)
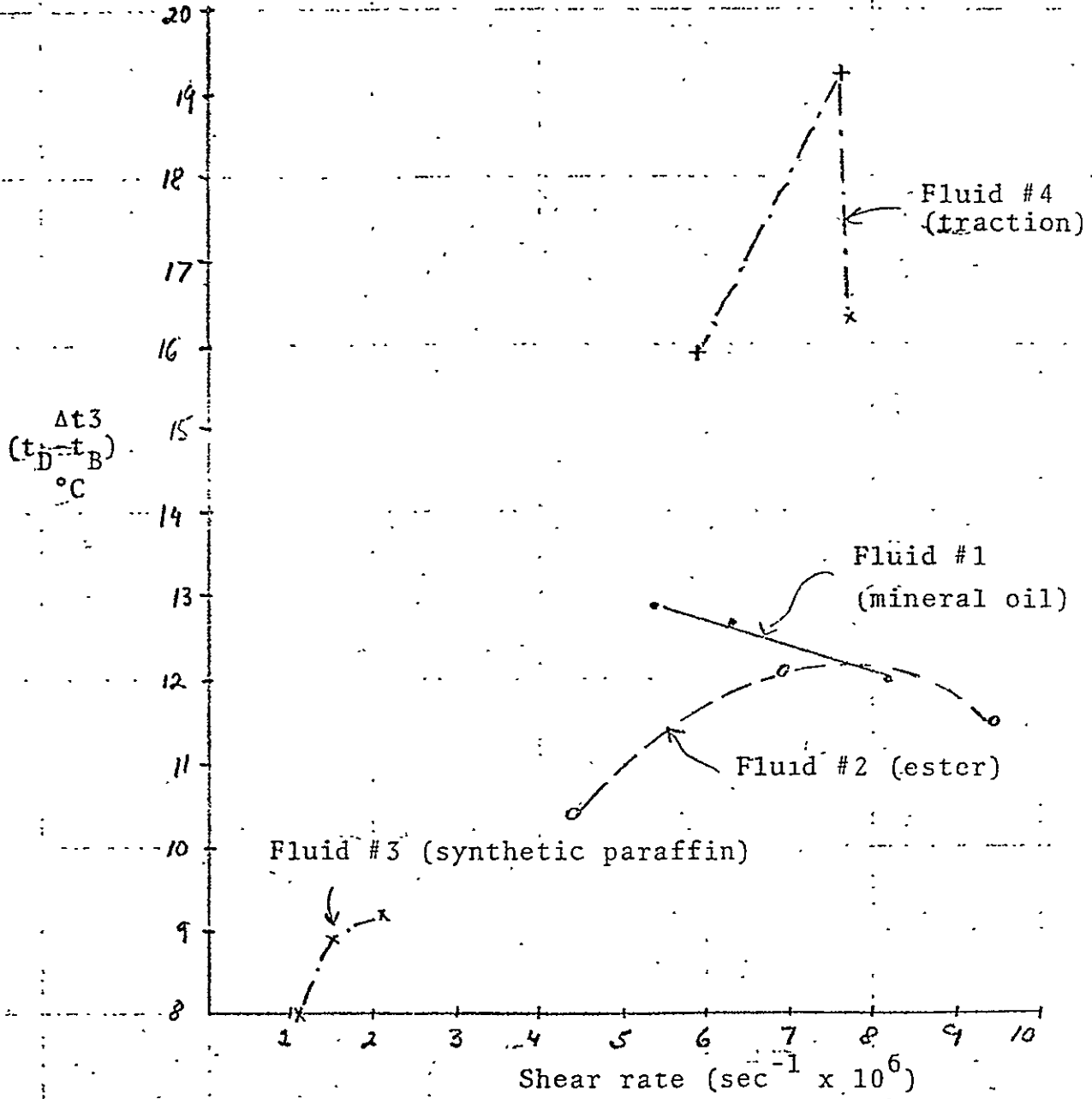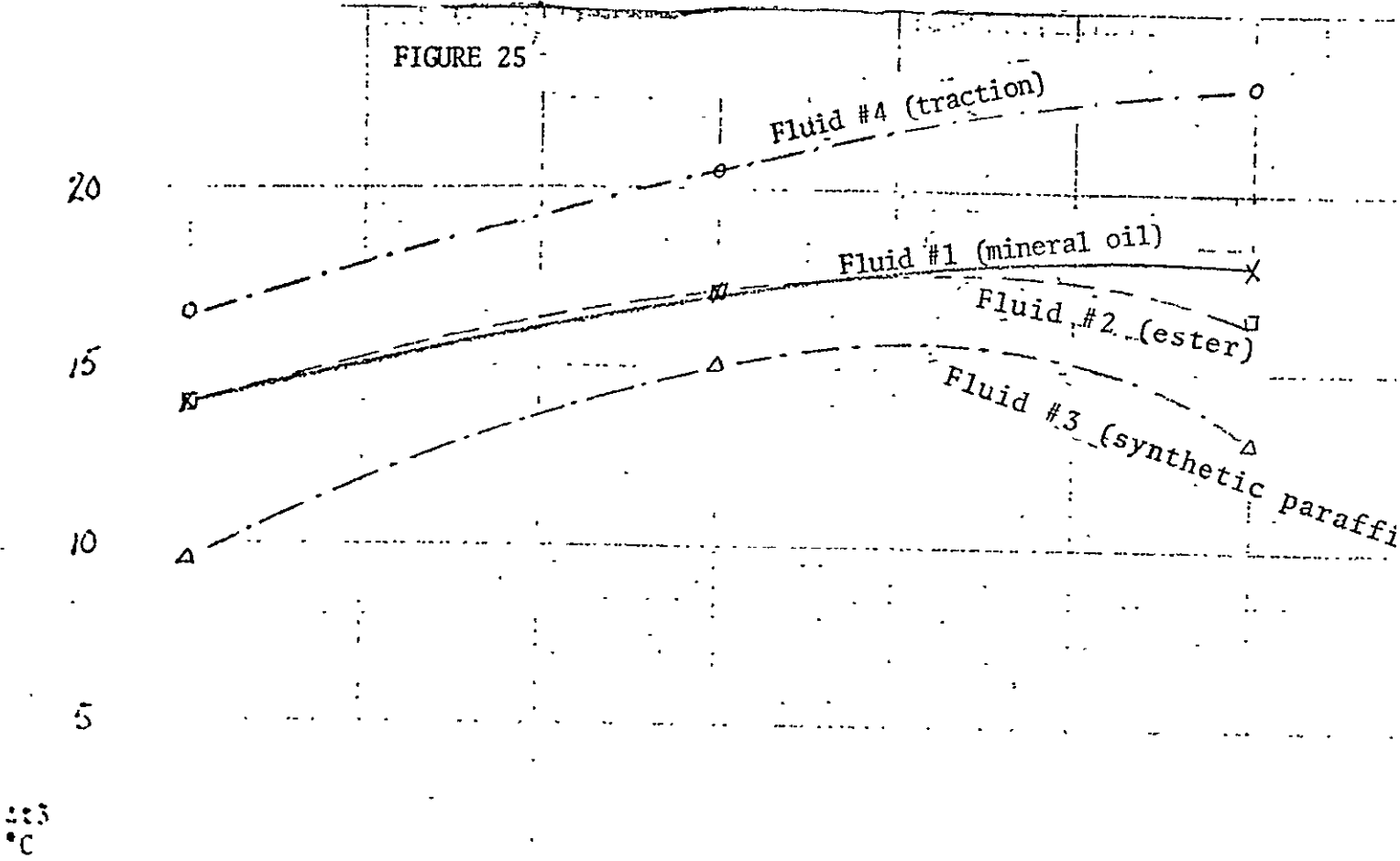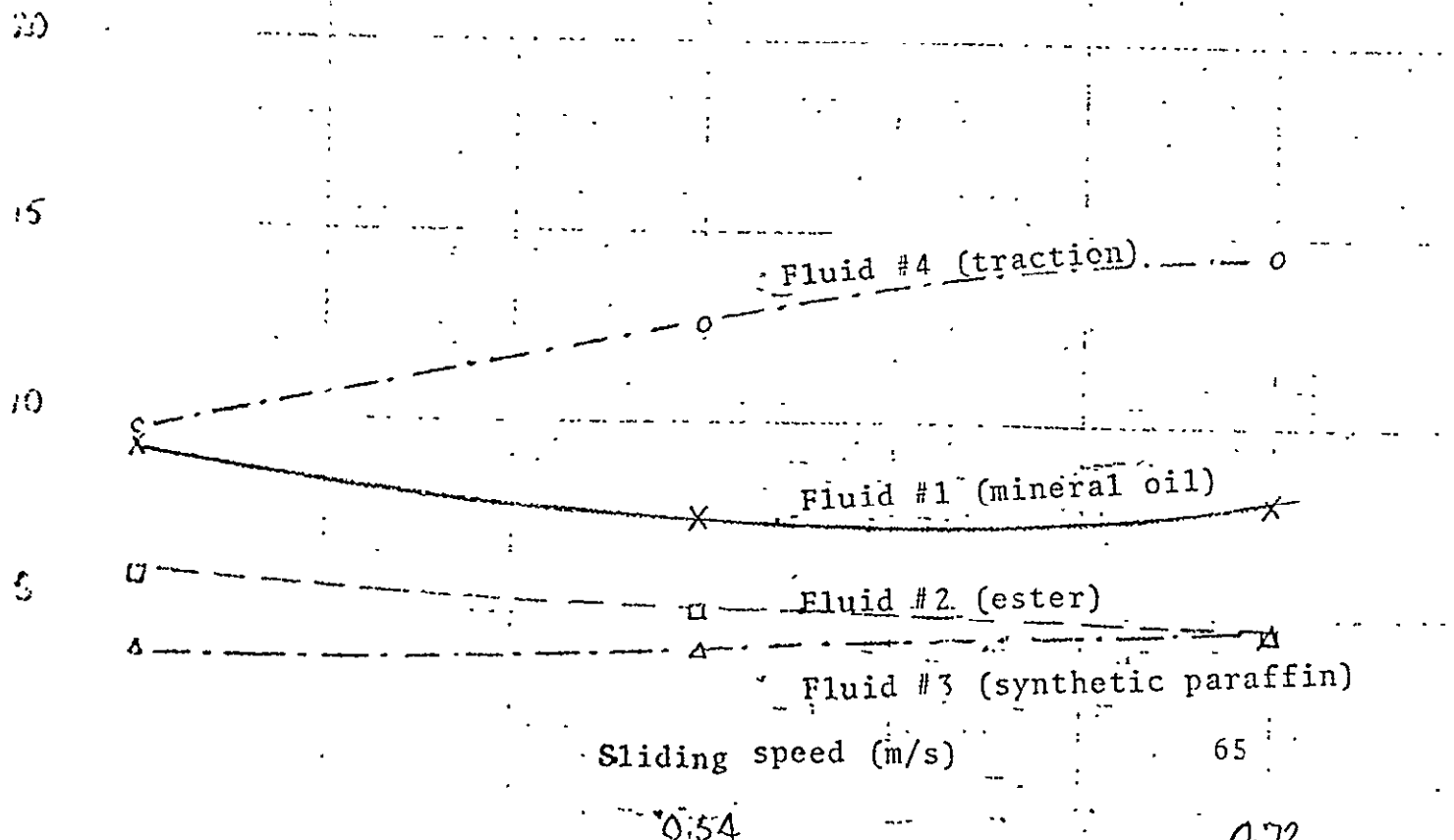
Sliding speed (m/s) 65

0.54 0.72

Δt3 VS LOAD @ CONST. SPEED

FIGURE 26

Fluid #4 (traction)

Fluid #1 (mineral oil)

Fluid #2 (ester)

Fluid #3 (synthetic paraffin)

Δt3 °C

U = 0.72

U = 0.36

Fluid No.	1	2	3	4
	X	◻	△	○

Fluid #4 (traction)

Fluid #1 (mineral oil)

Fluid #2 (ester)

Fluid #3 (synthetic paraffin)

Load (kg)

66

11

19

28
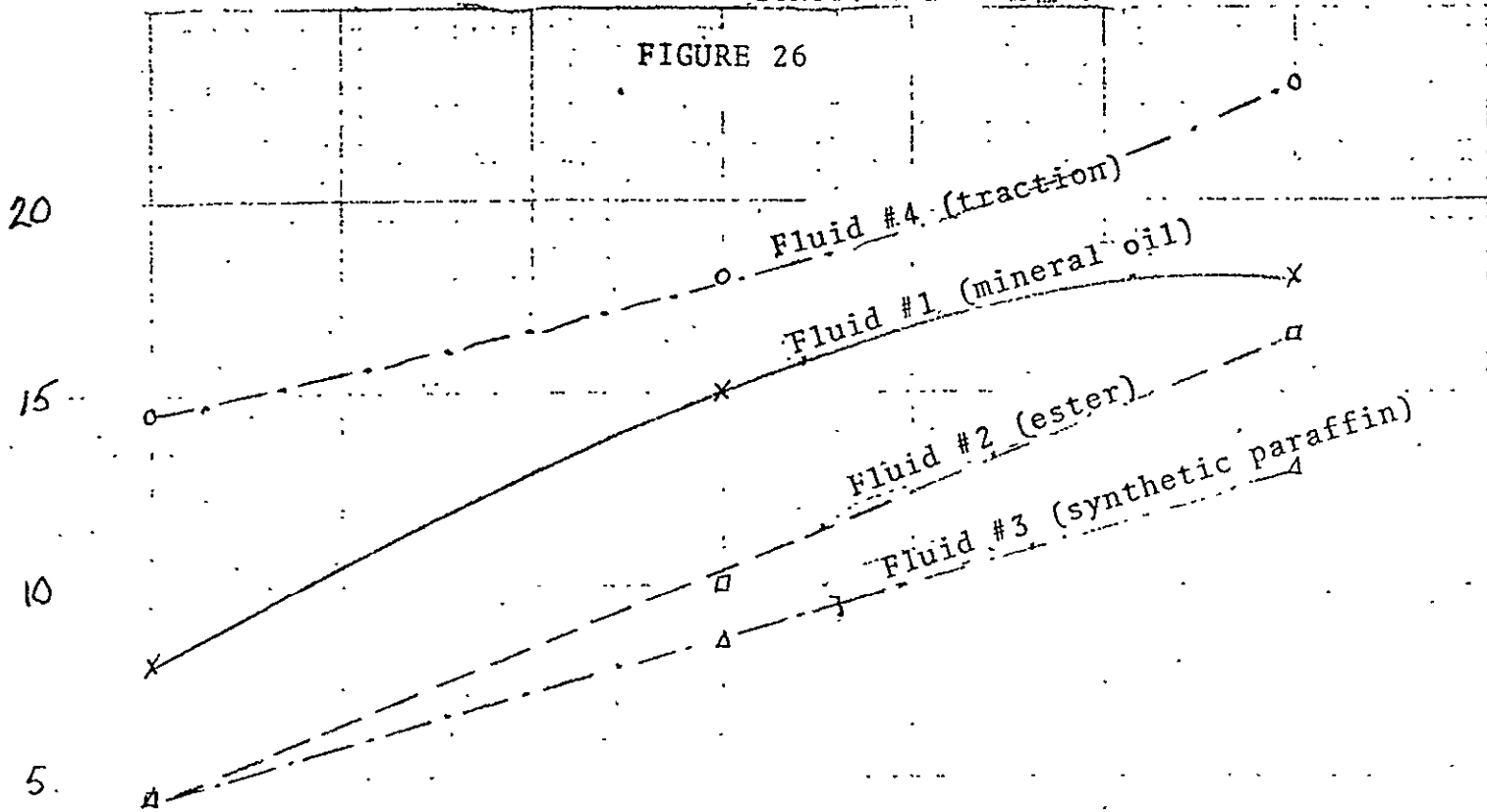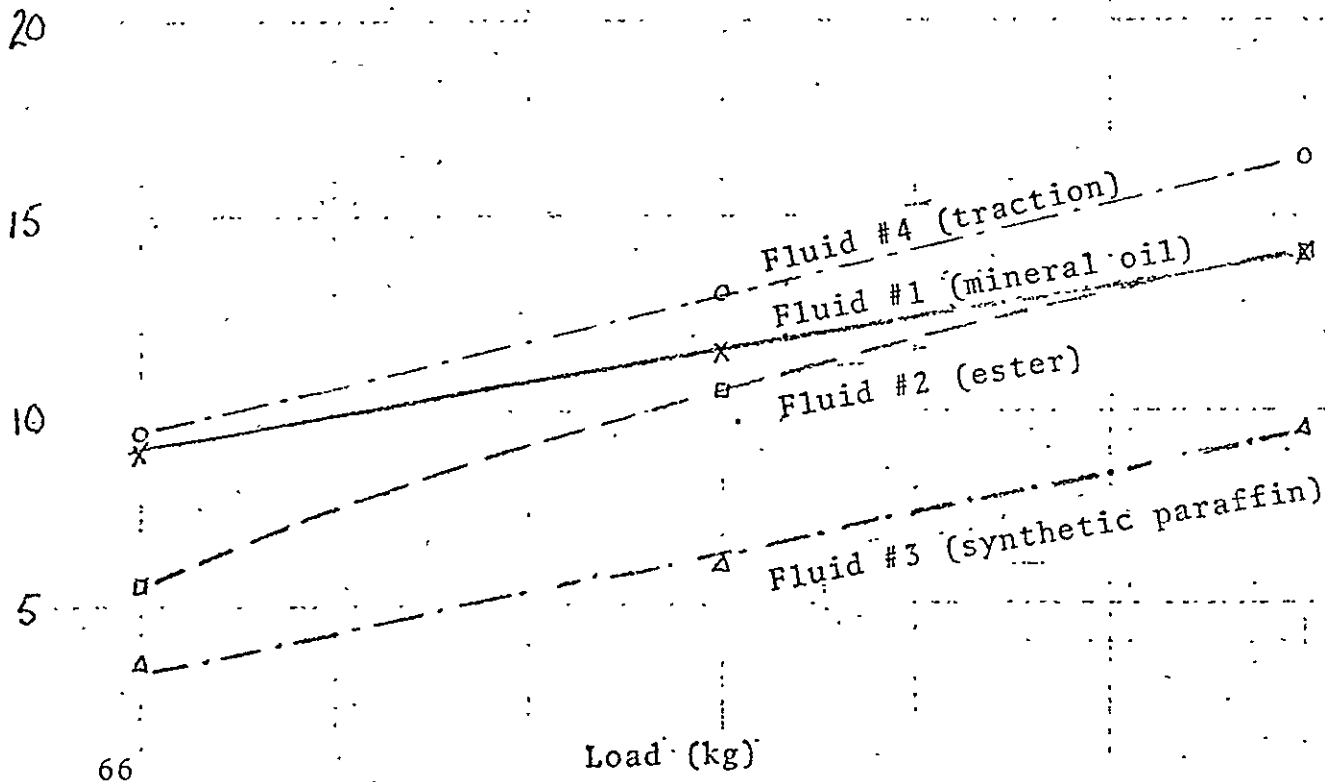
Δt2 VS SHEAR RATE

Figure 27

$\Delta t2$ °C. $(t_M - t_D)$
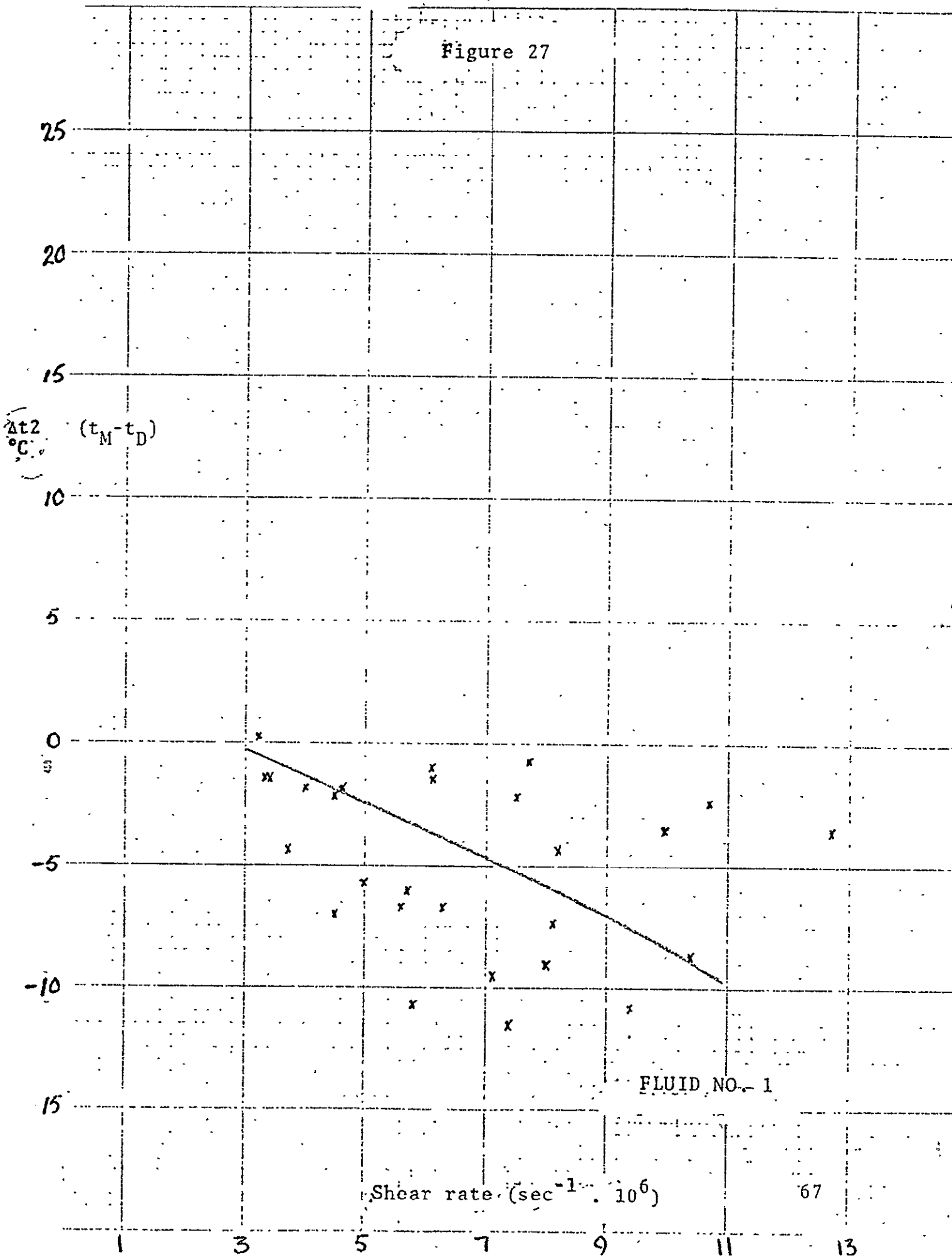
FLUID NO. 1

Shear rate $(sec^{-1} \cdot 10^6)$

67

Δt2 VS SHEAR RATE

FIGURE 28

FLUID NO. 2

$\Delta t2$ °C $(t_M - t_D)$

Shear rate (sec^{-1} . 10^6)

68
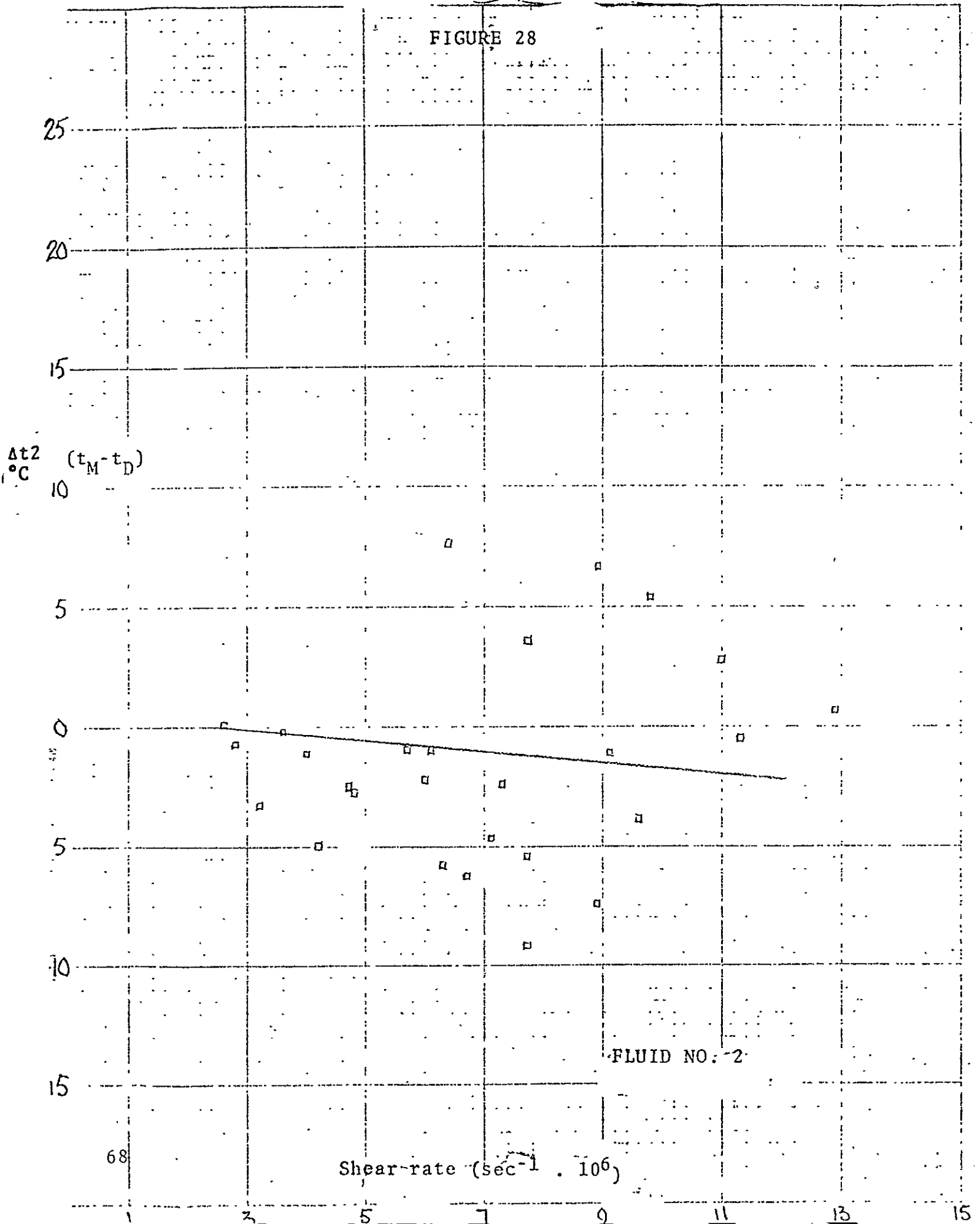
Δt2 VS SHEAR RATE

FIGURE 29

$\Delta t2$
$^\circ C$ $(t_M - t_D)$
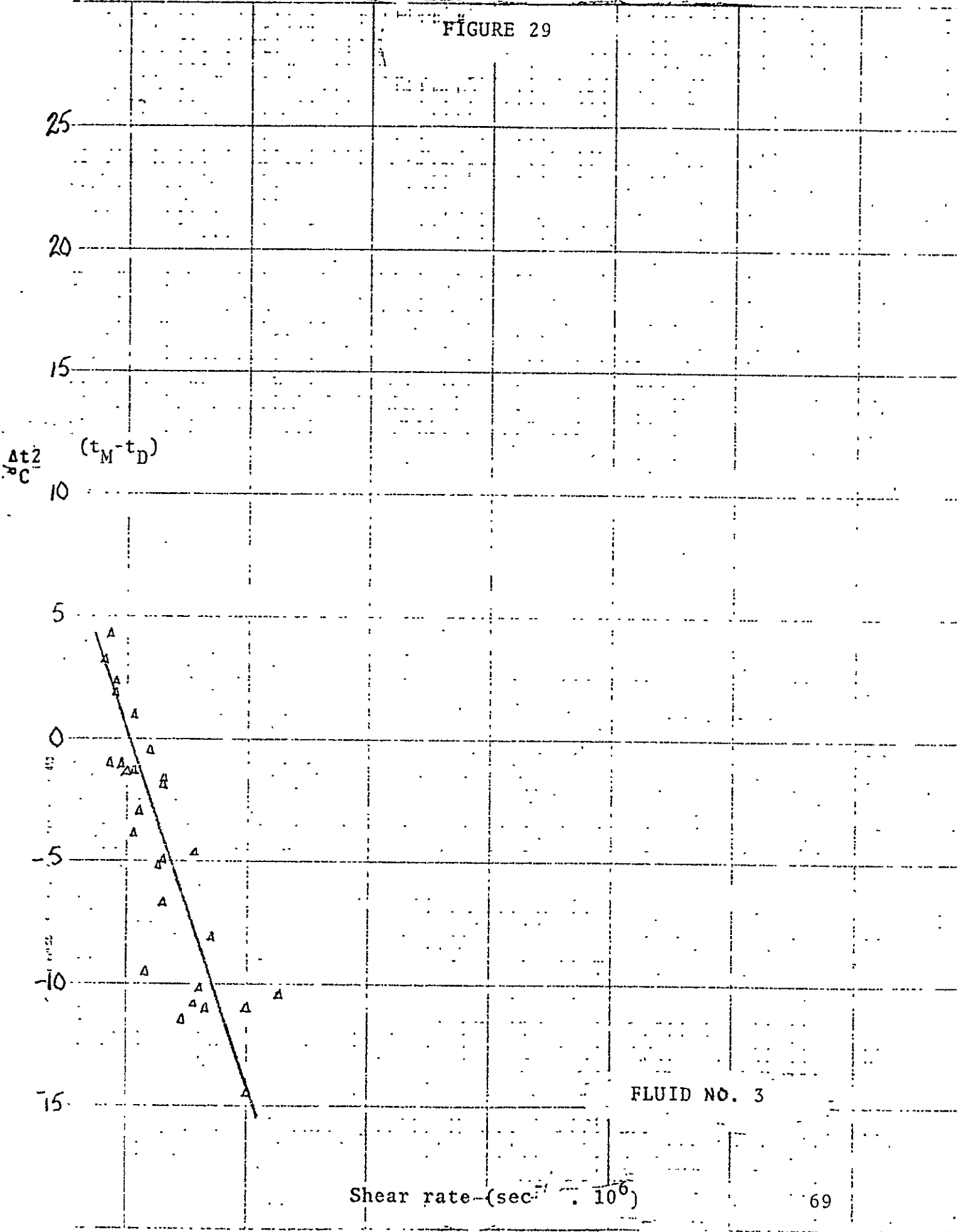
FLUID NO. 3

Shear rate-(sec^{-1} . 10^6)

69

Δt2 VS SHEAR RATE.

FIGURE 30
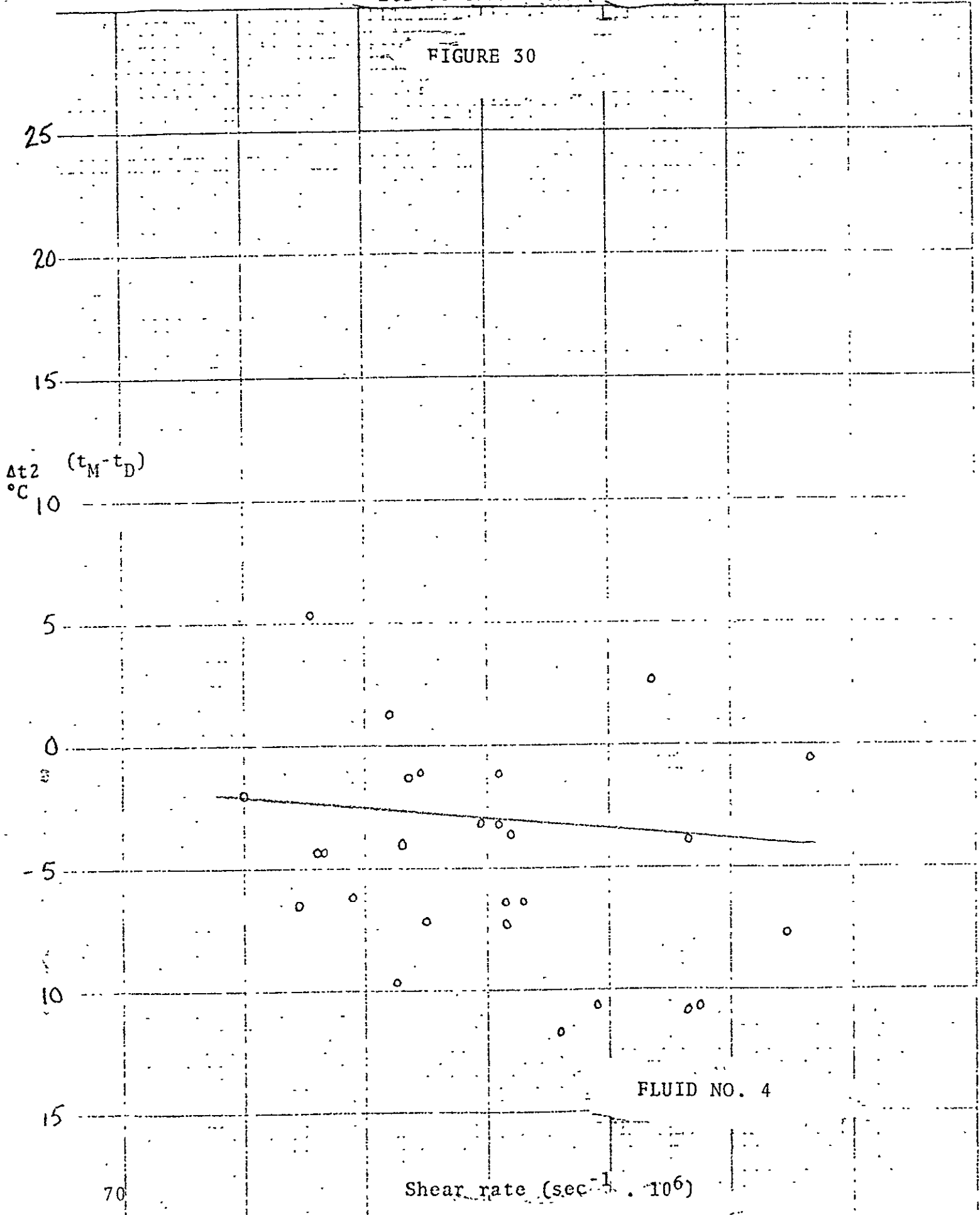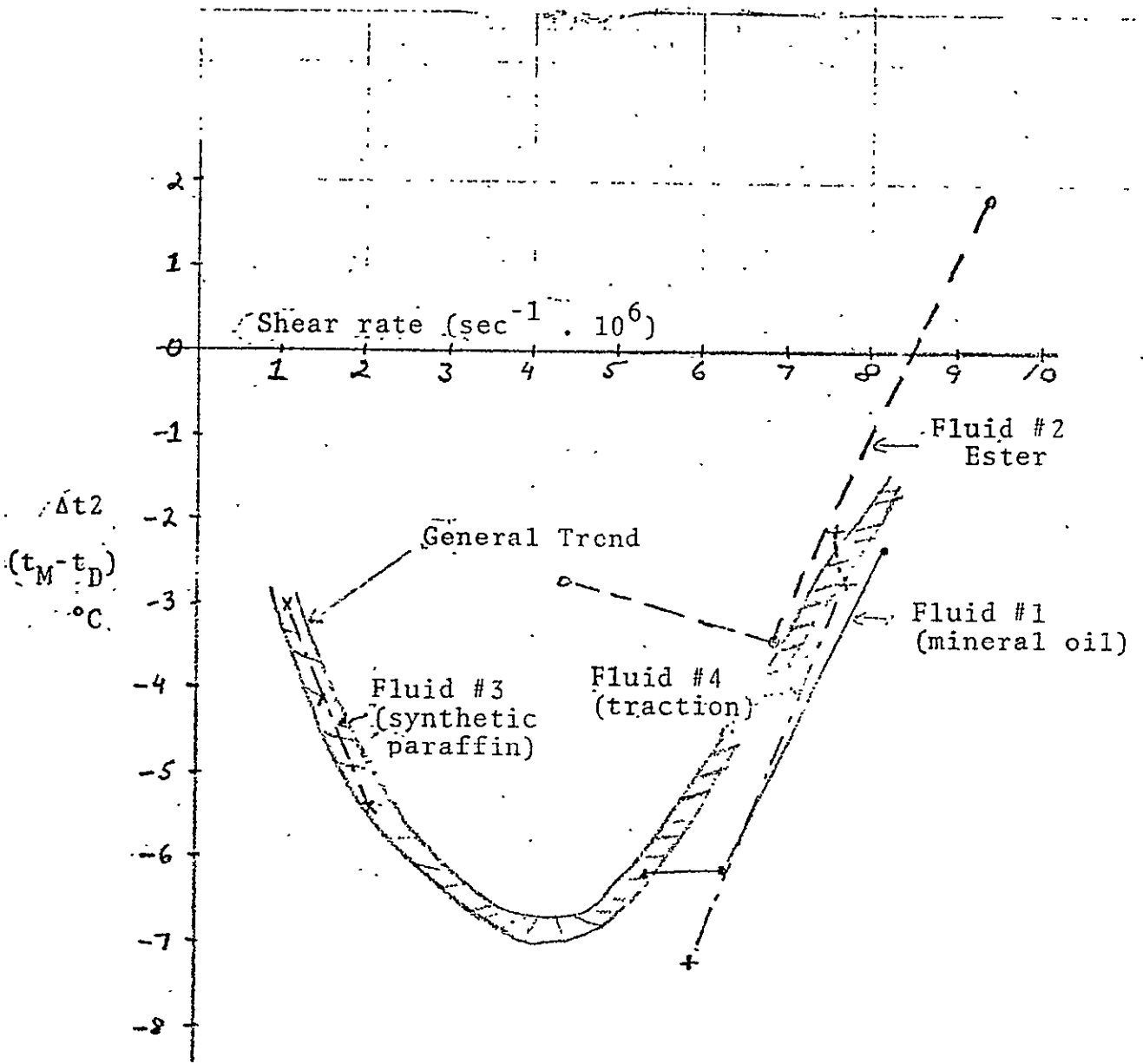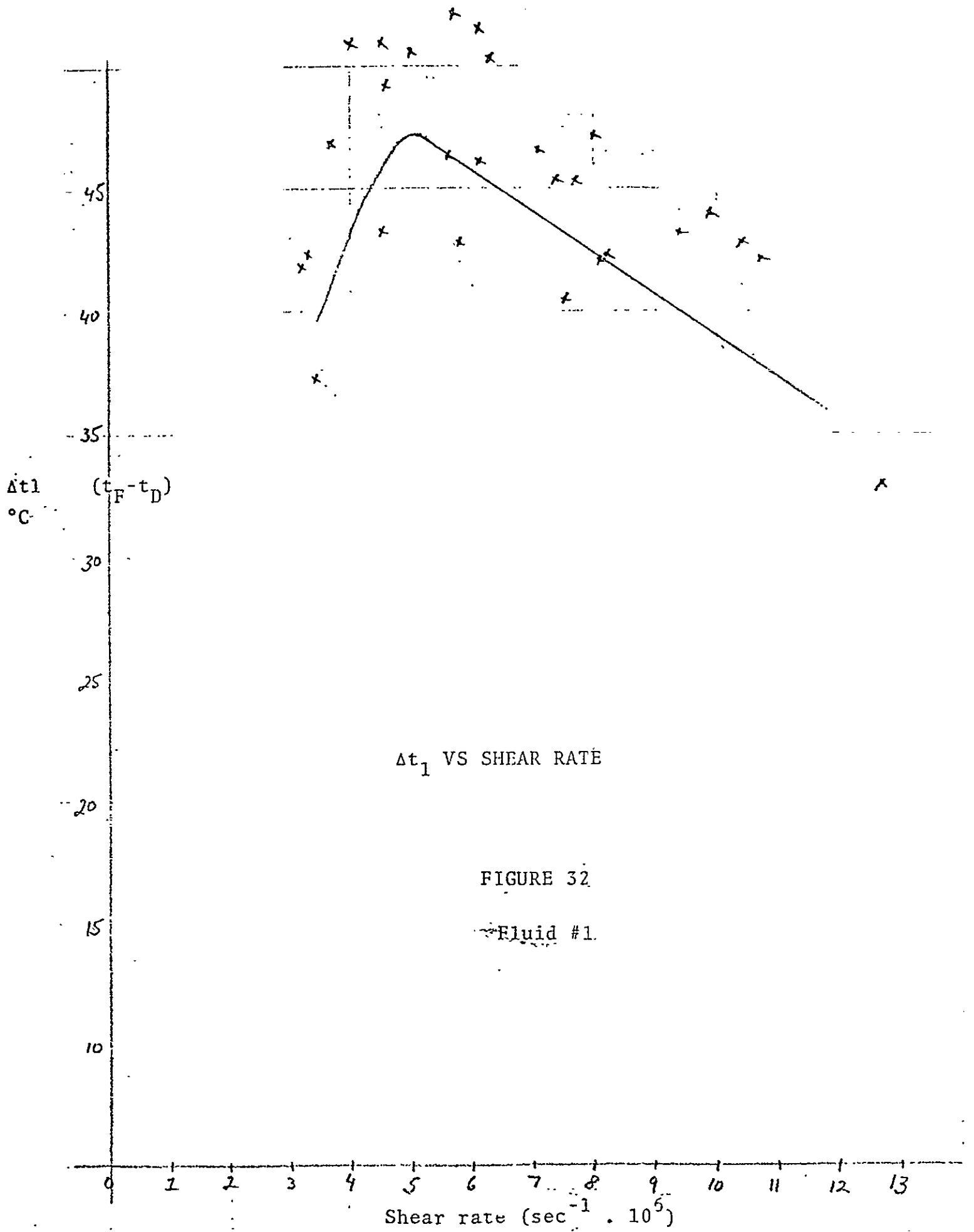
$\Delta t2$ $(t_M - t_D)$
°C
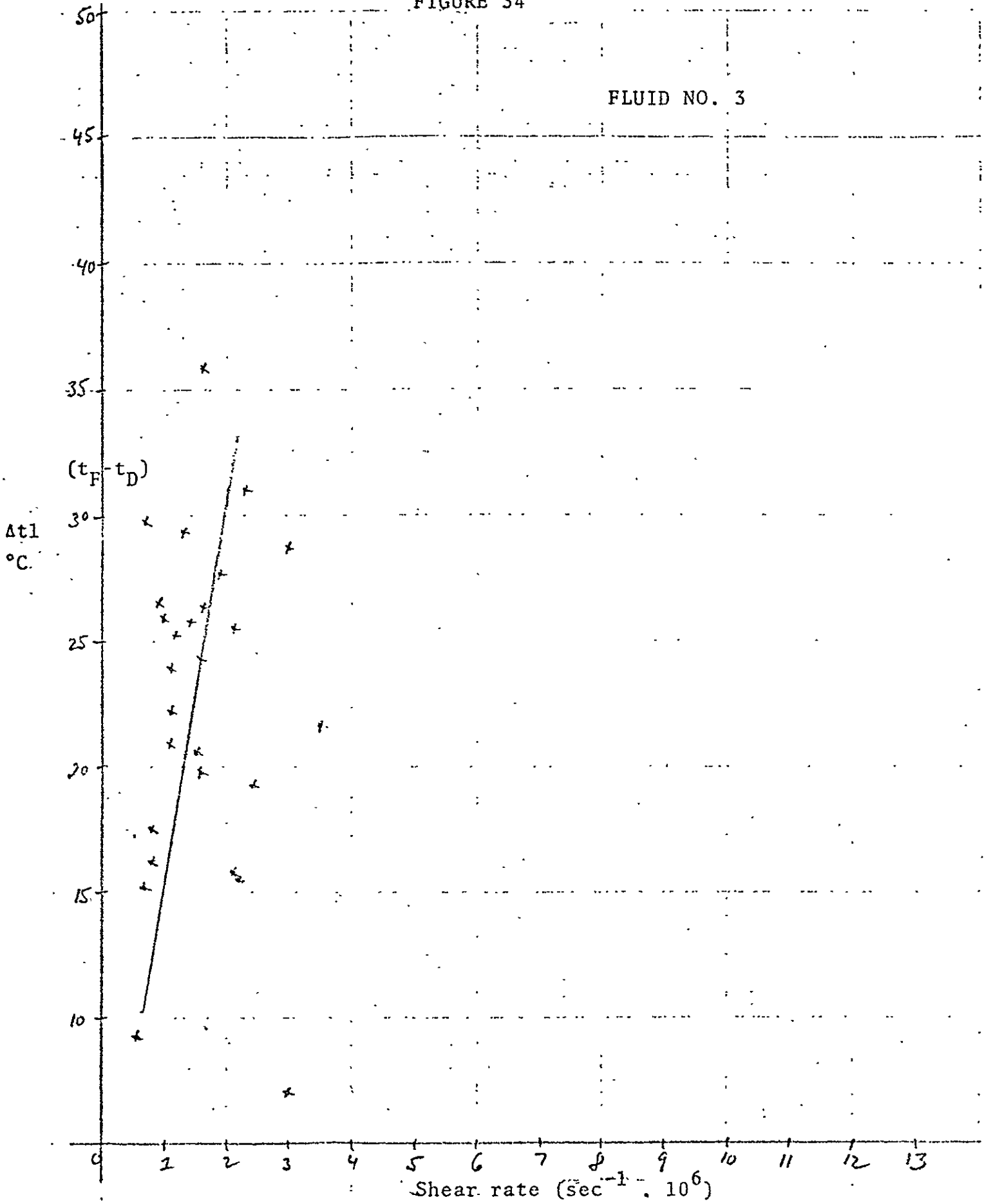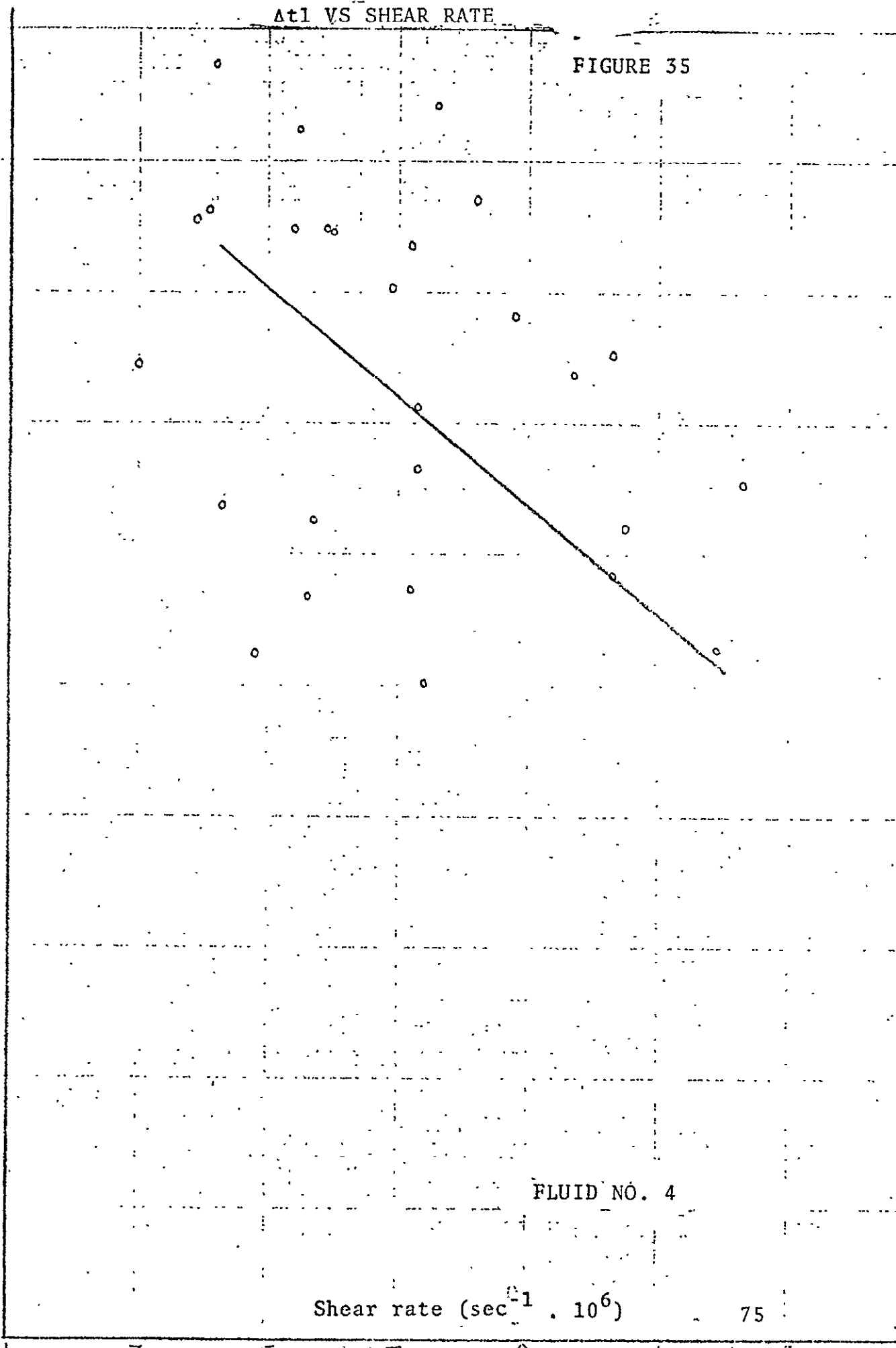
FLUID NO. 4

Shear rate (sec^{-1} . 10^6)

FIGURE 31

Δt2 AVERAGED OVER SPEED AND LOAD
VS AVERAGED SHEAR RATE

Δt_1 VS SHEAR RATE
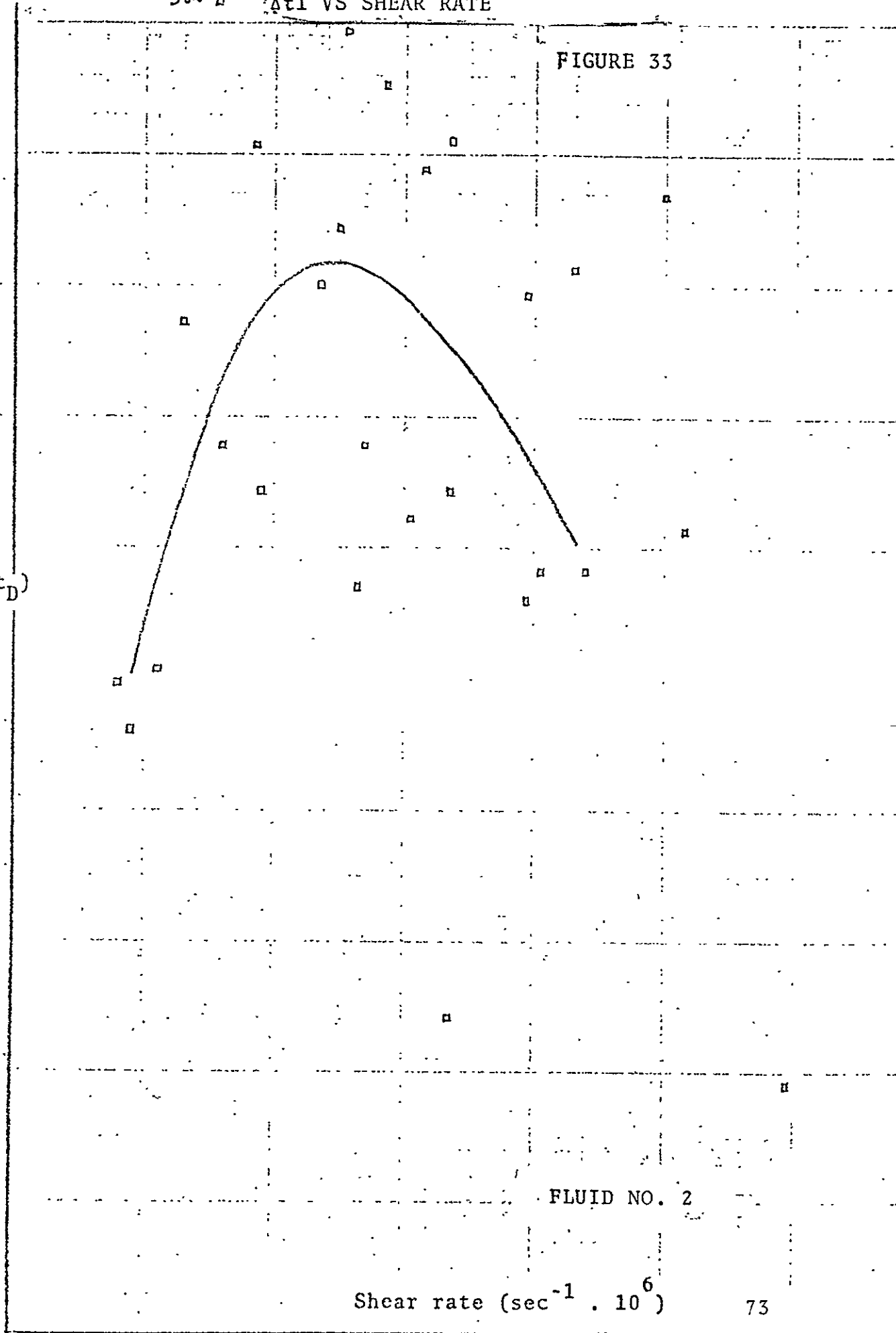
FIGURE 32

Fluid #1.

FIGURE 33

Δt1 VS SHEAR RATE

Δt1 $(t_F - t_D)$ °C

Shear rate (sec^{-1} . 10^6)

FLUID NO. 2

73

FIGURE 34

FLUID NO. 3

(t_F-t_D)

$\Delta t1$ °C.

Shear rate (sec^{-1} . 10^6)

74

Δt1 VS SHEAR RATE

FIGURE 35

FLUID NO. 4

Vertical axis: $(t_F - t_D)$, Δt1, °C

Horizontal axis: Shear rate (sec^{-1} . 10^6)

FIGURE 36

Δt_1 AVERAGED OVER SPEED AND LOAD
VS AVERAGED SHEAR RATE

Δt_1

$(t_F - t_D)$

°C

Fluid #4
(traction)

Fluid #1
(mineral oil)

Fluid #2
(ester)

General trend

Fluid #3
(synthetic paraffin)

Shear rate (sec^{-1} . 10^6)

76
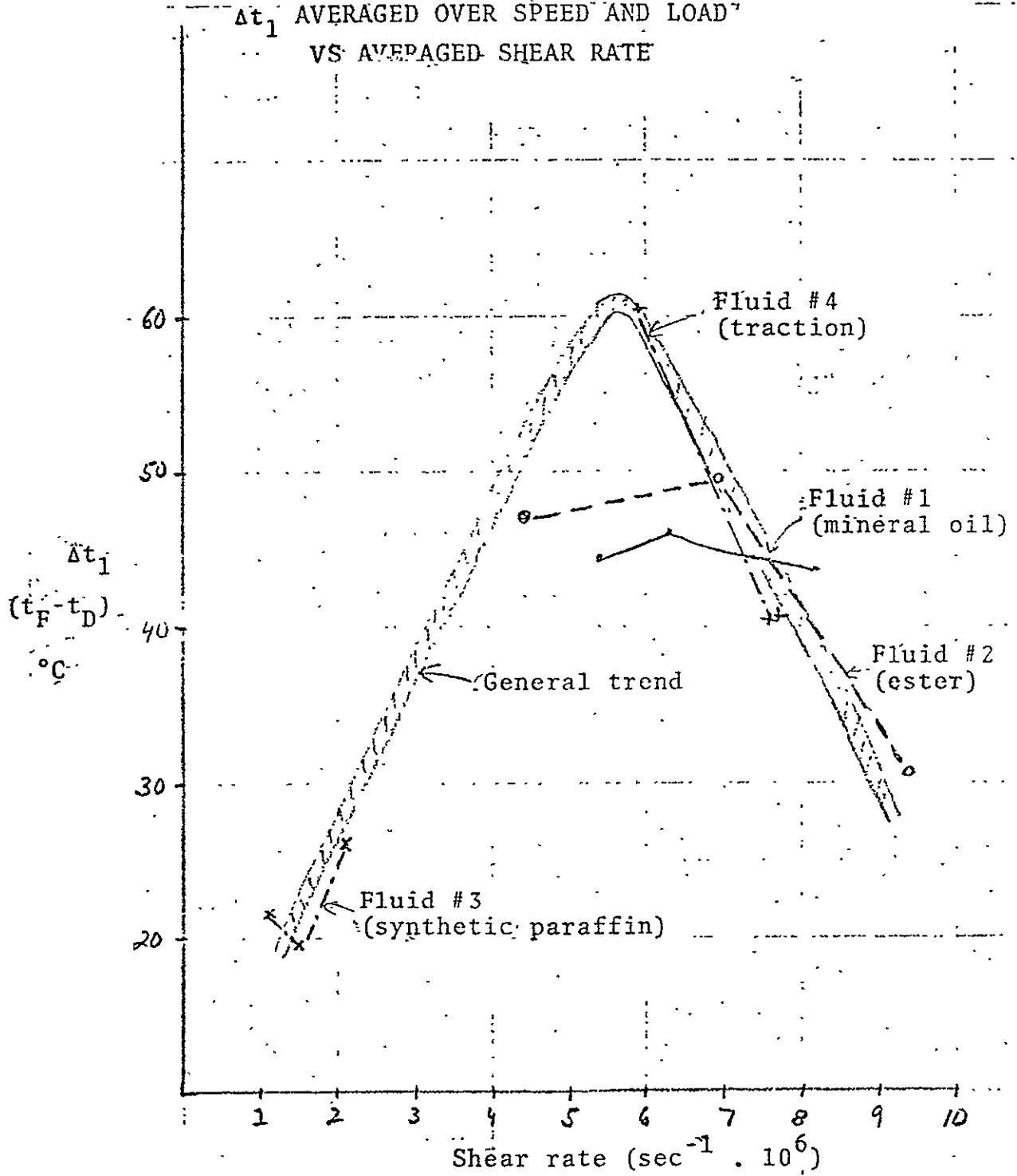
Δt_4 VS SHEAR RATE

FIGURE 37

Fluid #1 (NAPHTHENIC MINERAL OIL)

$(t_F - t_M)$

Δt_4

°C

Shear rate (sec^{-1} . 10^6)
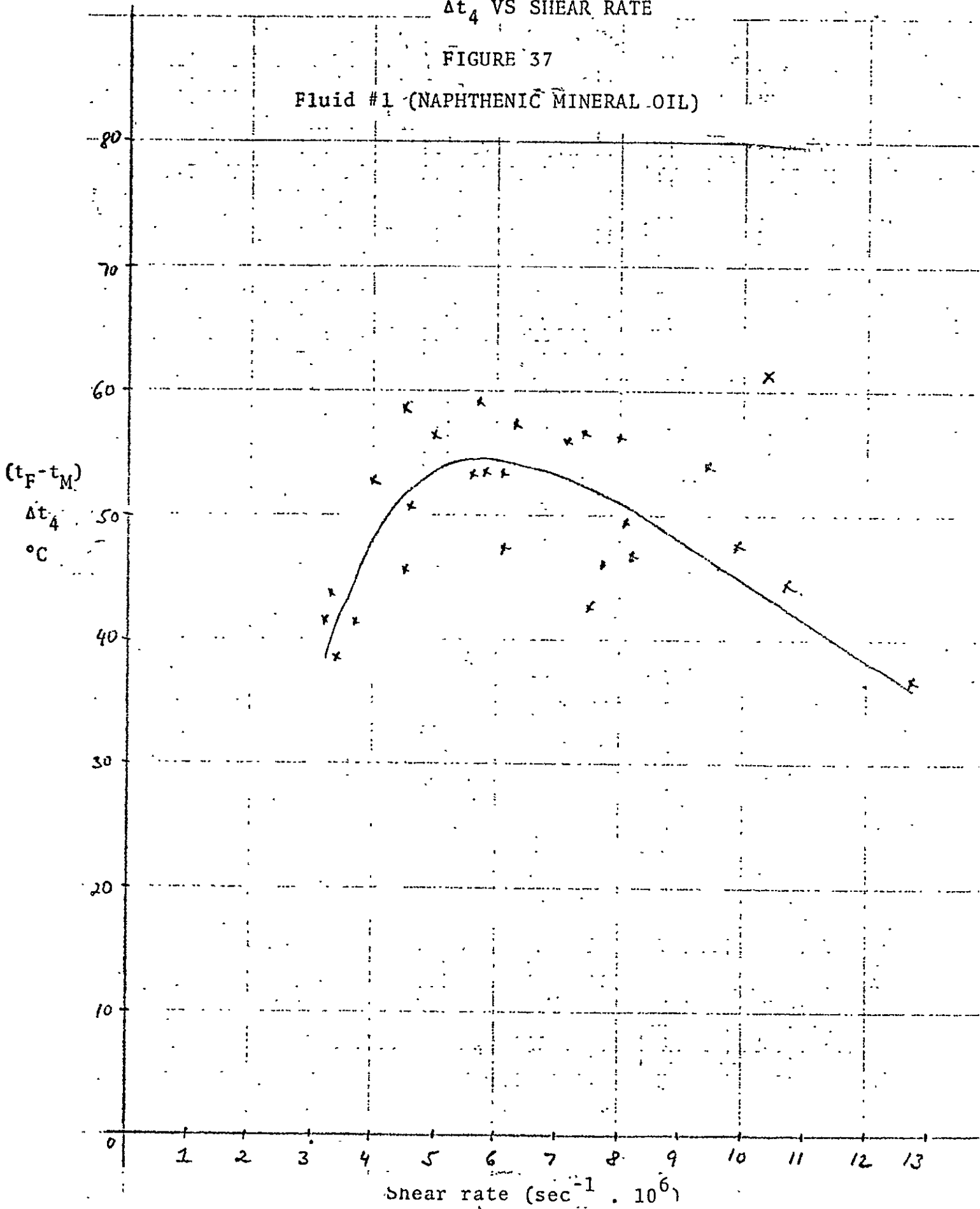
Δt4 VS SHEAR RATE

FIGURE 38

$(t_F - t_M)$

t4

°C

80

70

60

50

40

30

20

10

0

FLUID NO. 2

78

Shear rate (sec^{-1} . 10^6)

1   3   5   7   9   11   13   15
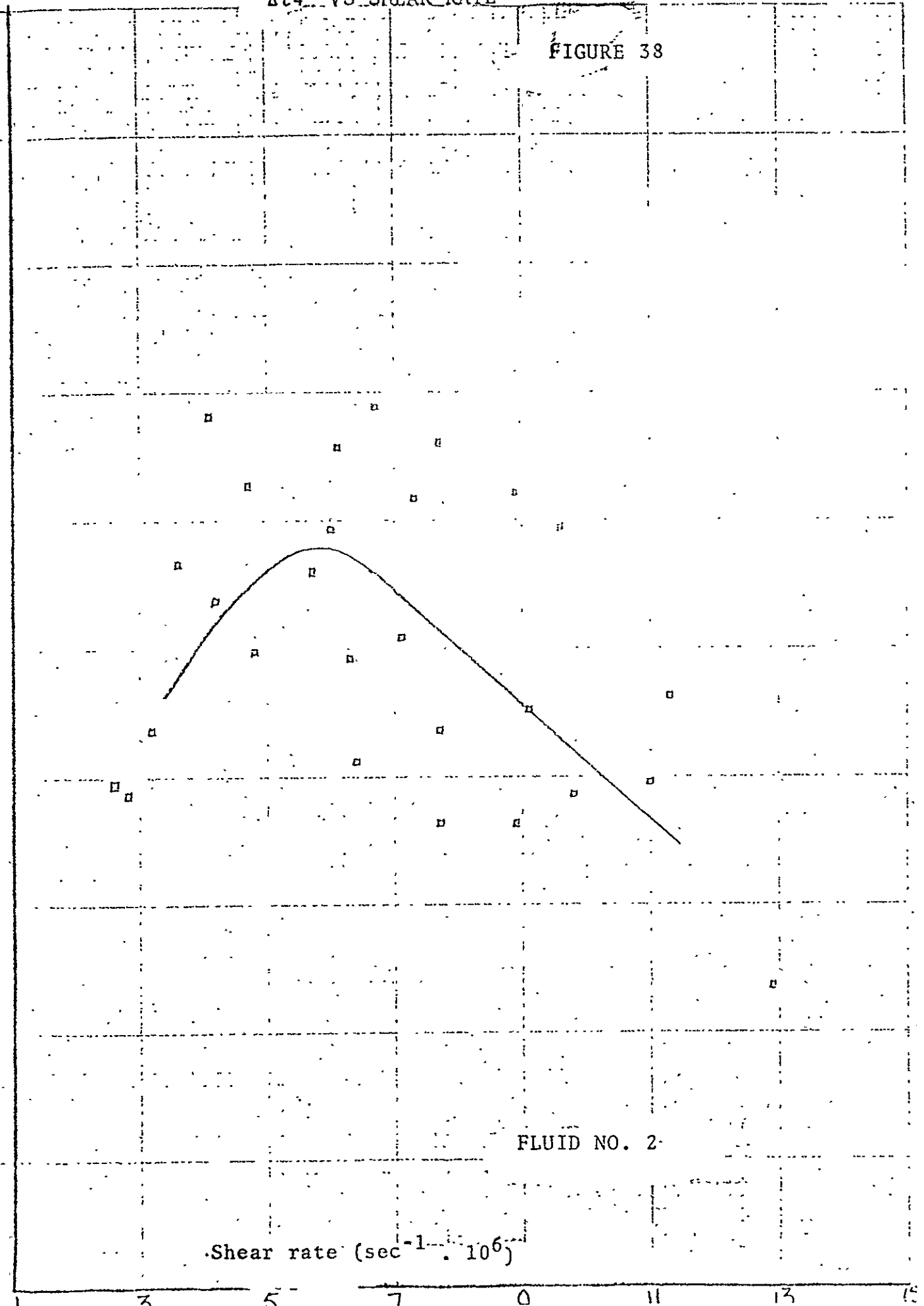
Δt_4 VS SHEAR RATE

FIGURE 39

FLUID #3 (SYNTHETIC PARAFFIN)

$(t_F - t_M)$

Δt_4

°C

Shear rate (sec^{-1} . 10^6)
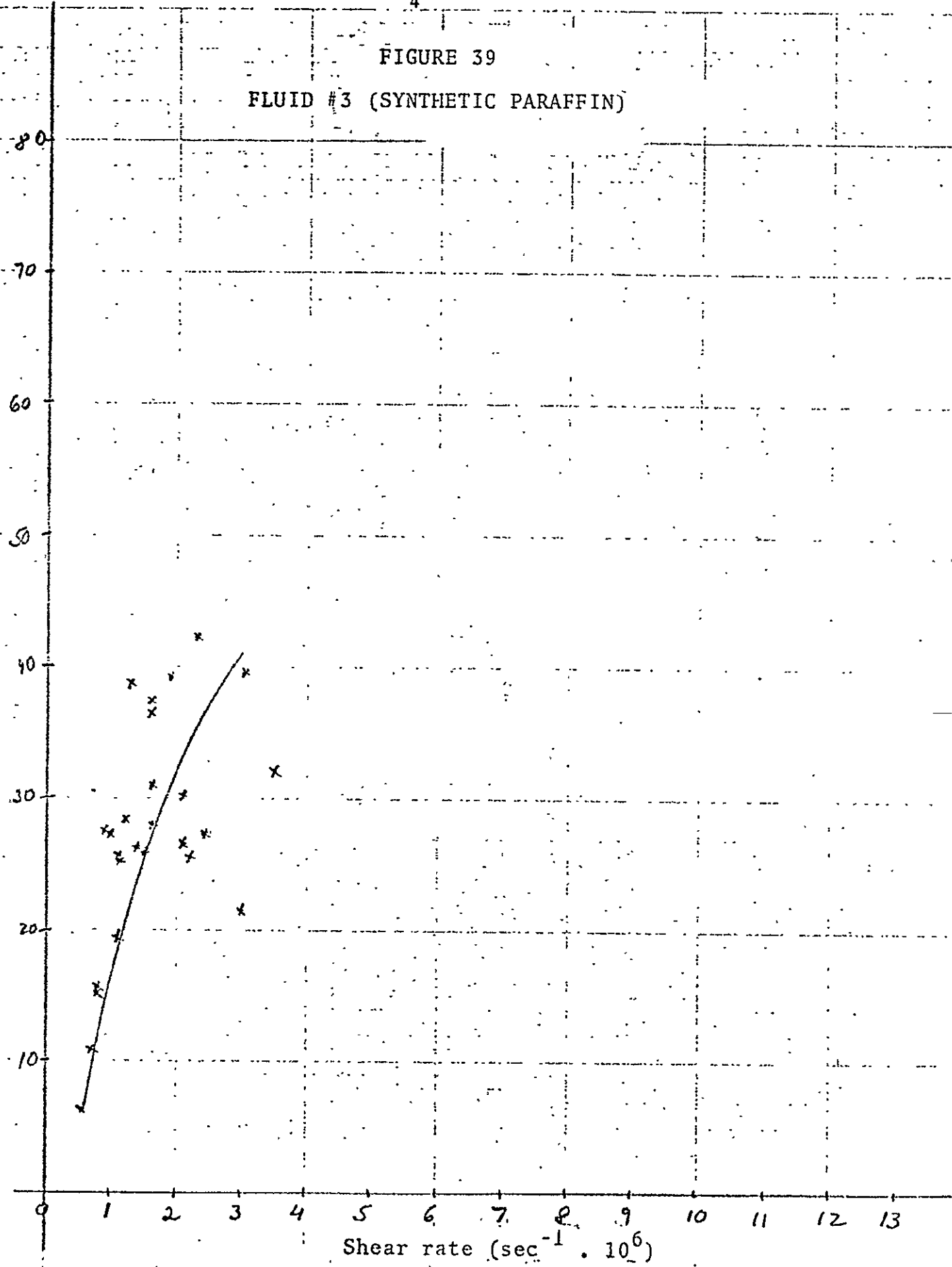
Δt4 VS SHEAR RATE

FIGURE 40

FLUID NO. 4

$(t_F - t_M)$
Δt4
°C

Shear rate (sec^{-1} . 10^6)

FIGURE 41

Δt4 AVERAGED OVER SPEED AND LOAD
VS AVERAGED SHEAR RATE
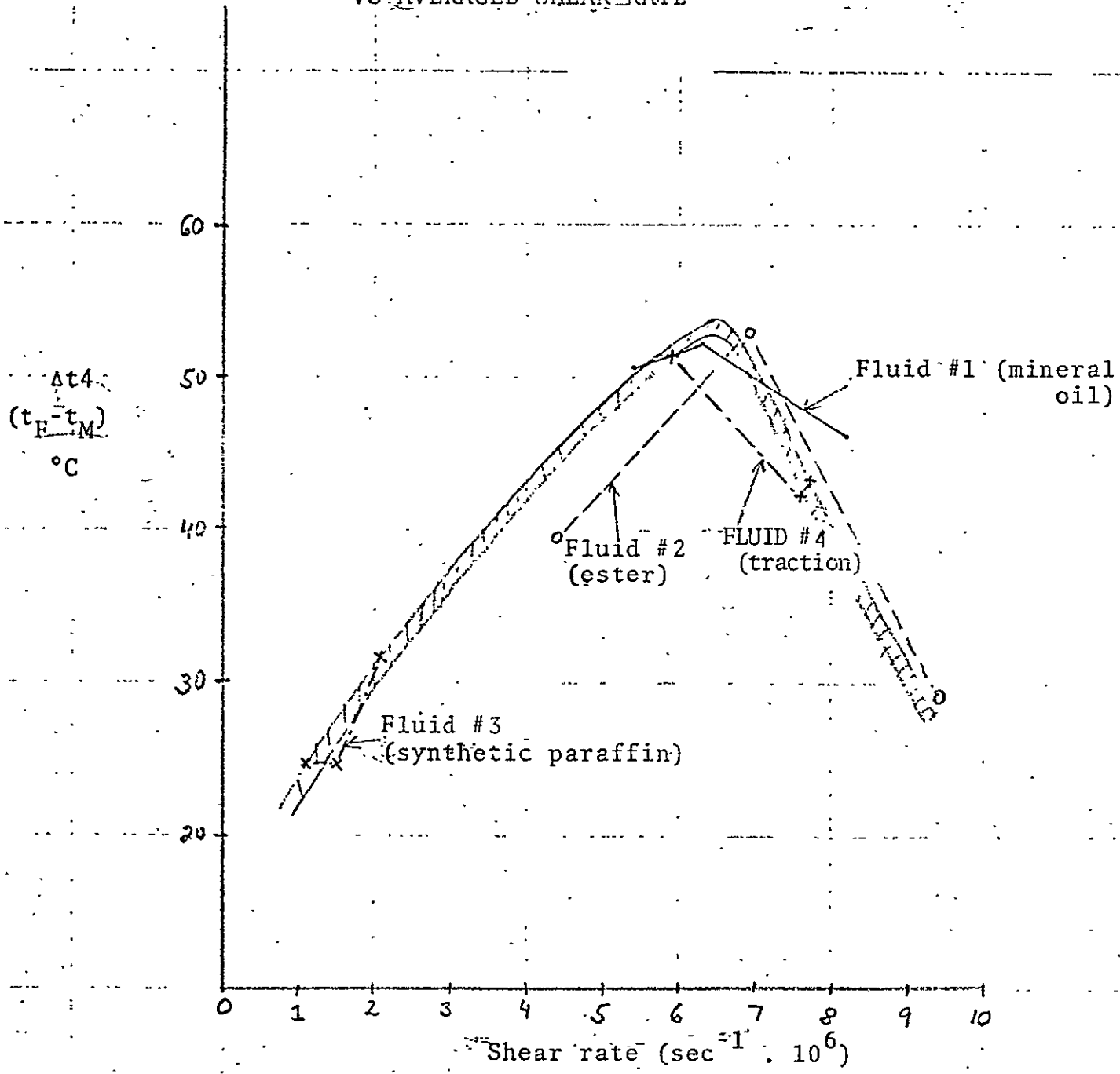
FIGURE 42

$\times \Delta t_1$ VS SHEAR RATE FOR ALL FLUIDS

$\Delta t1$
$(t_F - t_D)$
°C

Fluid #1

Fluid #2

Fluid #4

Fluid #3

Shear rate (sec^{-1} . 10^6)

82
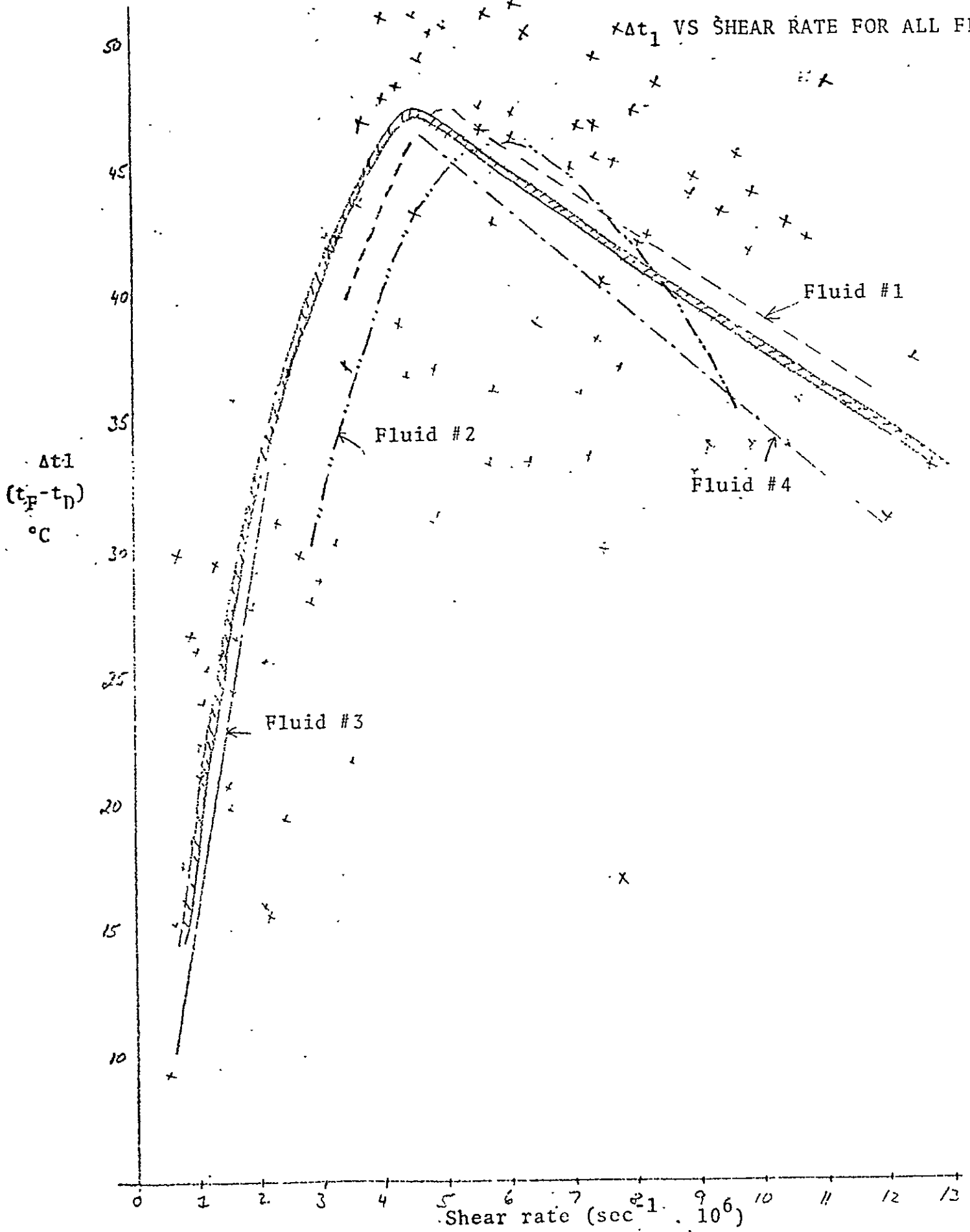
FIGURE 43

Δt_4 VS SHEAR RATE FOR ALL FLUIDS

$\Delta t4$
$(t_F - t_M)$
$^\circ C$

Fluid #4

Fluid #1

Fluid #2

Fluid #3

Shear rate (sec^{-1} ... 10^6)

83
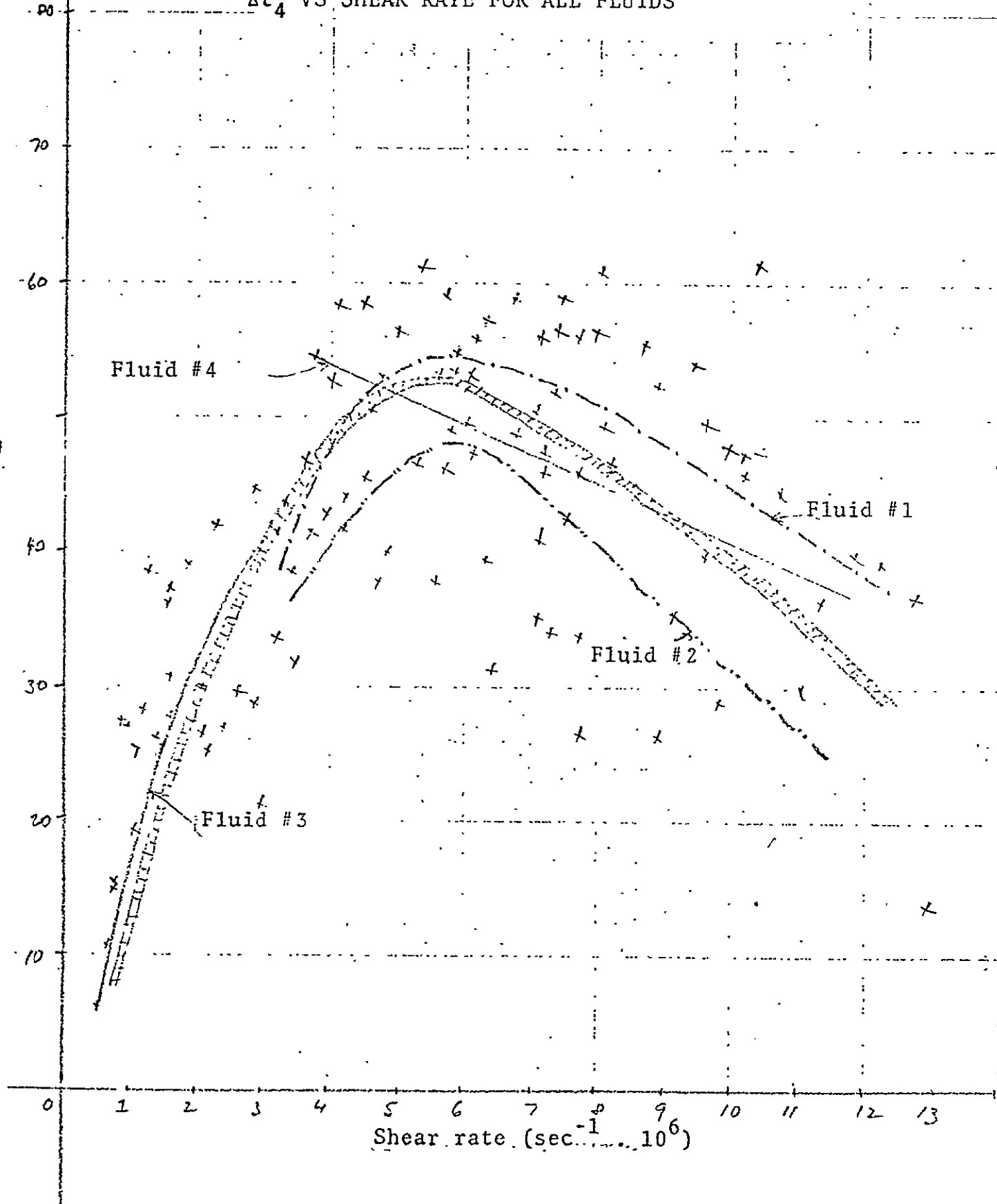
FIGURE 44

AVERAGE TEMPERATURE
DIFFERENCES COMPARED
FOR THE FOUR FLUIDS

REFERENCES

1. Lauer, J. L., "Study to Define Behavior of Liquid Lubricants in an Elastohydrodynamic Contact", NASA CR-134671, October, 1974.

2. Turchina, V., Sanborn, D. M., and Winer, W. O., "Temperature Measurements in Sliding Elastohydrodynamic Point Contacts", Trans. ASME, Journal of Lubrication Technology, Series F, Vol. 96, No. 3, pp. 464-71, July, 1974.

3. Lauer, J. L., and Peterkin, M. E., Developments in Applied Spectroscopy, Vol. 10, pp. 59-78, (Plenum Press, New York, 1972).
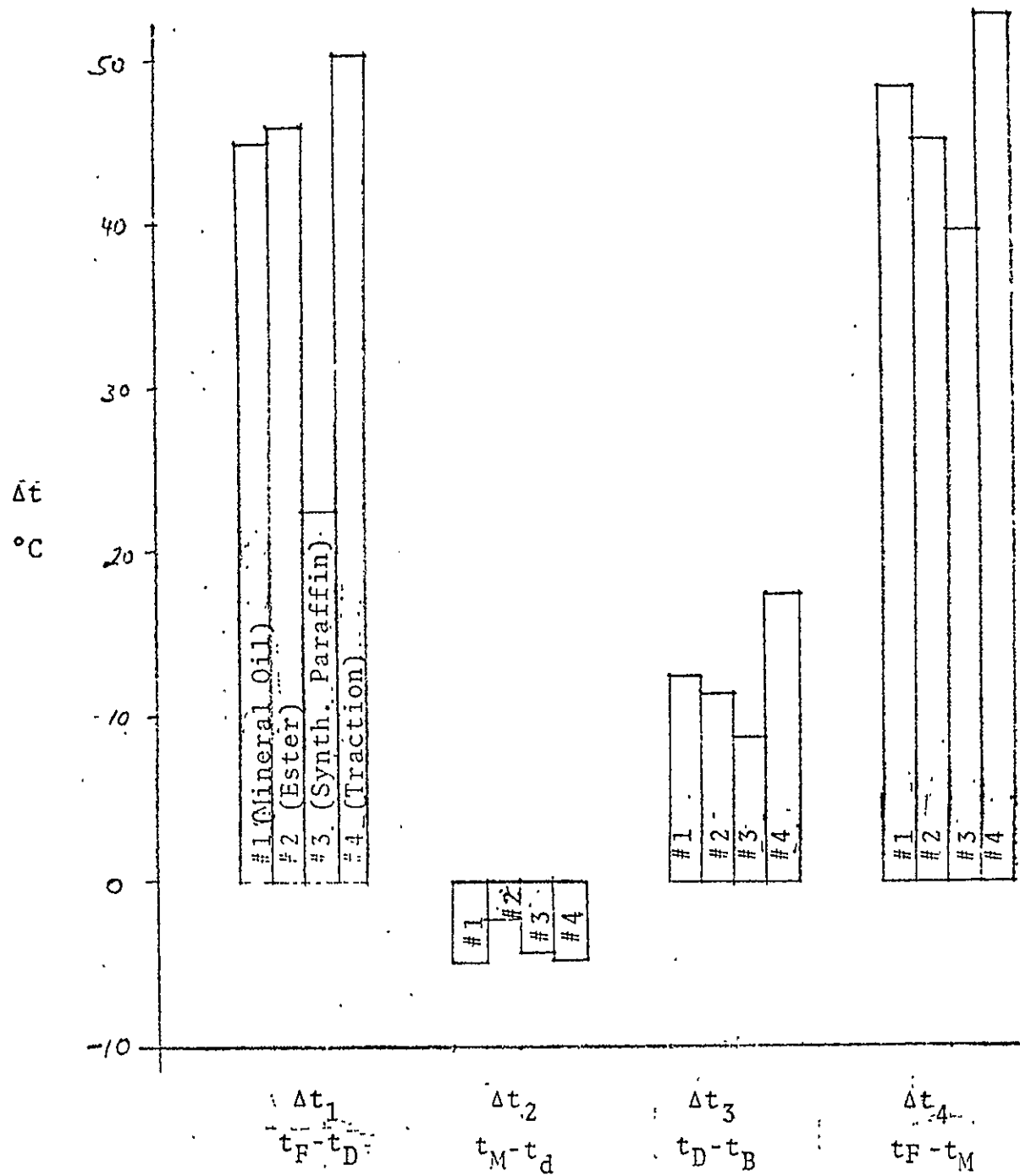
4. Low, M. J. D., and Coleman, I., Spectrochim. Acta, 22, 369 (1966).

5. McMahon, H. O., "Thermal Radiation from Partially Transparent Reflecting Bodies," J. of the Optical Society of America, Vol. 40, No. 6, pp. 376-80, 1950.

6. Viskanta, R., Hommert, P. J., and Groninger, G. L., "Spectral Remote Sensing of Temperature Distribution in Semi-transparent Solids Heated by an External Radiation Source", Applied Optics, Vol. 14, No. 2, pp. 428-37 (February 1975)

7. Stejskal, E. O., and Cameron, A., "Optical Interferometry Study of Film Formation in Lubrication of Sliding and/or Rolling Contacts," NASA CR-120842, MRC-SL-345, April 1972.

8. Sanborn, D. M., and Winer, W. O., "Fluid Rheological Effects in Sliding Elastohydrodynamic Point Contacts with Transient Loading: I.Film Thickness," Trans. ASME, Journal of Lubrication Technology, Series F, Vol. 93, pp. 262-271, April 1971.

9. Wedeven, L. D., Evans, D., and Cameron, A., "Optical Analysis of Ball Bearing Starvation", Trans. ASME, Journal of Lubrication Technology, Series F, Vol. 93; pp. 349-63 (July 1971).

10. Walther, C., "Characterizing Lubricating Oils by the Viscosity-Pole-Height," Proceedings of the World Petroleum Congress, 1973; London, 1934, pp. 419-20.

11. Jones, William R., Jr., Johnson, R. L., Winer, W. O., and Sanborn, D. M., "Pressure-Viscosity Measurements for Several Lubricants to 5.5x10^8 Newtons per Square Meter and 149°C," NASA, TN D-7736 (August 1974).

12. Born, M., and Wolf, E., "Principles of Optics", Pergamcon Press Ltd., Oxford, 1964.

13. Lauer, J. L., and Peterkin, M. E., "Low Temperature and Samll Sample Spectra Obtained by FTS with a Large Computer," in Developments in Applied Spectroscopy, Vol. 9, pp. 73-107 (1971).

14. Griffith, P. R., "Photometric Precision in Infrared Spectra Measured by Fourier Transform Spectroscopy; Applied Spectroscopy, 29, 11-24 (1975).

15. Gribov, L. A., "Intensity Theory for Infrared Spectra of Polyatomic Molecules." Translated from the Russian by P. P. Sutton. New York, Consultants Bureau, 1964.

16. Lauer, J. L., and Peterkin, M. E., "Infrared Emission Spectra of Elastohydrodynamic Contacts," Paper No. 74-LUB-10, Contributed to the ASLE/ASME Joint Lubrication Conference, Miami Beach, Fla., October 21-23, 1975.

17. Johnson, K. L. in Discussion of the Paper by Allen, C. M., Townsend, D. P., and Zaretsky, E. V., "Elastohydro-dynamic Lubrication of a Spinning Ball in a Non-conforming Groove," Trans. ASME, J. of Lubrication Technology, 89-96, January 1970.

18. Hirst, W., and Moore, A. J., "The Elastohydrodynamic Behaviour of Polyphenyl Ether," Proc. Roy. Soc., Series A, Vol. 344 pp. 403-426 (July 1975).

19. Crook, A. W., "Lubrication of Rollers", II. Film Thickness with Relation to Viscosity and Speed, III "A Theoretical Discussion of Friction and Temperature in the Oil Film." Phil. Trans. Roy. Soc. A., 254, 223, 237 (1961).

20. Cameron, A., "The Principles of Lubrication," Longmans Green & Co., Ltd., London 1966.

DISTRIBUTION LIST

CR-134973   NASA Contract NAS 3-18531

ADDRESSEE	NUMBER OF COPIES

NASA Lewis Research Center
21000 Brookpark Road
Cleveland, OH 44135
Attn: Contract Section A, MS 500-206   1
       Technology Utilization Office, MS 3-19   1

       Library, MS 60-3   2
       Report Control Office, MS 5-5   1
       N. T. Musial, MS 500-118   1
       A. Ginsburg, MS 5-3   1
       J. H. Weeks, MS 5-3   1

       W. R. Jones, MS 23-2   10
       W. R. Loomis, MS 23-2   1
       L. D. Wedeven, MS 23-2   1
       H. E. Sliney, MS 23-2   1
       W. J. Anderson, MS 23-2   1
       E. V. Zaretsky, MS 6-1   1
       G. J. Weden, MS 5-3   1

NASA Headquarters
Washington, DC 20546
Attn: N. F. Rekos (RLC)   1
      J. Maltz (RWM)   1

NASA Scientific and Technical Information Facility
P. O. Box 33
College Park, MD 20740
Attn: Acquisitions Branch   30

Air Force Aero Propulsion Laboratory
Wright Patterson AFB, OH 45433
Attn: Howard Jones, APFL/SFL   1
      J. F. Dill, APFL/SFL   1

Air Force Materials Laboratory
Wright Patterson AFB, OH 45433
Attn: Major L. Fehrenbacher, AFML/MBT   1
      C. E. Snyder, Jr., AFML/MBT   1
      G. J. Morris, AFML/MBT   1
      F. Brooks, AFML/MBT   1

Office of Naval Research
Code 411
Arlington, VA 22217
Attn: Lt. R. Miller   1

ADDRESSEE	NUMBER OF COPIES
Battelle Memorial Institute Columbus Laboratories 505 King Avenue Columbus, OH 43201 Attn: C. M. Allen	1
Chevron Research Company 576 Standard Avenue Richmond, CA 94802 Attn: D. Godfrey	1
Exxon Research & Engineering Company P. O. Box 51 Linden, NJ 07036 Attn: A. Beerbower	1
Midwest Research Institute 425 Volker Blvd. Kansas City, MO 64110 Attn: V. Hopkins	1
Mobil Research & Development Corp. P. O. Box 1025 Princeton, NJ 08540 Attn: C. N. Rowe P. E. Fowles	1 1
Southwest Research Institute P. O. Box 28510 San Antonio, TX 78284 Attn: P. M. Ku	1
Trans-Sonics, Inc. P. O. Box 326 Lexington, MA 02173 Attn: V. C. Westcott	1
Carnegie-Mellon University Dept. of Chemical Engineering Schenley Park Pittsburgh, PA 15213 Attn: T. Fort, Jr.	1
Pennsylvania State University Dept. of Chemical Engineering University Park, PA 16802 Attn: E. E. Klaus	1
Mr. E. E. Bisson 20786 Eastwood Avenue Fairview Park, OH 44126	1

ADDRESSEE	NUMBER OF COPIES
Northwestern University The Technology Institute Evanston, IL 60201 Attn: H. S. Cheng	1
Texaco Research Center Research & Technical Department Fundamental Research Station Beacon, NY 12508 Attn: R. Fein	1
University of Virginia Thornton Hall Charlottesville, VA 22091 Attn: J. J. Kauzlarich W. Jamison	1 1
University of Michigan Dept. of Mechanical Engineering Ann Arbor, MI 48105 Attn: K. Ludema	1
Georgia Institute of Technology School of Mechanical Engineering Atlanta, GA 30332 Attn: W. O. Winer D. M. Sanborn	1 1
Imperial College Dept. of Mechanical Engineering Exhibition Road London SW7 2BX England Attn: A. Cameron	1
National Engineering Laboratory East Kilbride, Glasgow Great Britain Attn: D. Scott	1
Mr. Robert L. Johnson 4503 W. 224 Street Fairview Park, OH 44126	1